SARCOMERE DYNAMICS DURING CONTRACTION-INDUCED INJURY TO PERMEABILIZED SINGLE MUSCLE FIBERS

by

Appaji Panchangam

A dissertation submitted in partial fulfillment
of the requirements for the degree of
Doctor of Philosophy
(Biomedical Engineering)
in The University of Michigan
2008

Doctoral Committee:

Professor John A. Faulkner, Chair
Professor Douglas C. Noll
Professor Duncan G. Steel
Assistant Research Scientist Dennis R. Claflin
Assistant Research Scientist Mark L. Palmer

to

pandu

amma

nayanamma

ACKNOWLEDGMENTS

I would like to thank my committee for the help and guidance they have provided. My advisor, John Faulkner, has been a great inspiration both in the process of scientific inquiry and the process of life. His guidance, support and mentorship are invaluable. My co-advisor, Dennis Claflin, has been phenomenally helpful in various matters related to my work in the lab as well as matters in my personal life. Mark Palmer has spent a tremendous amount of time in helping me and I thank him for all the discussions ranging from science to spirituality. I thank you all and appreciate your patience and the time you have taken to help me in this process.

I would like to thank all the members of the Muscle Mechanics Lab for their assistance. In particular, I would like to express my gratitude for the assistance given by Cheryl A. Hassett, without her assistance I would not have been able to complete my experiments. Jane Heibel has been a great help in so many things that enable several everyday activities.

I would like to thank Prof. Matt O'Donnell and Russell Witte for introducing me to several signal processing and data representation techniques.

I would like to thank Mike Stucky for bringing me up to speed on this project.

I would like to thank Susan V. Brooks for serving on my Qualifying committee and for her help and support.

Even though many of my family members do not know what this is all about, they supported my pursuit whole-heartedly. I like to thank them for all the support and encouragement.

TABLE OF CONTENTS

LIST OF FIGURES

Figures

CHAPTER 1

INTRODUCTION

Skeletal muscles (Fig. 1.1) can be injured by their own contractions. Such contraction-induced injury is a leading cause of the loss of mobility in the rapidly increasing population of elderly people (Faulkner et al., 1990; Garrett, Jr., 1990; Pope and Tarlov, 1991). The concept of skeletal muscles being injured by their own contractions was suggested more than a century ago by the experiments of Hough (Hough, 1902). After performing repeated contractions of the finger flexor muscles of humans until fatigued, subjects reported experiencing soreness several hours later. Furthermore, these subjects reported increased soreness over the following 2–3 days. This phenomenon, termed, delayed onset of muscle soreness by Hough, has since been recognized as a universal phenomenon experienced by people of all ages while performing a wide variety of daily-life activities.

The early investigations in the study of contraction-induced injury were predominantly at the whole body level of humans (Asmussen, 1956; Hough, 1902; Newham et al., 1983c; Schwane et al., 1983). While these early investigations highlighted the importance of studying the phenomenon of contraction-induced injury, a preliminary understanding of the factors involved in the injury came from the mechanistic studies performed at the level of single skeletal muscles from animals (Armstrong, 1990; Faulkner et al., 1993; McCully and Faulkner, 1985; Proske and

Morgan, 2001; Stauber, 1989; Talbot and Morgan, 1996). Despite the primary focus on the whole body and at the single skeletal muscle levels, a number of insightful studies have investigated the underlying mechanisms of contraction-induced injury in single fibers or permeabilized single fibers (Brooks et al., 1995; Brown and Hill, 1991; Edman et al., 1981; Faulkner et al., 1993; Macpherson et al., 1996; Macpherson et al., 1997). This dissertation focuses on studies of the initial mechanisms that lead to the development of contraction-induced injury in permeabilized single fibers of skeletal muscles.

Characterization of contraction-induced injury

Direct evidence of injury

To conclude the occurrence of contraction-induced damage, investigators have relied upon direct evidence of the changes to muscle structure (Warren et al., 1999). The direct evidence was obtained using histology (Armstrong et al., 1983; Friden et al., 1983; Jones et al., 1986; McCully and Faulkner, 1985), or electron microscopy (Friden et al., 1983; Macpherson et al., 1996; Newham et al., 1983b; Ogilvie et al., 1988). Manifestations of the damage (Fig. 1.2) revealed with these techniques have included, (*i*) Z-line streaming (Friden et al., 1983; Lieber et al., 1991; Newham et al., 1983b; Ogilvie et al., 1988), (*ii*) loss of thick and thin filament overlap with intact Z-lines (Newham et al., 1983b; Wood et al., 1993), (*iii*) gaps in A-bands (Ogilvie et al., 1988), and (*iv*) complete disruption of the sarcomeres (Newham et al., 1983b; Ogilvie et al., 1988; Wood et al., 1993). Common to all of these manifestations is the observation that the damage is localized to small, but randomly distributed groups of sarcomeres that are both in parallel and in series with intact sarcomeres.

Limitations of the direct measures

Despite the diagnostic value, the direct observation techniques have important limitations. Since the focal damage is random, the histological images and electron micrographs do not provide suitable means to quantify the injury (McCully and Faulkner, 1985). Histological and electron microscopic evaluations require expensive and time-consuming preparations of the muscle samples. Furthermore, only images of a thin section of the sample are obtained at any one time. Consequently, the identification of the exact section that contains the representative damage becomes challenging.

Indirect measures of injury

Several indirect measures of the contraction-induced damage to muscles, including subjective reports of muscle soreness (Asmussen, 1956; Hough, 1902; Komi and Buskirk, 1972; Newham et al., 1983c; Schwane et al., 1983), release of muscle-specific enzymes (Armstrong et al., 1983; Newham et al., 1983a; Sargeant and Dolan, 1987; Schwane et al., 1983), increased influx of calcium (Jackson et al., 1984; Jones et al., 1984), and a reduced capacity to generate isometric force (Davies and White, 1981; Friden et al., 1983; Hough, 1902; McCully and Faulkner, 1985), have been reported. Of all these indirect measures, reduced capacity to develop maximum isometric force can be measured immediately following contraction-induced damage and appears to provide the most reliable and quantitative measure of the magnitude of damage (McCully and Faulkner, 1985).

Factors resulting in contraction-induced injury

During physical activities, skeletal muscles develop active force in three modes of contractions: shortening, isometric, and lengthening (Faulkner, 2003). Of these three types of contractions, only lengthening contractions result in contraction-induced damage (McCully and Faulkner, 1985). The injury develops in two stages: a first stage that consists of an initial injury immediately after the lengthening contraction, and a second stage that develops during a 24–72 hour period following the occurrence of the initial injury (Armstrong et al., 1983; Faulkner et al., 1989; Jones et al., 1986; McCully and Faulkner, 1985; McCully and Faulkner, 1986). Electron micrographs of contraction-induced injury also confirm the chronology by showing that the damage to muscle fibers is localized to specific areas initially and, with time, becomes more diffuse and generalized (Friden et al., 1983; Newham et al., 1983b).

Factors resulting in the initial injury

Several factors have been proposed as causes of the initial injury including, metabolic (Lieber et al., 1991; West-Jordan et al., 1991), chemical (Duan et al., 1990; Duncan, 1987; Jones et al., 1984), and mechanical (Brooks et al., 1995; Macpherson et al., 1996; McCully and Faulkner, 1986; Newham et al., 1983b; Warren et al., 1993b; Warren et al., 1993a). Decreased levels of metabolic factors such as ATP (Lieber et al., 1991; West-Jordan et al., 1991) and decreased intracellular pH (West-Jordan et al., 1991) were proposed to initiate a sequence of events that then lead to the initial injury. The metabolic cost of lengthening contractions is low compared with the energy cost during other types of contractions (Curtin and Davies, 1973). The lower metabolic cost of

lengthening contractions is not consistent with the view that injury due to lengthening contractions has a metabolic origin.

The primary chemical factor implicated in the initial injury is intracellular calcium (Duan et al., 1990; Duncan, 1987; Duncan and Jackson, 1987; Wrogemann and Pena, 1976). Some experimental results have suggested that the ultrastructural damage during muscle contractions might occur due to a net influx of calcium (Jackson et al., 1984; Jackson et al., 1987; Jones et al., 1984), moving down the large electrochemical gradient, which then activates calcium mediated degradative pathways (Armstrong, 1990; Jackson, 1993). Although muscles that underwent lengthening contractions showed an increase in intracellular [Ca^{2+}], injured muscles appear to buffer the extra calcium (Lowe et al., 1994). If increased intracellular [Ca^{2+}] is the cause of contraction-induced damage, permeabilized single muscle fibers that, by definition, lack an intact cell membrane, should undergo contraction-induced damage irrespective of the mode of contraction, whereas, permeabilized single fibers are damaged only during a lengthening contraction (Macpherson et al., 1996; Macpherson et al., 1997). Thus, chemical factors are not likely to cause the initial injury.

Mechanical factors

A number of investigators have proposed that the initial mechanism of contraction-induced injury is a mechanical event (Brooks et al., 1995; Macpherson et al., 1996; Morgan, 1990; Talbot and Morgan, 1998; Warren et al., 1993a; Wood et al., 1993). Following protocols of repeated lengthening contractions of whole muscles, the force deficits measured immediately afterwards correlated with one or more of: (i) the peak force during the initial lengthening contraction (McCully and Faulkner, 1986; Warren et

al., 1993a), (ii) the magnitude of strain during each lengthening contraction (Lieber and Friden, 1993; Talbot and Morgan, 1998), and (iii) the muscle length at which the lengthening contractions were initiated (Talbot and Morgan, 1998). When activated muscles were injured by a single stretch protocol, where fatigue effects are absent, Brooks et al. (Brooks et al., 1995) showed that the mechanical work done to stretch the muscles was the best predictor of the force deficit. These studies strongly support the mechanical nature of the initial event in contraction-induced injury.

Underlying mechanisms of initial mechanical injury

The descriptions of injury at the ultrastructural level vary widely from loss of thick and thin filament overlap to complete disruption of the sarcomeres (see 'Direct evidence of injury'; Fig. 1.2). While the evidence suggested that the initial events resulting in injury were mechanical, the precise structures within the sarcomeres that were most susceptible to damage have not been established conclusively. Despite the lack of specific details as to which sarcomeric structures were the most susceptible to damage, the focal nature of the sarcomere disruption suggested that some sarcomeres within the volume of the muscle are more susceptible to contraction-induced damage than the others.

Non-uniformities within single fibers

The concept of non-uniform distribution of the contractile material within a single muscle fiber was first proposed by Hill (Hill, 1953). He proposed that a single muscle fiber, with a length hundreds of times greater than its diameter, would not likely develop a uniform strength along its entire length. This concept of non-uniform strength was

expanded further by Abbott et al. (Abbott and Aubert, 1952) who suggested that the stronger regions have greater resistance to stretch compared with the weaker regions. These early investigations considered the possibility of regional variations within a single fiber, even before the sarcomere was recognized as the basic functional unit within single fibers. After the sliding filament theory of muscle contraction was proposed (Huxley, 1957; Huxley and Hanson, 1954), Huxley and Peachey (Huxley and Peachey, 1961) showed that the lengths of sarcomeres (L_s) along a given fiber are not uniform. Subsequently, non-uniform distribution of L_s was reported in resting intact single fibers (Burton et al., 1989; Huxley and Peachey, 1961; Julian and Morgan, 1979), mechanically skinned fibers (Hellam and Podolsky, 1969; Julian and Moss, 1980), and segments of chemically permeabilized single fibers (Julian and Moss, 1980; Macpherson et al., 1997; Schoenberg and Podolsky, 1972). Since the force generated by a sarcomere (Fig. 1.3) varies with its length (Gordon et al., 1966; Stephenson and Williams, 1982), the non-uniformity in L_s has important implications during lengthening contractions of single fibers.

Sarcomere length non-uniformities during lengthening contractions

When passive fibers with non-uniform L_s along the length are activated maximally, stronger sarcomeres shorten at the expense of weaker sarcomeres (Hill, 1953). Consequently, the non-uniformity in L_s of a single fiber is increased during a maximal activation compared with the resting condition (Burton et al., 1989; Julian et al., 1978; Julian and Morgan, 1979; Julian and Moss, 1980). When maximally activated fibers are subsequently stretched, longer sarcomeres are lengthened by neighboring sarcomeres that are at shorter lengths (Edman et al., 1981; Julian and Morgan, 1979;

Lombardi and Piazzesi, 1990). Based on these observations Morgan (Morgan, 1990) proposed a model that describes non-uniform behavior of sarcomeres during a lengthening contraction. To explain the force responses during stretches of maximally activated fibers, Morgan hypothesized that some sarcomeres undergo extreme elongation at undamped and uncontrolled rates until overlap of thick and thin filaments is lost. Despite the attractiveness of this hypothesis in explaining the focal contraction-induced damage, the uncontrolled elongation of sarcomeres has not been observed directly.

Excessive lengthening can damage the sarcomeres

Experiments on passive intact single fibers showed that when sarcomeres were stretched to lengths consistent with the loss of thick and thin filament overlap, significant deficits in the force were produced (Higuchi et al., 1988). In contrast, when fibers were stretched to shorter lengths where filament overlap was still maintained, there was no evidence of damage. Electron microscopic evaluations of the fibers that were stretched to loss of filament overlap showed that thin filaments did not reenter the thick filament complex properly (Trombitas et al., 1993). In addition, when skinned single fibers were stretched beyond loss of filament overlap, the titin molecules were pulled from their attachment sites on the thick filaments (Wang et al., 1993). Titin is a giant molecule that spans the half-sarcomere, connecting A-bands to I-bands and Z-lines (Furst et al., 1988; Maruyama et al., 1985), and is the primary contributor to the passive tension produced in single fibers (Magid and Law, 1985; Prado et al., 2005). These results suggest that during lengthening contractions, any sarcomeres that are stretched to lengths consistent with the loss of filament overlap will have impairments of both the passive elastic and contractile properties of the sarcomeres.

Electron microscopic evaluations

Brown and Hill (Brown and Hill, 1991) stretched maximally activated intact single fibers, held them at the longer lengths, and then fixed them rapidly while still activated. Electron micrographs obtained from these fixed samples showed the loss of thick and thin filament overlap and Z-line streaming, and to a lesser degree, the formation of gaps in the A-bands. Although this evidence seems to support Morgan's theory, the interpretations must be viewed cautiously as all sarcomeres in the electron micrographs appear to have been extended. If a few sarcomeres elongated uncontrollably, as predicted by Morgan, then the remaining intact sarcomeres were not expected to lengthen significantly, whereas, the intact sarcomeres were also lengthened. Another limitation of this study is that no quantitative analysis was done to show if the applied fiber strain was balanced with the observed sarcomere strain.

To overcome the limitations of the earlier study by Brown and Hill (Brown and Hill, 1991), Talbot and Morgan (Talbot and Morgan, 1996) stretched activated muscles from toads and fixed them rapidly without allowing the muscles to relax. Subsequently, in the electron micrographs of these fixed muscles, the investigators showed some over-stretched half-sarcomeres. Also, using these electron micrographs, they computed the strain within the over-stretched and the intact half-sarcomeres and balanced the total observed strain with the applied strain. Although, these quantitative analyses of strain provided some support to Morgan's theory, since the analyses were done on electron micrographs of only a few sections of the muscle, the data are not convincing that the strains of each of the half-sarcomeres contained in the entire muscle were taken into account. Furthermore, the process of rapid fixation of muscles was not characterized to

assure that the observed disordering of the sarcomere structures was not due to fixation artifacts (Telley et al., 2006).

Regional differences in susceptibility to the initial injury

Using laser diffraction in permeabilized single fibers, Macpherson et al. (1997) measured mean L_s in five discrete regions, hereafter termed 'sectors,' along the fiber once during the maximal activation prior to a lengthening contraction and once after the fibers were returned to their original lengths following the lengthening contraction (Macpherson et al., 1997). Following the lengthening contraction that involved a 40% stretch of the fibers, the sarcomeres in sectors that were at longest mean L_s prior to the stretch, were estimated to have stretched the most. Fibers were subsequently relaxed and fixed for electron microscopic evaluations. In the electron micrographs, the sectors with longest pre-stretch L_s contained the largest number of focally damaged sarcomeres. Consequently, Macpherson's study provided indirect support for the hypothesis that contraction-induced injury is caused by groups of sarcomeres that are at longer lengths in activated fibers and are then stretched excessively, when compared with the serially connected sarcomeres at shorter lengths. The observation of sector-level differences in the susceptibility to contraction-induced injury provided the impetus to measure L_s during lengthening contractions of permeabilized single fibers in a spatially resolved fashion that constitutes the main measurement methodology in this dissertation.

Laser diffraction

Due to periodic variation in the protein density along the axis of single fibers, the single fiber can be approximated as a linear diffraction grating (Cleworth and Edman,

1972). The technique of laser diffraction has been used widely to assess mean L_s of sarcomeres contained in a small volume of the fiber illuminated by the laser (Cleworth and Edman, 1972; Kawai and Kuntz, 1973; Leung, 1983; Rudel and Zite-Ferenczy, 1979). The advantages of the laser diffraction technique are: (*i*) a superior signal-to-noise ratio and complete utilization of the dynamic range of the light detectors compared with direct optical imaging (Julian and Moss, 1980; Krueger and Denton, 1992; Myers et al., 1982; Roos et al., 1980), (*ii*) minimal optics and consequently the minimization of the effects of aberrations that pose significant challenges in optical imaging techniques, and (*iii*) the inexpensive availability of lasers and optical-to-electrical conversion systems.

Multiple-sector measurements of L_s with laser diffraction

Lieber et al. (Lieber et al., 1983) used laser diffraction for multiple-sector estimation of L_s in intact single fibers during fixed-end contractions. These investigators translated the fiber axially through a stationary laser beam during the rest periods between multiple tetani and obtained continuous records of L_s of multiple sectors of the contracting fiber. This measurement technique required a reproducible behavior of the sector-level L_s in order to reconstruct the sarcomere behavior from the multiple time-resolved records of L_s. This approach is not suitable for the studies of contraction-induced injury because lengthening contractions cause ultrastructural damage causing the diffraction properties of the sarcomere system to be permanently altered within a single contraction.

In contrast to Lieber's approach, Macpherson (Macpherson et al., 1997) measured L_s of five discrete sectors of a permeabilized single fiber within the same contraction by translating the laser beam from one sector to the other while the fiber remained

stationary. With Macpherson's approach, the time required for each set of five measurements was ~5 s. Such a long measurement time is suitable only when the fibers are in a steady state, but is not suitable for capturing the dynamic behavior of sarcomeres during a lengthening contraction. The ideal of rapid measurements of L_s of multiple sectors within single fibers has not been met before due to challenges involved in the development of suitable instrumentation. This dissertation addresses and resolves these problems in methodology associated with the rapid measurements.

Permeabilized single fibers

To date, permeabilized single fibers provide the best available preparation to test specific hypotheses related to the role of sarcomeres in contraction-induced injury. The conditions of pH, ATP, [Ca^{2+}], and the temperature at which the permeabilized single fibers are subjected to contraction-induced injury can be controlled precisely. Additionally with these preparations, the average characteristics of the contractile apparatus contained in small segment of a given fiber alone can be studied. As permeabilized single fibers lack continuous and intact membranes, the mechanical performance of these fibers is less stable than that of intact single fibers (Brenner, 1993; Chase and Kushmerick, 1988; Galler and Hilber, 1994; Hilber and Galler, 1998; Martyn and Gordon, 1992; Sweeney et al., 1987). Despite the increased instability of these fibers, stable sarcomere spacing and mechanical performance can be maintained for up to 10 min (Hilber and Galler, 1998).

Aims

The working hypothesis of the present study is that, during a lengthening contraction, the contraction-induced damage to sarcomeres is initiated when some susceptible sarcomeres undergo steady elongation at high rates to reach a strain that causes disruption in these sarcomeres. Based on the working hypothesis, we tested the following hypotheses in permeabilized single fibers from *soleus* muscles of adult male rats: (*i*) during the lengthening of maximally activated permeabilized single fibers, the sectors that contain longer sarcomeres during the preceding isometric activation period undergo more elongation than the regions that contain shorter sarcomeres; (*ii*) severe lengthening contractions increase the variability in L_s for passive fibers; and (*iii*) during the course of a severe lengthening contraction all the sectors of permeabilized single fibers exhibit stable lengthening behavior.

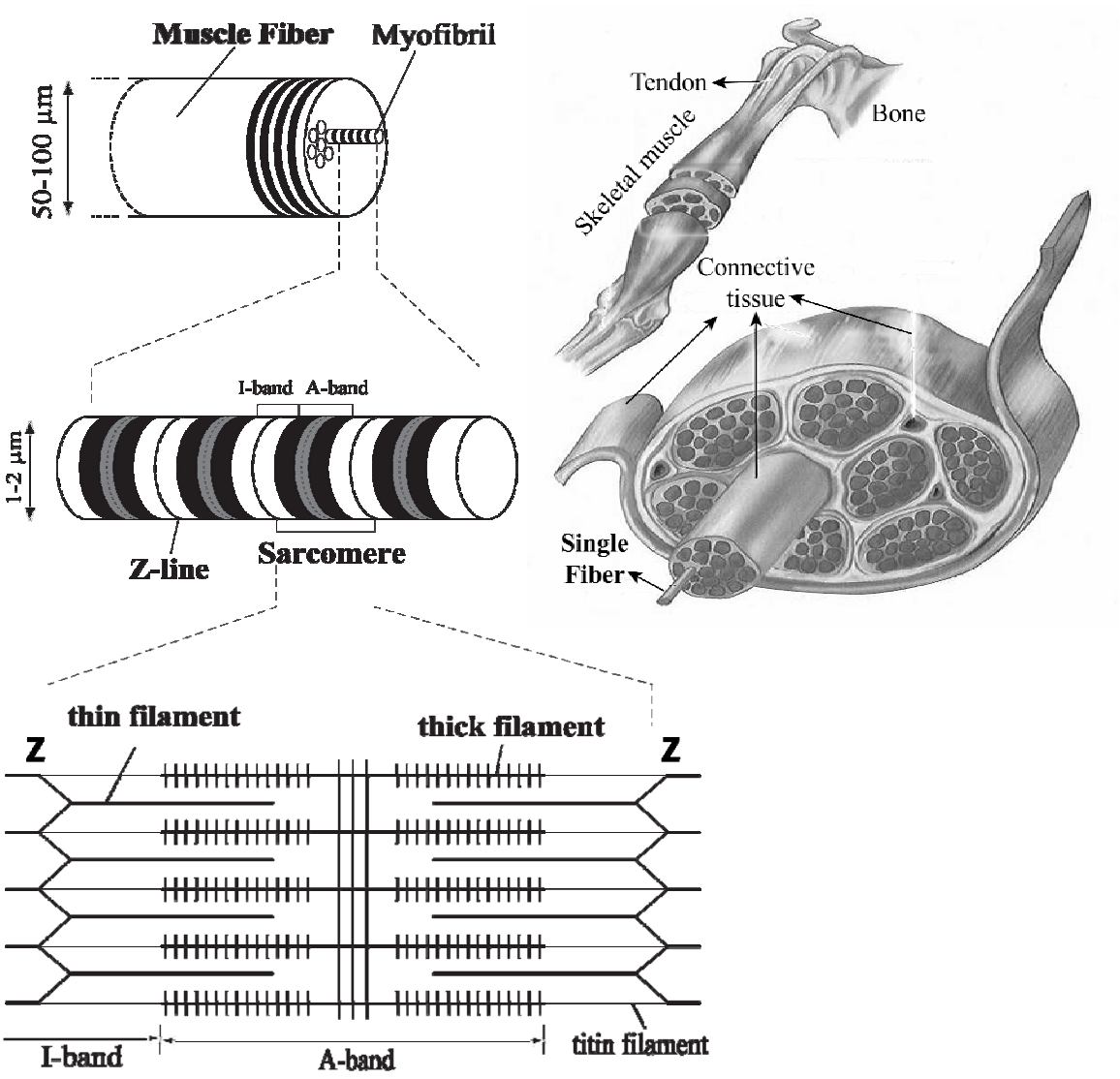

FIGURE 1.1: Hierarchical structure of skeletal muscle (not drawn to scale).

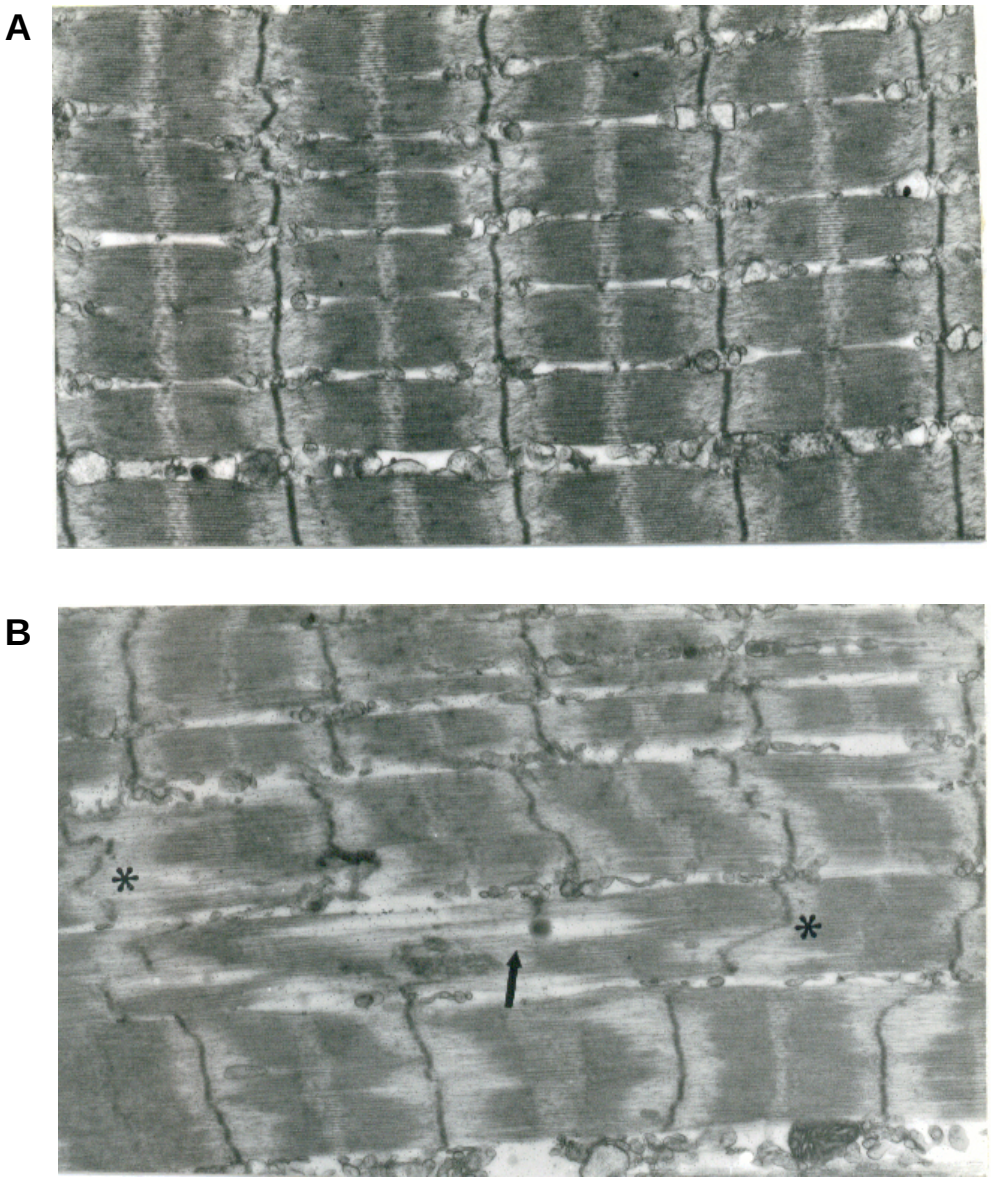

FIGURE 1.2: Electron micrographs of permeabilized single fibers from *soleus* muscles of rat before and after a single lengthening contraction of strain magnitude 40%. (*A*) A section of a relaxed fiber before the lengthening contraction showing series and parallel arrangement of sarcomeres. (*B*) Disrupted sarcomeres showing Z-line streaming (*), gaps in the A-bands (arrow), and misalignment of Z-lines. Source: Macpherson et al. 1996.

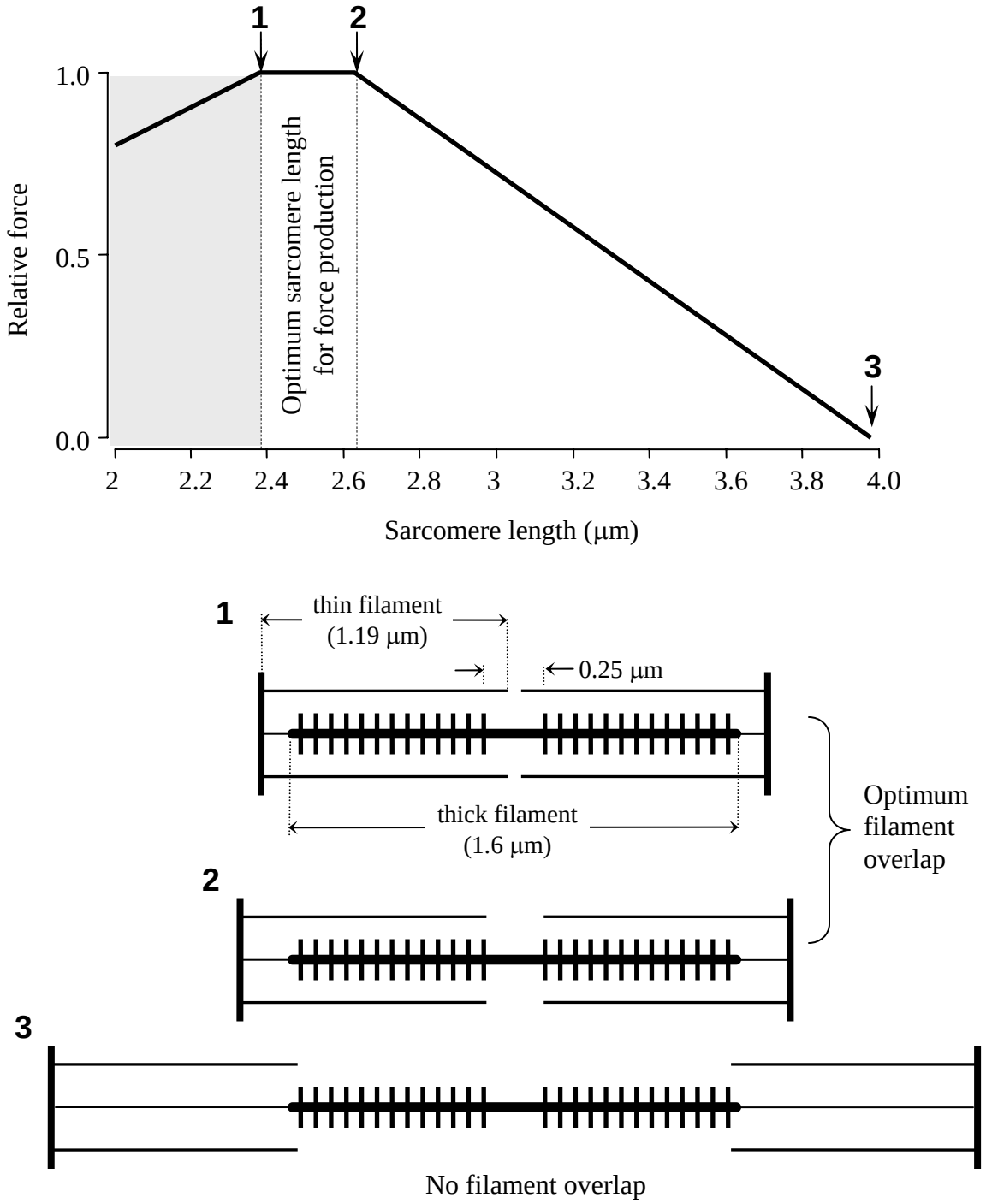

FIGURE 1.3: Sarcomere length-force relationship for *soleus* muscles of rat. The shaded region is not well characterized. Source: Stephenson et al. 1982.

References

Abbott, B. C. and X. M. Aubert. 1952. The force exerted by active striated muscle during and after change of length. *J Physiol* 117:77-86.

Armstrong, R. B. 1990. Initial events in exercise-induced muscular injury. *Med. Sci. Sports Exerc.* 22:429-435.

Armstrong, R. B., R. W. Ogilvie, and J. A. Schwane. 1983. Eccentric exercise-induced injury to rat skeletal muscle. *J Appl. Physiol* 54:80-93.

Asmussen, E. 1956. Observations on experimental muscular soreness. *Acta Rheumatol. Scand.* 2:109-116.

Brenner, B. 1993. Dynamic actin interaction of cross-bridges during force generation: implications for cross-bridge action in muscle. *Adv. Exp. Med. Biol.* 332:531-542.

Brooks, S. V., E. Zerba, and J. A. Faulkner. 1995. Injury to muscle fibres after single stretches of passive and maximally stimulated muscles in mice. *J. Physiol* 488:459-469.

Brown, L. M. and L. Hill. 1991. Some observations on variations in filament overlap in tetanized muscle fibres and fibres stretched during a tetanus, detected in the electron microscope after rapid fixation. *J. Muscle Res. Cell Motil.* 12:171-182.

Burton, K., W. N. Zagotta, and R. J. Baskin. 1989. Sarcomere-Length Behavior Along Single Frog-Muscle Fibers at Different Lengths During Isometric Tetani. *Journal of Muscle Research and Cell Motility* 10:67-84.

Chase, P. B. and M. J. Kushmerick. 1988. Effects of pH on contraction of rabbit fast and slow skeletal muscle fibers. *Biophys. J.* 53:935-946.

Cleworth, D. R. and K. A. Edman. 1972. Changes in sarcomere length during isometric tension development in frog skeletal muscle. *J Physiol* 227:1-17.

Curtin, N. A. and R. E. Davies. 1973. Chemical and Mechanical Changes During Stretching of Activated Frog Skeletal-Muscle. *Cold Spring Harbor Symposia on Quantitative Biology* 37:619-626.

Davies, C. T. and M. J. White. 1981. Muscle weakness following eccentric work in man. *Pflugers Arch.* 392:168-171.

Duan, C., M. D. Delp, D. A. Hayes, P. D. Delp, and R. B. Armstrong. 1990. Rat skeletal muscle mitochondrial [Ca2+] and injury from downhill walking. *J Appl. Physiol* 68:1241-1251.

Duncan, C. J. 1987. Role of calcium in triggering rapid ultrastructural damage in muscle: a study with chemically skinned fibres. *J Cell Sci.* 87 (Pt 4):581-594.

Duncan, C. J. and M. J. Jackson. 1987. Different mechanisms mediate structural changes and intracellular enzyme efflux following damage to skeletal muscle. *J Cell Sci.* 87:183-188.

Edman, K. A., G. Elzinga, and M. I. Noble. 1981. Critical sarcomere extension required to recruit a decaying component of extra force during stretch in tetanic contractions of frog skeletal muscle fibers. *J Gen. Physiol* 78:365-382.

Faulkner, J. A. 2003. Terminology for contractions of muscles during shortening, while isometric, and during lengthening. *J Appl. Physiol* 95:455-459.

Faulkner, J. A., S. V. Brooks, and J. A. Opiteck. 1993. Injury to skeletal muscle fibers during contractions: conditions of occurrence and prevention. *Phys. Ther.* 73:911-921.

Faulkner, J. A., S. V. Brooks, and E. Zerba. 1990. Skeletal muscle weakness and fatigue in old age: underlying mechanisms. *Annu. Rev. Gerontol. Geriatr.* 10:147-166.

Faulkner, J. A., D. A. Jones, and J. M. Round. 1989. Injury to skeletal muscles of mice by forced lengthening during contractions. *Q. J Exp. Physiol* 74:661-670.

Friden, J., M. Sjostrom, and B. Ekblom. 1983. Myofibrillar damage following intense eccentric exercise in man. *Int. J. Sports Med.* 4:170-176.

Furst, D. O., M. Osborn, R. Nave, and K. Weber. 1988. The organization of titin filaments in the half-sarcomere revealed by monoclonal antibodies in immunoelectron microscopy: a map of ten nonrepetitive epitopes starting at the Z line extends close to the M line. *J Cell Biol.* 106:1563-1572.

Galler, S. and K. Hilber. 1994. Unloaded shortening of skinned mammalian skeletal muscle fibres: effects of the experimental approach and passive force. *J. Muscle Res. Cell Motil.* 15:400-412.

Garrett, W. E., Jr. 1990. Muscle strain injuries: clinical and basic aspects. *Med. Sci. Sports Exerc.* 22:436-443.

Gordon, A. M., A. F. Huxley, and F. J. Julian. 1966. The variation in isometric tension with sarcomere length in vertebrate muscle fibres. *J. Physiol* 184:170-192.

Hellam, D. C. and R. J. Podolsky. 1969. Force measurements in skinned muscle fibres. *J Physiol* 200:807-819.

Higuchi, H., T. Yoshioka, and K. Maruyama. 1988. Positioning of actin filaments and tension generation in skinned muscle fibres released after stretch beyond overlap of the actin and myosin filaments. *J Muscle Res. Cell Motil.* 9:491-498.

Hilber, K. and S. Galler. 1998. Improvement of the measurements on skinned muscle fibres by fixation of the fibre ends with glutaraldehyde. *J. Muscle Res. Cell Motil.* 19:365-372.

Hill, A. V. 1953. The mechanics of active muscle. *Proc. R. Soc. Lond B Biol. Sci.* 141:104-117.

Hough, T. 1902. Ergographic studies in muscular soreness. *Am J Physiol* 7:76-92.

Huxley, A. F. 1957. Muscle structure and theories of contraction. *Prog. Biophys. Biophys. Chem.* 7:255-318.

Huxley, A. F. and L. D. Peachey. 1961. The maximum length for contraction in vertebrate straiated muscle. *J Physiol* 156:150-165.

Huxley, H. and J. Hanson. 1954. Changes in the cross-striations of muscle during contraction and stretch and their structural interpretation. *Nature* 173:973-976.

Jackson, M. J. 1993. Molecular mechanisms of muscle damage. *Mol. Cell Biol. Hum. Dis. Ser.* 3:257-282.

Jackson, M. J., D. A. Jones, and R. H. Edwards. 1984. Experimental skeletal muscle damage: the nature of the calcium-activated degenerative processes. *Eur. J Clin. Invest* 14:369-374.

Jackson, M. J., A. J. Wagenmakers, and R. H. Edwards. 1987. Effect of inhibitors of arachidonic acid metabolism on efflux of intracellular enzymes from skeletal muscle following experimental damage. *Biochem. J* 241:403-407.

Jones, D. A., M. J. Jackson, G. McPhail, and R. H. Edwards. 1984. Experimental mouse muscle damage: the importance of external calcium. *Clin. Sci. (Lond)* 66:317-322.

Jones, D. A., D. J. Newham, J. M. Round, and S. E. Tolfree. 1986. Experimental human muscle damage: morphological changes in relation to other indices of damage. *J Physiol* 375:435-448.

Julian, F. J. and D. L. Morgan. 1979. Intersarcomere dynamics during fixed-end tetanic contractions of frog muscle fibres. *J. Physiol* 293:365-378.

Julian, F. J. and R. L. Moss. 1980. Sarcomere length-tension relations of frog skinned muscle fibres at lengths above the optimum. *J. Physiol* 304:529-539.

Julian, F. J., M. R. Sollins, and R. L. Moss. 1978. Sarcomere length non-uniformity in relation to tetanic responses of stretched skeletal muscle fibres. *Proc. R. Soc. Lond B Biol. Sci.* 200:109-116.

Kawai, M. and I. D. Kuntz. 1973. Optical diffraction studies of muscle fibers. *Biophys. J* 13:857-876.

Komi, P. V. and E. R. Buskirk. 1972. Effect of eccentric and concentric muscle conditioning on tension and electrical activity of human muscle. *Ergonomics* 15:417-434.

Krueger, J. W. and A. Denton. 1992. High resolution measurement of striation patterns and sarcomere motions in cardiac muscle cells. *Biophys. J* 61:129-144.

Leung, A. F. 1983. Light diffractometry for determining the sarcomere length of striated muscle: an evaluation. *J. Muscle Res. Cell Motil.* 4:473-484.

Lieber, R. L. and J. Friden. 1993. Muscle damage is not a function of muscle force but active muscle strain. *J. Appl. Physiol* 74:520-526.

Lieber, R. L., K. P. Roos, B. A. Lubell, J. W. Cline, and R. J. Baskin. 1983. High-speed digital data acquisition of sarcomere length from isolated skeletal and cardiac muscle cells. *IEEE Trans. Biomed. Eng* 30:50-57.

Lieber, R. L., T. M. Woodburn, and J. Friden. 1991. Muscle damage induced by eccentric contractions of 25% strain. *J Appl. Physiol* 70:2498-2507.

Lombardi, V. and G. Piazzesi. 1990. The contractile response during steady lengthening of stimulated frog muscle fibres. *J. Physiol* 431:141-171.

Lowe, D. A., G. L. Warren, D. A. Hayes, M. A. Farmer, and R. B. Armstrong. 1994. Eccentric contraction-induced injury of mouse soleus muscle: effect of varying [Ca2+]. *J Appl. Physiol* 76:1445-1453.

Macpherson, P. C., R. G. Dennis, and J. A. Faulkner. 1997. Sarcomere dynamics and contraction-induced injury to maximally activated single muscle fibres from soleus muscles of rats. *J. Physiol* 500:523-533.

Macpherson, P. C., M. A. Schork, and J. A. Faulkner. 1996. Contraction-induced injury to single fiber segments from fast and slow muscles of rats by single stretches. *Am. J. Physiol* 271:C1438-C1446.

Magid, A. and D. J. Law. 1985. Myofibrils bear most of the resting tension in frog skeletal muscle. *Science* 230:1280-1282.

Martyn, D. A. and A. M. Gordon. 1992. Force and stiffness in glycerinated rabbit psoas fibers. Effects of calcium and elevated phosphate. *J. Gen. Physiol* 99:795-816.

Maruyama, K., T. Yoshioka, H. Higuchi, K. Ohashi, S. Kimura, and R. Natori. 1985. Connectin filaments link thick filaments and Z lines in frog skeletal muscle as revealed by immunoelectron microscopy. *J Cell Biol.* 101:2167-2172.

McCully, K. K. and J. A. Faulkner. 1985. Injury to skeletal muscle fibers of mice following lengthening contractions. *J. Appl. Physiol* 59:119-126.

McCully, K. K. and J. A. Faulkner. 1986. Characteristics of lengthening contractions associated with injury to skeletal muscle fibers. *J. Appl. Physiol* 61:293-299.

Morgan, D. L. 1990. New insights into the behavior of muscle during active lengthening. *Biophys. J.* 57:209-221.

Myers, J., R. Tirosh, R. C. Jacobson, and G. H. Pollack. 1982. Phase-locked loop measurement of sarcomere length with high time resolution. *IEEE Trans. Biomed. Eng* 29:463-466.

Newham, D. J., D. A. Jones, and R. H. Edwards. 1983a. Large delayed plasma creatine kinase changes after stepping exercise. *Muscle Nerve* 6:380-385.

Newham, D. J., G. McPhail, K. R. Mills, and R. H. Edwards. 1983b. Ultrastructural changes after concentric and eccentric contractions of human muscle. *J. Neurol. Sci.* 61:109-122.

Newham, D. J., K. R. Mills, B. M. Quigley, and R. H. Edwards. 1983c. Pain and fatigue after concentric and eccentric muscle contractions. *Clin. Sci. (Lond)* 64:55-62.

Ogilvie, R. W., R. B. Armstrong, K. E. Baird, and C. L. Bottoms. 1988. Lesions in the rat soleus muscle following eccentrically biased exercise. *Am J Anat.* 182:335-346.

Pope, A. M. and A. R. Tarlov. 1991. Disability in America: Toward a National Agenda for Prevention. National Academy Press.

Prado, L. G., I. Makarenko, C. Andresen, M. Kruger, C. A. Opitz, and W. A. Linke. 2005. Isoform diversity of giant proteins in relation to passive and active contractile properties of rabbit skeletal muscles. *J Gen. Physiol* 126:461-480.

Proske, U. and D. L. Morgan. 2001. Muscle damage from eccentric exercise: mechanism, mechanical signs, adaptation and clinical applications. *J. Physiol* 537:333-345.

Roos, K. P., R. J. Baskin, R. L. Lieber, J. W. Cline, and P. J. Paolini. 1980. Digital data acquisition and analysis of striated muscle diffraction patterns with a direct memory access microprocessor system. *Rev. Sci. Instrum.* 51:762-767.

Rudel, R. and F. Zite-Ferenczy. 1979. Interpretation of light diffraction by cross-striated muscle as Bragg reflexion of light by the lattice of contractile proteins. *J. Physiol* 290:317-330.

Sargeant, A. J. and P. Dolan. 1987. Human muscle function following prolonged eccentric exercise. *Eur. J Appl. Physiol Occup. Physiol* 56:704-711.

Schoenberg, M. and R. J. Podolsky. 1972. Length-force relation of calcium activated muscle fibers. *Science* 176:52-54.

Schwane, J. A., S. R. Johnson, C. B. Vandenakker, and R. B. Armstrong. 1983. Delayed-onset muscular soreness and plasma CPK and LDH activities after downhill running. *Med. Sci. Sports Exerc.* 15:51-56.

Stauber, W. T. 1989. Eccentric action of muscles: physiology, injury, and adaptation. *Exerc. Sport Sci. Rev.* 17:157-185.

Stephenson, D. G. and D. A. Williams. 1982. Effects of sarcomere length on the force-pCa relation in fast- and slow-twitch skinned muscle fibres from the rat. *J. Physiol* 333:637-653.

Sweeney, H. L., S. A. Corteselli, and M. J. Kushmerick. 1987. Measurements on permeabilized skeletal muscle fibers during continuous activation. *Am. J. Physiol* 252:C575-C580.

Talbot, J. A. and D. L. Morgan. 1996. Quantitative analysis of sarcomere non-uniformities in active muscle following a stretch. *J. Muscle Res. Cell Motil.* 17:261-268.

Talbot, J. A. and D. L. Morgan. 1998. The effects of stretch parameters on eccentric exercise-induced damage to toad skeletal muscle. *J. Muscle Res. Cell Motil.* 19:237-245.

Telley, I. A., R. Stehle, K. W. Ranatunga, G. Pfitzer, E. Stussi, and J. Denoth. 2006. Dynamic behaviour of half-sarcomeres during and after stretch in activated rabbit psoas myofibrils: sarcomere asymmetry but no 'sarcomere popping'. *J. Physiol* 573:173-185.

Trombitas, K., G. H. Pollack, J. Wright, and K. Wang. 1993. Elastic properties of titin filaments demonstrated using a "freeze-break" technique. *Cell Motil. Cytoskeleton* 24:274-283.

Wang, K., R. McCarter, J. Wright, J. Beverly, and R. Ramirez-Mitchell. 1993. Viscoelasticity of the sarcomere matrix of skeletal muscles. The titin-myosin composite filament is a dual-stage molecular spring. *Biophys. J* 64:1161-1177.

Warren, G. L., D. A. Hayes, D. A. Lowe, and R. B. Armstrong. 1993a. Mechanical factors in the initiation of eccentric contraction-induced injury in rat soleus muscle. *J. Physiol* 464:457-475.

Warren, G. L., D. A. Hayes, D. A. Lowe, B. M. Prior, and R. B. Armstrong. 1993b. Materials fatigue initiates eccentric contraction-induced injury in rat soleus muscle. *J Physiol* 464:477-489.

Warren, G. L., D. A. Lowe, and R. B. Armstrong. 1999. Measurement tools used in the study of eccentric contraction-induced injury. *Sports Med.* 27:43-59.

West-Jordan, J. A., P. A. Martin, R. J. Abraham, R. H. Edwards, and M. J. Jackson. 1991. Energy metabolism during damaging contractile activity in isolated skeletal muscle: a 31P-NMR study. *Clin. Chim. Acta* 203:119-134.

Wood, S. A., D. L. Morgan, and U. Proske. 1993. Effects of repeated eccentric contractions on structure and mechanical properties of toad sartorius muscle. *Am. J. Physiol* 265:C792-C800.

Wrogemann, K. and S. D. J. Pena. 1976. Mitochondrial Calcium Overload - General Mechanism for Cell Necrosis in Muscle Diseases. *Lancet* 1:672-674.

CHAPTER 2

MAGNITUDE OF SARCOMERE EXTENSION CORRELATES WITH INITIAL SARCOMERE LENGTH DURING LENGTHENING OF ACTIVATED SINGLE FIBERS FROM *SOLEUS* MUSCLE OF RATS

Introduction

Skeletal muscle is routinely subjected to three types of contractions: shortening, isometric (fixed-length), and lengthening (Faulkner, 2003). Of the three, only lengthening contractions are capable of producing muscle injury (McCully and Faulkner, 1985). Structural damage to muscle fibers is evident by electron microscopy immediately following stretches of maximally activated whole muscle groups (Newham et al., 1983; Friden et al., 1983; Ogilvie et al., 1988), whole muscles (Wood et al., 1993; Brooks et al., 1995; Talbot and Morgan, 1998), intact single fibers (Brown and Hill, 1991) and permeabilized single fibers (Macpherson et al., 1996). In each case, the damage is localized within single sarcomeres or small groups of sarcomeres that are distributed randomly among intact sarcomeres. The extent of the injury sustained during lengthening contractions of whole muscles (Brooks et al., 1995; Hunter and Faulkner, 1997; Talbot and Morgan, 1998) and segments of permeabilized single fibers (Macpherson et al., 1996) is effected by a combination of mechanical factors that include the initial length, the strain, the stress during the stretch, and the work done during the stretch.

While the gross mechanical factors that lead to injury have been identified, the underlying causative factors and events are described only through a theoretical model (Morgan, 1990). The model supports the premise that the injury is due to non-uniformity in sarcomere lengths (L_s) and predicts that during a lengthening contraction some sarcomeres at longer lengths are stretched beyond filament overlap, whereas shorter sarcomeres are strained, but maintain some filament overlap. Some support exists for the relationship between L_s heterogeneity and the magnitude of injury (Patel et al., 2004). Although L_s heterogeneity has been implicated as the leading cause of excessive stretch and subsequent damage to localized groups of sarcomeres during lengthening contractions, this hypothesis has not been supported by definitive evidence.

Macpherson et al. (Macpherson et al., 1997) used laser diffraction to measure L_s sequentially in five discrete locations along permeabilized single fibers to demonstrate that regions of an activated fiber containing the longest sarcomeres prior to stretch showed the highest number of over-stretched and disrupted sarcomeres as observed in electron micrographs obtained after the fibers were returned to their original length, a finding consistent with the sarcomere non-uniformity hypothesis. They also reported that, after the activated fibers were returned to original length following the stretch, the sarcomeres in the injured regions were estimated to be at longer lengths than they were prior to the stretch. Since they did not measure L_s of the activated fibers at the peak of the stretch, it is not clear that the L_s prior to the stretch had any influence on the strain of a region during the stretch. The purpose of the present investigation was to test the hypothesis that during lengthening of maximally activated permeabilized fibers, regions that contain longer sarcomeres during the preceding isometric activation period undergo

more stretch than the regions containing shorter sarcomeres. Testing this hypothesis required simultaneous measurement of lengths of all serially-connected groups of sarcomeres during stretches of activated fibers. We developed a technique that approximates this ideal by measuring the L_s within 20 contiguous sections of a fiber during stretches within 2 ms.

Materials and methods

Permeabilized single fiber preparation

Adult male rats (n = 5; age 6–10 months) were anaesthetized with an intraperitoneal injection of sodium pentobarbitone (50 mg kg^{-1}) with supplemental doses administered as needed to prevent response to tactile stimuli. The *soleus* muscles were exposed and the proximal and distal tendons were isolated. The tendons were cut and both muscles removed from the hindlimb. The muscles were placed immediately in cold (~4°C) skinning solution (see 'solutions,' below). After the muscles were removed, the rats were euthanized with an overdose of sodium pentobarbitone (100 mg kg^{-1}) and a bilateral pneumothorax procedure was performed. All experimental procedures were approved by the University of Michigan Committee on the Use and Care of Animals and in accordance with the *Guide for the Care and Use of Laboratory Animals* [DHHS Publication No. 85–23 (NIH), Revised 1985, Office of Science and Health Reports, Bethesda, MD 20892]. Bundles of fibers approximately 5 mm in length and 1–2 mm in diameter were dissected from the *soleus* muscles. Following dissection, bundles were immersed for 30 minutes in skinning solution to which the non-ionic detergent Brij 58 was added (0.5% w/v). Fiber bundles were subsequently placed in storage solution and

maintained for 24 hrs at 4°C before being stored at –20°C for periods of up to 4 months for use.

Experimental apparatus

Permeabilized single fibers were mounted on two short lengths of 29-gauge (OD = 330 μm) stainless-steel thin-wall tubing in a fluid exchange bath (1.1H × 0.6W × 0.5D cm) containing relaxation solution maintained at 15°C (Fig. 2.1). One length of tubing was attached to a force transducer (Model 403A, Aurora Scientific, Inc.) and the other was attached to the lever arm of a servomotor (Model 322C, Aurora Scientific, Inc.). To begin an experiment, a bundle of fibers was removed from the storage solution and placed in relaxing solution for 25 min at 4°C. With dark-field illumination and a dissecting microscope, permeabilized single fiber segments ("fibers") were pulled from the bundle with fine forceps. Isolated fibers were transferred to the bath and the ends of the fibers secured to the tubing with two 10-0 monofilament nylon suture ties. A typical preparation is shown in Fig. 2.1 *B*, with only the innermost two of the four sutures within the image frame. Approximate resting L_s was determined through projection of the laser diffraction pattern produced by the middle section of the fiber onto a calibrated target screen. The fiber length was then adjusted to obtain the desired L_s by translating the servomotor using a micrometer drive. Fiber length (L_f) was defined as the length between the innermost ties when mean L_s was 2.5 μm (Fig. 2.1 *B*). The length of the fiber being probed optically (L_{op}) was obtained by measuring from the end of the force transducer tubing to the end of the servomotor tubing and then subtracting the width of the laser spot (Fig. 2.1 *B*). The cross-sectional area (CSA) of fibers was measured as described later in

this section and the force measurements were normalized by the CSA to obtain stress (kN m^{-2}).

The bathing solution was changed using a fluid exchange system. Fluid from the bath was emptied in ~700 ms by opening a solenoid valve to a vacuum line. Fresh solution was delivered to the chamber by a syringe pump at the rate of 0.3 ml s^{-1}. The process of exchanging the fluid was computer-controlled and took approximately 2 s. Bath temperature was maintained at 15°C using feedback-controlled Peltier devices. Relaxed single fibers were activated by first soaking them in a low-[Ca^{2+}] pre-activating solution for 3 min and then exposing them to high-[Ca^{2+}] activating solution. The pre-activating solution was weakly-buffered for Ca^{2+}, allowing very rapid activation and force development upon introduction of the activating solution (Moisescu and Thieleczek, 1978).

Solutions

The skinning solution was composed of (mM): K-propionate, 125; imidazole, 20; EGTA, 5; $MgCl_2$, 2; ATP, 2; maintained at a pH of ~7.0 and storage solution: K-propionate, 125; imidazole, 20; EGTA, 5; $MgCl_2$, 2; ATP, 2; glycerol, 50% (v/v); maintained at a pH of ~7.0. The relaxing solution (pCa ~9.0) was composed of (mM): HEPES, 90; Mg (total), 10.3; Mg^{2+}, 1.0; EGTA, 50; ATP, 8.0; CrP, 10.0; NaN_3, 1.0; Na (total), 36; K (total), 125; pH 7.1. The pre-activating solution was composed of (mM): HEPES, 90; Mg (total), 8.50; Mg^{2+}, 1.0; EGTA, 0.10; HDTA, 50; ATP, 8.0; CrP, 10.0; NaN_3, 1.0; Na (total), 36; K (total), 125; pH 7.1. The activating solution (pCa ~4.5) contained (mM): HEPES, 90; Mg (total), 8.12; Mg^{2+}, 1.0; EGTA, 50; Ca^{2+} (total), 50; ATP, 8.0; CrP, 10.0; NaN_3, 1.0; Na (total), 36; K (total), 125; pH 7.1.

L_s measurements

L_s measurements were made from the diffraction patterns that resulted from trans-illumination of a small volume of the fiber with a laser beam having e^{-2} beam width of ~180 μm (based on Gaussian intensity distribution, ~66% of the laser intensity was concentrated in the central 90 μm; ~35 sarcomeres in series). A diode laser operating at a wavelength of 650 nm was used. Translation of the laser spot was accomplished with a slow shear wave TeO_2 acousto-optic beam deflector (AOBD; Model N45070-6, NEOS Technologies, Inc.), driven by a digital RF synthesizer oscillator (Model N640410-200-2ASDFS, NEOS Technologies, Inc.). The resulting diffraction patterns were captured with a 2048-element charge-coupled device linear array sensor (Model LD3543PGK, Perkin Elmer Optoelectronics, Inc.) and a frame grabber (Model PCI-1428, National Instruments, Corp.). A complete interrogation of the length of the fiber segment (L_{op}) was accomplished by translating the laser beam through 20 contiguous spots, hereafter referred to as 'sectors,' and scanning the diffraction patterns on the sensor that were produced by each sector. A complete readout from the sensor, referred to as a 'scan,' was a sequence of 2048 unsigned 8-bit integers that represented the intensity profile of the diffraction pattern. At each sector on the fiber, the laser spot was locked for 100 μs and one scan of the diffraction pattern was acquired. Thus the time taken to complete one full cycle of 20 scans, hereafter referred to as a 'sweep,' was 2 ms. For a given contraction protocol, servomotor and AOBD command arrays were pre-calculated and stored in the computer. Command arrays were updated to the respective instruments at a rate of 10 k updates s^{-1}. All inputs and outputs were gated by a single trigger pulse generated simultaneously on several trigger lines on a real-time system integration bus. The

diffraction, servo and force data were captured simultaneously at 10 k s^{-1} and stored by computer. A custom LabVIEW™ (National Instruments, Corp.) program controlled the instruments and acquired and saved the data.

The diffraction data from one full sweep of a fiber (a matrix of 20 × 2048 elements) is shown in Fig. 2.2 *A* as a grayscale image. Each scan was pre-processed with a low-pass filter and folded along the centroid of the zero-order (0°) intensity profile (Fig. 2.2). The intensity profiles of the two first-orders (–1° and +1°), thus falling on each other, were averaged to obtain the mean first-order (1°) profile. At any time point, L_s for a given sector was calculated based on the distance between the peak locations of 0° and 1° profiles, by using the standard grating equation, $\lambda = L_s \cdot sin\theta$, where θ is the diffraction angle between the undiffracted (0°) and the diffracted (1°) beams and λ is the wavelength of the laser. Both the +1° and –1° orders were used (by obtaining 1°) in the L_s calculation in order to minimize volume diffraction effects (Rudel and Zite-Ferenczy, 1979; Rudel and Zite-Ferenczy, 1980; Goldman and Simmons, 1984). The 1° peak locations were estimated using the centroid method (Kawai and Kuntz, 1973) given in the following equation:

$$\hat{p} = \frac{\sum_p I(p) \cdot p}{\sum_p I(p)} \tag{1}$$

where, $I(p)$ is intensity at pixel p and $\hat{p}$ is the centroid of the sequence I.

Determination of fiber cross-sectional area (CSA)

After adjusting L_s to ~2.5 μm, each fiber was imaged digitally from above and then from the side using a prism embedded in the chamber wall. Diameter pairs were measured from the images at 5 equally-spaced locations along the midsection of the fiber

with custom image-analysis software developed in Matlab™ (Mathworks, Inc.). CSA was calculated for each of the 5 locations based on the assumption of an elliptical fiber cross-section. Fiber CSA was calculated as the mean of the 5 individual measurements.

Sweeping

Sweeping was accomplished by generating a stair-step waveform of total amplitude proportional to the length of the sweep and using it as the input to the RF driver of the AOBD to translate the laser beam along the fiber in equally-spaced steps (Fig. 2.3). When the length of the fiber was changed the intervals were adjusted proportionally to ensure the entire L_{op} was interrogated. The stair-step waveforms were pre-calculated for a given fiber length change protocol and stored in the computer.

Experimental Protocol

Mean resting L_s was set to ~2.7 μm before the lengthening contraction protocol was initiated because the mean L_s within L_{op} shortens up to 6% during the isometric activation phase prior to the stretch. The resting L_s value was chosen to ensure that the stretches of the activated fibers occurred with mean L_s in the middle of the plateau region or early part of the descending limb (Close, 1972; Stephenson and Williams, 1982) of the length-tension relationship (see Discussion). Activated fibers (n = 22) were then lengthened by a single stretch of magnitude 0.27 L_f. The velocity of the stretch was 0.54 $L_f\ s^{-1}$ (Fig. 2.4 *A*). Following the stretch, the fibers were returned to the original length at the same speed. Immediately upon return to original length, the fibers were shortened rapidly (step shortening) by a length of 0.22 L_f and held for 40 ms. Fibers were then returned rapidly to their original lengths (step stretch) and allowed to generate maximum isometric force (Fig. 2.4). The step shortening-return maneuver was performed to

establish the true zero of the force transducer. Following the single activated stretch protocol the fibers were relaxed for 15 minutes and then activated again to measure the post-stretch isometric force. A typical stress response of a fiber to the single stretch protocol is shown in Fig. 2.4 *B*.

Force deficit measurements

Force deficit (Macpherson et al., 1996), the percentage reduction in peak isometric force (P_o) following stretch of an activated fiber, was calculated from the isometric force generated by a maximally activated single fiber before and after the single stretch protocol. Post-stretch force was measured twice, once during the first activation after a fiber was returned to its original length (Fig. 2.4) and once during a subsequent isometric activation, 15 min after the lengthening contraction. The force deficit was calculated using the mean value of the two post-stretch isometric force measurements.

Selection criteria

Diffraction patterns produced by the fibers during maximal isometric activation prior to stretch were visually inspected and fibers were rejected without replacement if the diffraction patterns were faint or diffuse. Fibers that had gross markers of damage at the end of the protocol (tears, etc.) were also rejected. During maximal isometric activation, compliant sectors at the ends of the fiber, near the attachment points (see Discussion) were identified using a rate-limiting filter and those sectors were eliminated from subsequent analyses. The rate-limiting filter algorithm assumed that the middle 10 sectors of the fiber were fully functional. The inclusion criterion for a new sector R on the right half of the fiber (sector numbers 16–20) was: L_s of R must be less than L_s of R − 1 + ½ × SD of L_s of all the accepted sectors. The algorithm continued to the right only if

sector R was included in the set of accepted sectors. Similarly, when including sectors in the left half of the fiber (sector numbers 5–1): sector R was accepted only if L_s of R was less than L_s of R + 1 + ½ × SD of L_s of all the accepted sectors. The algorithm proceeded to the left only if sector R was accepted. Sector selection within one half of the fiber was carried out independently from the other half and the final set of accepted sectors was obtained by the union of the sectors accepted in each half.

Statistical Analysis

To determine differences between relative stretch magnitudes at different pre-stretch L_s, the relative stretch magnitudes of sectors were grouped according to the pre-stretch L_s of the sector (Fig. 2.7 *B*), and then group means were assessed by a univariate one-way analysis of variance (ANOVA). If the *F*-statistic of the ANOVA showed significance, the differences were determined by Tukey's HSD *post hoc* tests for multiple comparisons. The level of significance was set *a priori* at $p < 0.05$. Linear regression models were used to determine the influence of pre-stretch L_s on stretch magnitude (Fig. 2.6) and relative stretch magnitude (Fig. 2.7 *A*), and strain on force deficit (Fig. 2.8). The correlation coefficient (r, Pearson's product moment) and the significance level of the correlation are presented.

Results

The lengths of the fibers were $L_f = 1.37 \pm 0.14$ (mean ± SD, n = 16) and $L_{op} = 1.05 \pm 0.11$ mm. The CSA was 6490 ± 1410 μm^2 (range = 4370–10210), P_o was 0.86 ± 0.17 mN, and stress was 135 ± 25 kN m^{-2}. For each fiber, the L_s for all sectors was computed from the diffraction patterns captured just prior to and at the peak of the

stretch. The rate-limiting filter described in 'Materials and Methods' was applied to the pre-stretch L_s profile to identify the functional sectors (Fig. 2.5). Of 320 sectors from the 16 fibers, 245 functional sectors were identified for further analyses; the remaining 75 sectors were excluded. The number of sectors retained for analyses varied among fibers (range = 11–20 sectors). For the accepted sectors (termed, collectively, the 'accepted segment') of each fiber we computed, 1) the mean pre-stretch L_s, 2) the increase in L_s for each sector, and 3) the mean increase in L_s. For the accepted segments, the mean pre-stretch L_s was 2.54 ± 0.12 μm (range = 2.33–2.73) and the mean increase in L_s ranged from 0.37 to 0.83 μm.

In general, non-uniform distribution of the stretch was observed along activated fibers, a finding consistent with previous reports (Julian and Morgan, 1979; Lombardi and Piazzesi, 1990; Macpherson et al., 1997; Panchangam et al., 2006). Fig. 2.6 *A* shows representative diffraction patterns of an activated fiber prior to and at the peak of the stretch. For the same fiber, Fig. 2.6 *B* is a plot of the increase in L_s against pre-stretch L_s for the sectors in the accepted segment, showing that sectors with pre-stretch L_s longer than the mean L_s underwent a greater increase in L_s than the mean (top-right quadrant). Similarly, sectors with shorter pre-stretch L_s underwent a smaller increase in L_s than the mean (bottom-left quadrant).

Fig. 2.7 *A* shows the relationship between the relative pre-stretch L_s, calculated as the ratio of pre-stretch sector L_s to the mean L_s of the accepted segment, and the relative increase in L_s of a sector, the ratio of the increase in sector L_s to the mean L_s increase for all sectors in the accepted segment. The figure was obtained by pooling the data from all accepted sectors of the 16 fibers (245 data points). The graph indicates that if a sector

was initially at a L_s longer than the mean, then it extended more than the mean during the stretch. Such sectors fall into the top-right quadrant of the graph. Similarly, the sectors in the bottom-left quadrant began with shorter pre-stretch L_s and stretched less than the mean stretch. For Fig. 2.7 *B* the relative increases in L_s for all 245 sectors were assigned to one of six groups according to the pre-stretch L_s values. The groups were distributed equally over a range of 2.25–2.85 μm with an interval of size 0.1 μm and the means and 95% confidence interval bars for the individual groups are shown. The group means correlated with the mid-interval value of the *x* axis ($r = 0.88$, $p = 0.02$). One-way ANOVA of the group means resulted in a significant *F*-statistic ($F = 8.31$). *Post hoc* multiple comparisons of mean values among the groups showed differences as indicated in Fig. 2.7 *B*. These tests revealed a biphasic relationship between pre-stretch L_s and relative increase in L_s, with the increase in L_s being independent of pre-stretch L_s in the range of 2.25–2.60 μm followed by an increasing trend for values of pre-stretch L_s greater than 2.60 μm. The pre-stretch L_s value at which the change in the trend of the relative increases in L_s occurred coincided approximately with the beginning of the descending limb of the length-tension relationship for *soleus* muscles of rats (Close, 1972; Stephenson and Williams, 1982) (Fig. 2.7 *B*).

Although the strain applied to all fibers during the active stretches was 27 % of L_f, the accepted segments of the fibers underwent varied magnitudes of sarcomere strain (range = 15.7–32.2 % of mean pre-stretch L_s). Furthermore, the force deficits observed in the present study varied among fibers, with a range of 7.0–33.5 $\%P_o$ (18.9 ± 8.9 $\%P_o$, mean ± SD). While the observed values for the force deficits were higher and more variable than the values reported previously for permeabilized single fibers of *soleus*

muscles of rats stretched at similar velocities (Macpherson et al., 1996), values for the force deficits correlated with the sarcomere strain in the accepted segments ($r = 0.82$, $p < 0.0001$, Fig. 2.8), an observation that is consistent with previous observations of permeabilized single fibers maximally activated and stretched (Macpherson et al., 1996).

Discussion

Uniqueness of the measurement technique

Testing the hypothesis that sarcomere extensibility increases with increasing L_s requires snapshots of the L_s of serially connected sectors of activated fibers before and at the peak of stretch. The laser diffraction technique has been used widely in L_s measurements and was selected for our study because this technique: (1) offers superior signal-to-noise ratio and complete utilization of the dynamic range of the detectors, when compared with direct optical imaging (Julian and Moss, 1980; Roos et al., 1980; Myers et al., 1982; Krueger and Denton, 1992), (2) requires minimal optics and consequently minimizes the effects of aberrations that pose significant challenges in optical imaging techniques, and (3) provides inexpensive availability of the light sources and optical-to-electrical conversion systems used in this technique. To test the hypothesis, we modified the measurement methodology of laser diffraction from a traditional single-point measurement to a multiple-point measurement approach by rapid translation of the laser beam. Multiple-point estimation of L_s has been made by Lieber et al. (Lieber et al., 1983) in intact single fibers by axially translating the fiber through a stationary laser beam during the rest periods between multiple tetani. The system described by Lieber et al. relied upon the repeatability of L_s behavior of a sector among multiple tetani and is not suitable for studying L_s behavior during protocols that cause irreversible changes.

Macpherson et al. (Macpherson et al., 1997) translated the laser beam along a stationary segment of permeabilized fiber to obtain spatially resolved L_s information within a single contraction, but the long measurement time (~5 s) required to make a complete set of L_s measurements rendered this technique unsuitable for our study. The requirement of near-simultaneous measurement of L_s of multiple sectors within single fibers has not been met before. We accomplished this by rapidly deflecting the laser beam to measure L_s along the full length of a permeabilized single fiber segment in 2 ms. Although the diffraction pattern for each sector was acquired sequentially, the short duration of acquisition approximated a snapshot of the L_s of the full fiber.

The laser sweeping used in this study proceeds along the fiber with uniform step sizes. The results, however, indicate that stretches were distributed non-uniformly along the fiber. This necessarily results in some sector mismatch. That is, a given sector number will not correspond to exactly the same sarcomere population from sweep to sweep. Analyses of the current data indicate that such mismatches were modest, averaging 18% for all sectors analyzed with only 1% of the sectors exceeding 50%. Furthermore, the spatial frequency content of the L_s profiles both before and at the peak of the stretch was very low (–3dB frequency < 0.07 cycles sector^{-1}), making any errors introduced by the contamination or loss of sarcomeres within a given sector insignificant.

Compliant end-sectors

In permeabilized single fiber preparations, the sectors near the ends tend to lengthen during maximal isometric activation due to increased compliance of the sub-functional sarcomeres that are compromised by the attachment procedure (Brenner, 1983; Chase and Kushmerick, 1988; Martyn and Gordon, 1992; Galler and Hilber, 1994; Hilber

and Galler, 1998). The increased end-compliance might be due to several factors. Visual inspection of the fiber preparations showed a noticeable change in aspect ratio of the fiber near the ends (Julian and Moss, 1980). Consequently, myofibrils passing through the curved boundaries near the end sectors are not parallel to the fiber axis. In these sectors, the component of the generated tension parallel to the fiber axis would be less than that in other sectors where the aspect ratio is preserved. The change in aspect ratio is also likely to indicate an altered myofilament lattice, contributing further to the reduced tension generation capability of those sectors. Due to this increased compliance at the ends, fully functional sectors in the middle of the fiber shorten at the expense of the end sectors, causing them to lengthen. Our data suggest that during maximal activation, the lengthening of sarcomeres near the attachment points can extend as far as 200 μm toward the fiber mid-point. Furthermore, the change in L_s from sub-functional segments to functional segments, as shown by our data, is gradual. Consequently, the simple criteria of shortening or lengthening of sarcomeres during maximal activation is not sufficient for identifying the boundary between functional and sub-functional sectors. Instead, the curvature of the relationship between sector number and L_s is a better indicator of this boundary. The rate-limiting filter described in 'Materials and Methods' identifies an increasing trend in L_s near the ends and determines the boundary between sub-functional and functional sectors in each half of the fiber.

A comparative study by Hilber and Galler (Hilber and Galler, 1998) on reliability of experiments using permeabilized single fibers with and without glutaraldehyde fixation of the fiber ends showed that results were comparable in the two preparation types only when the experimental duration was short. Fixing the ends with

glutaraldehyde improved the reliability and stability of the experiments that involved longer periods of activation. They also showed by simple visual observation that the laser diffraction patterns in activated preparations without glutaraldehyde fixation were less stable and deteriorated quickly with time. The activation times in our experimental protocols were ~20 s, much less than the periods of 3–30 min reported in the study of Hilber et al. The short activation times coupled with our acceptance criteria based on visual inspection of the quality of the laser diffraction patterns, ensured that the stability of the preparations used in the present study was not an issue.

Non-uniformity of stretch along the fiber

An activated stretch was not distributed uniformly among the sectors of a fiber; regions of the fiber with longer pre-stretch L_s absorbed a relatively higher proportion of the stretch. The negative slope of the descending limb of the length-tension relationship has been implicated in the development of L_s non-uniformities at longer lengths (Gordon et al., 1966a; Gordon et al., 1966b). According to theoretical models, when serially connected sarcomeres are stretched on the descending limb, the longest sarcomeres, being the weakest due to reduced opportunity for cross-bridge formation, are expected to stretch more than the shortest. With stretch, the opportunity for cross-bridge formation decreases further and, with this positive feedback, it has been proposed that the longest sarcomeres undergo a rapid and uncontrolled lengthening until the force is completely borne by passive elements (Morgan, 1990). While uncontrolled lengthening of sarcomeres cannot be observed with laser diffraction, our results generally support the idea that regions of a fiber with longer sarcomeres stretch more.

Relationship between strain and injury

Numerous studies in single fibers, including the present study, have shown the correlation between sarcomere strain and the magnitude of injury (Brooks et al., 1995; Brooks and Faulkner, 1996; Macpherson et al., 1996). The correlation between pre-stretch L_s and the magnitude of the injury has also been shown in single fibers and whole muscles (Newham et al., 1988; Lieber and Friden, 1993; Macpherson et al., 1997; Talbot and Morgan, 1998; Butterfield and Herzog, 2006). Despite these experimental observations, the connection between pre-stretch L_s and sarcomere strain have been drawn solely on a theoretical basis. The finding of greater numbers of disrupted sarcomeres in permeabilized single fiber sectors with the longest pre-stretch L_s (Macpherson et al., 1997) and of more severe injury following lengthening contractions initiated at longer muscle lengths (Talbot and Morgan, 1996; Talbot and Morgan, 1998) imply a relationship between pre-stretch L_s and injury via strain. Since the tension generation capability of sarcomeres decreases as they are extended beyond an optimum length, sarcomeres longer than optimum within a serially connected system are expected to become progressively weaker with stretch. Such sarcomeres are predicted to absorb a high proportion of the stretch imposed on the system. The results of our study support this prediction by direct observation and consequently provided a direct explanation for the observations of Macpherson et al. (Macpherson et al., 1997) and Talbot et al. (Talbot and Morgan, 1998).

Summary

We developed a technique to measure spatially resolved L_s rapidly along the lengths of segments of permeabilized single fibers and demonstrated that stretches of

activated fibers are distributed non-uniformly along the fiber length. We also observed that this non-uniformity during stretch is due to sectors with longer sarcomeres stretching more than sectors with shorter sarcomeres. These results support the hypothesis that injury induced by lengthening contractions is caused by groups of sarcomeres that are at longer lengths in activated fibers and are then stretched excessively when compared with their serially connected, shorter neighbors.

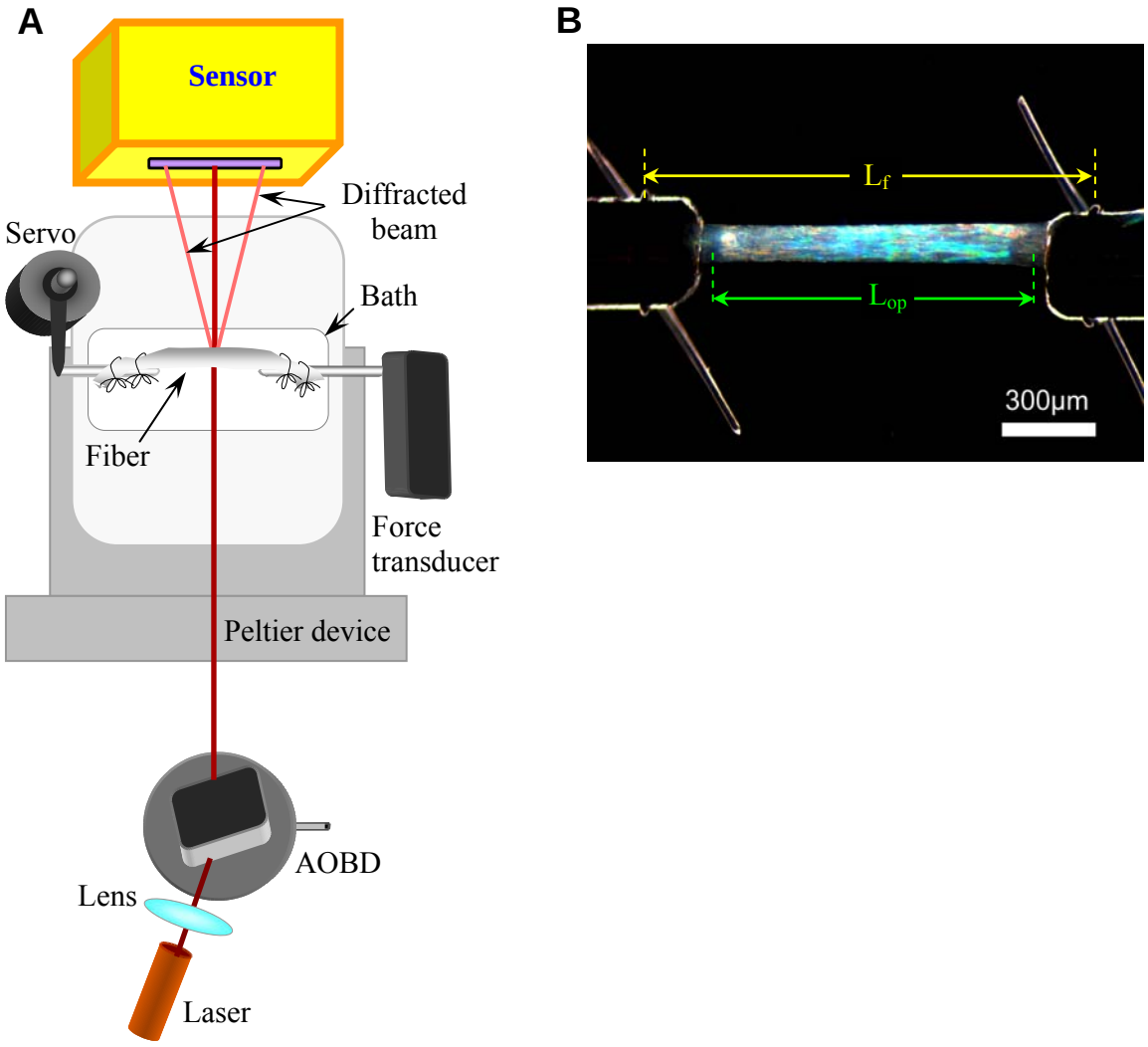

FIGURE 2.1: Experimental setup. (*A*) Schematic diagram of the experimental apparatus. (*B*) Top view of a sample fiber (under dark-field illumination) mounted in the bath showing only the two innermost ties. Force-producing length (L_f) and the investigation length (L_{op}) were measured as indicated in the figure with the L_s of a central section adjusted to ~2.5 µm.

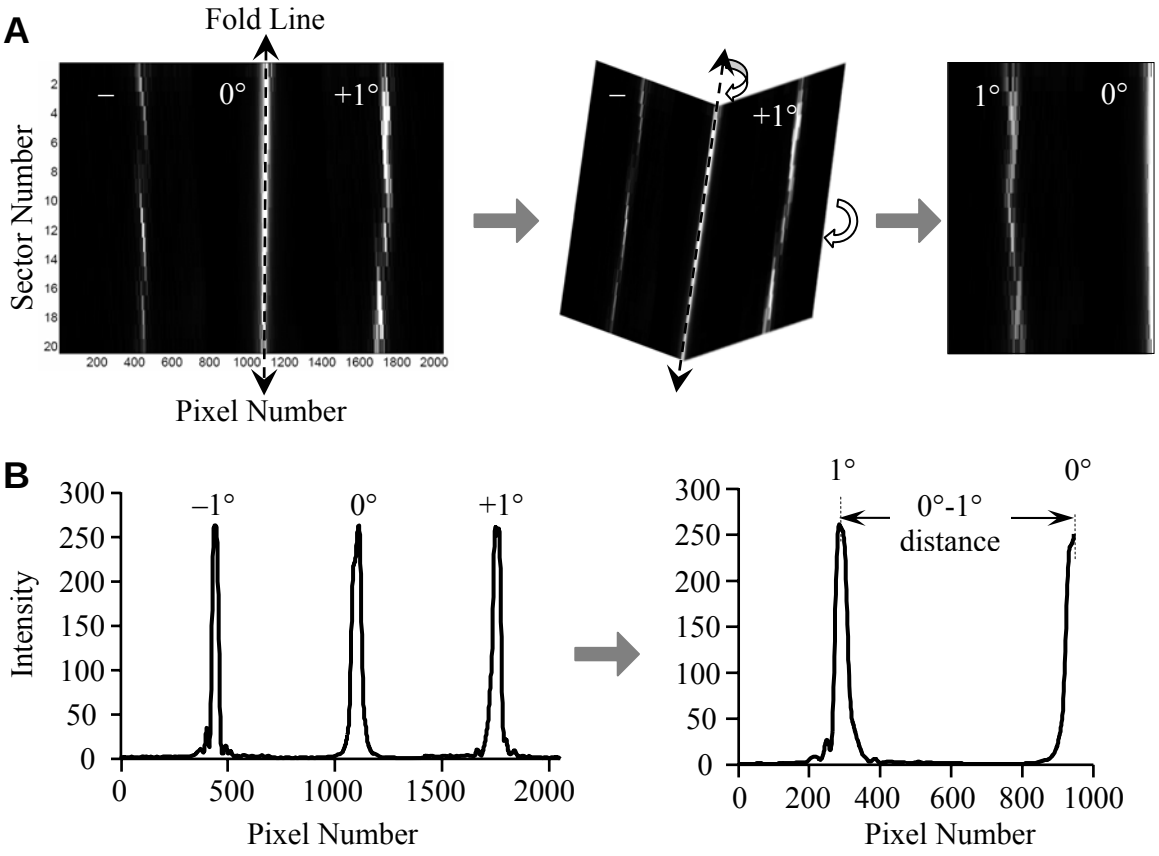

FIGURE 2.2: Method of determination of the diffraction angle. (*A*) Scheme for obtaining the 1° diffraction patterns from the –1° and +1°. The grayscale map (left) represents the diffraction data (all 20 scans) from a full sweep of the fiber. The *x* axis of the map represents the pixel number and the *y* axis, the sector number. The grayscale intensity of the image is proportional to the 8-bit intensity of the diffraction patterns (black, 0 to white, 255). The dashed line represents the fold line obtained by fitting a straight line to the centroids of the zero-order (0°) intensity profiles. (*B*) A typical 8-bit intensity profile (left) of the diffraction pattern corresponding to sector 10 of the grayscale map The intensity on the *y* axis is in arbitrary units (0–255). The intensity profile in the right panel corresponds to the 1° and left-half of the 0°. The distance between the 1° and 0° peak locations (separation in pixels × the pixel size) and the fiber-to-sensor distance were used to compute the diffraction angle.

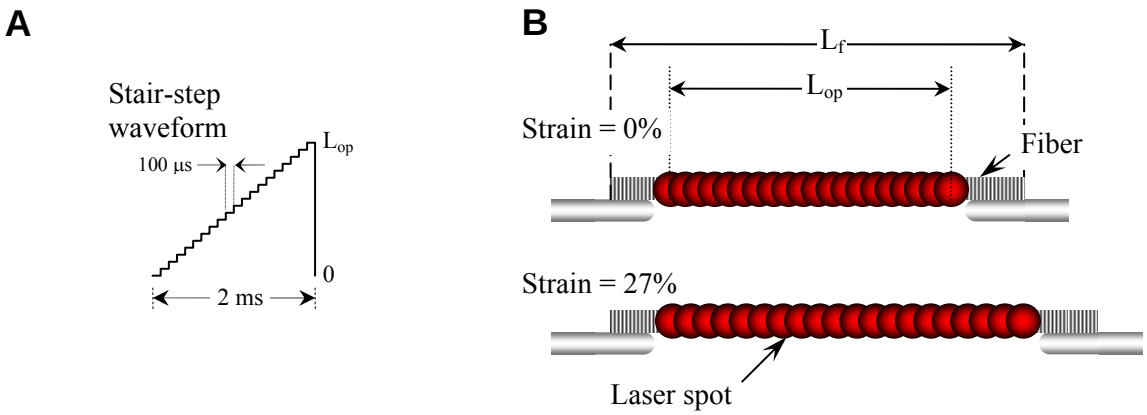

FIGURE 2.3: Translation of the laser beam during a sweep. (*A*) A typical stair-step waveform representing one complete sweep. The step height corresponds to the separation distance between the centers of two adjacent sectors and the step width to the duration of time that the laser spot was locked at the sector. (*B*) An illustration of the sweeping with overlapping laser spots. When fiber length was increased, the separation between the adjacent laser spots was increased such that the entire L_{op} span continued to be interrogated.

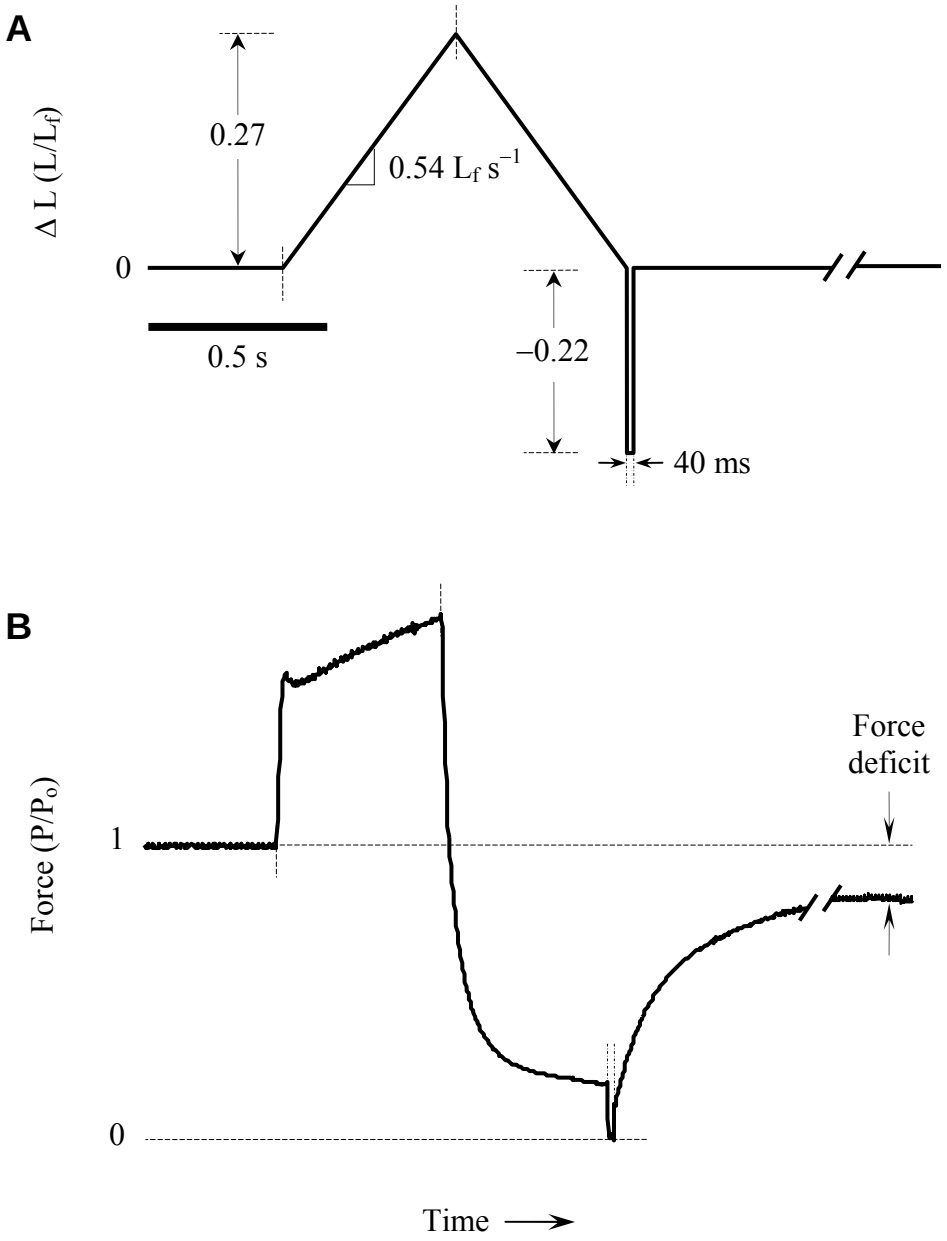

FIGURE 2.4: Experimental protocol. (*A*) Change in fiber length during the single stretch lengthening contraction protocol. Activated fibers were subjected to 27% stretch followed by shortening at constant speed. Immediately after the fibers were returned to original length a step - shortening and stretch maneuver was inserted to indicate the zero of the force transducer on the force record. (*B*) A typical force response of the fiber to the single stretch protocol on the same time scale as shown in panel *A*. At the peak of the stretch, the fiber stress increased by ~2-fold. The zero of the force transducer was established during the 40 ms hold following the step-shortening of the fiber. Following the stretch, steady-state isometric stress was reassessed and used in force deficit calculations.

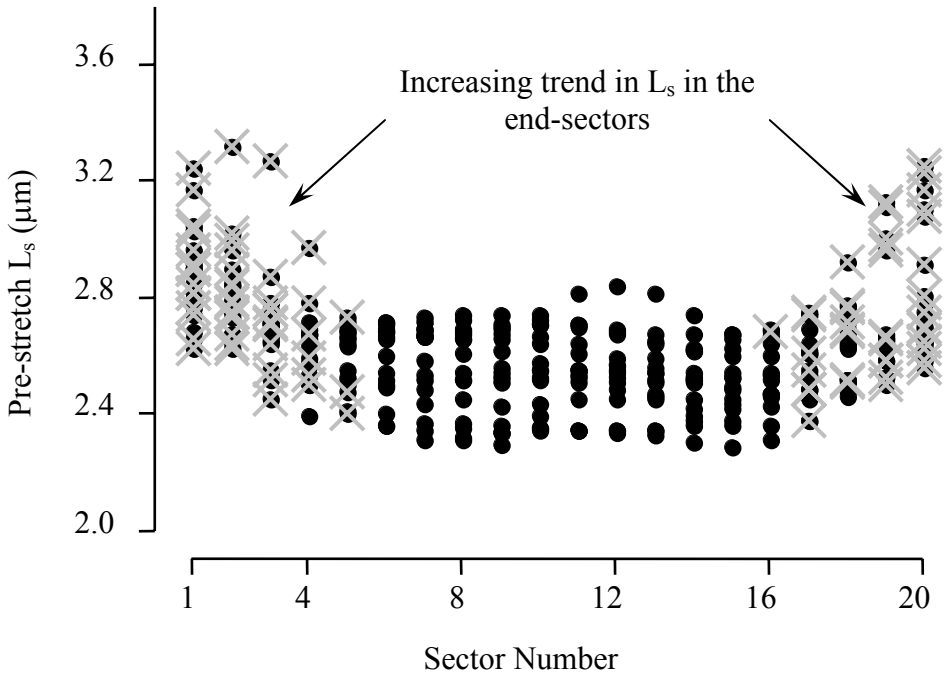

FIGURE 2.5: Sector exclusion map. The rate-limiting filter was applied to the pre-stretch L_s profiles (●) of each fiber. The data shown in the figure corresponds to all 320 sectors from the 16 fibers used in the study. Using the rate-limiting filter, a total of 75 sectors were identified as sub-functional and were eliminated (⊗) from subsequent analyses. Note the increasing trend in pre-stretch L_s near the end-sectors.

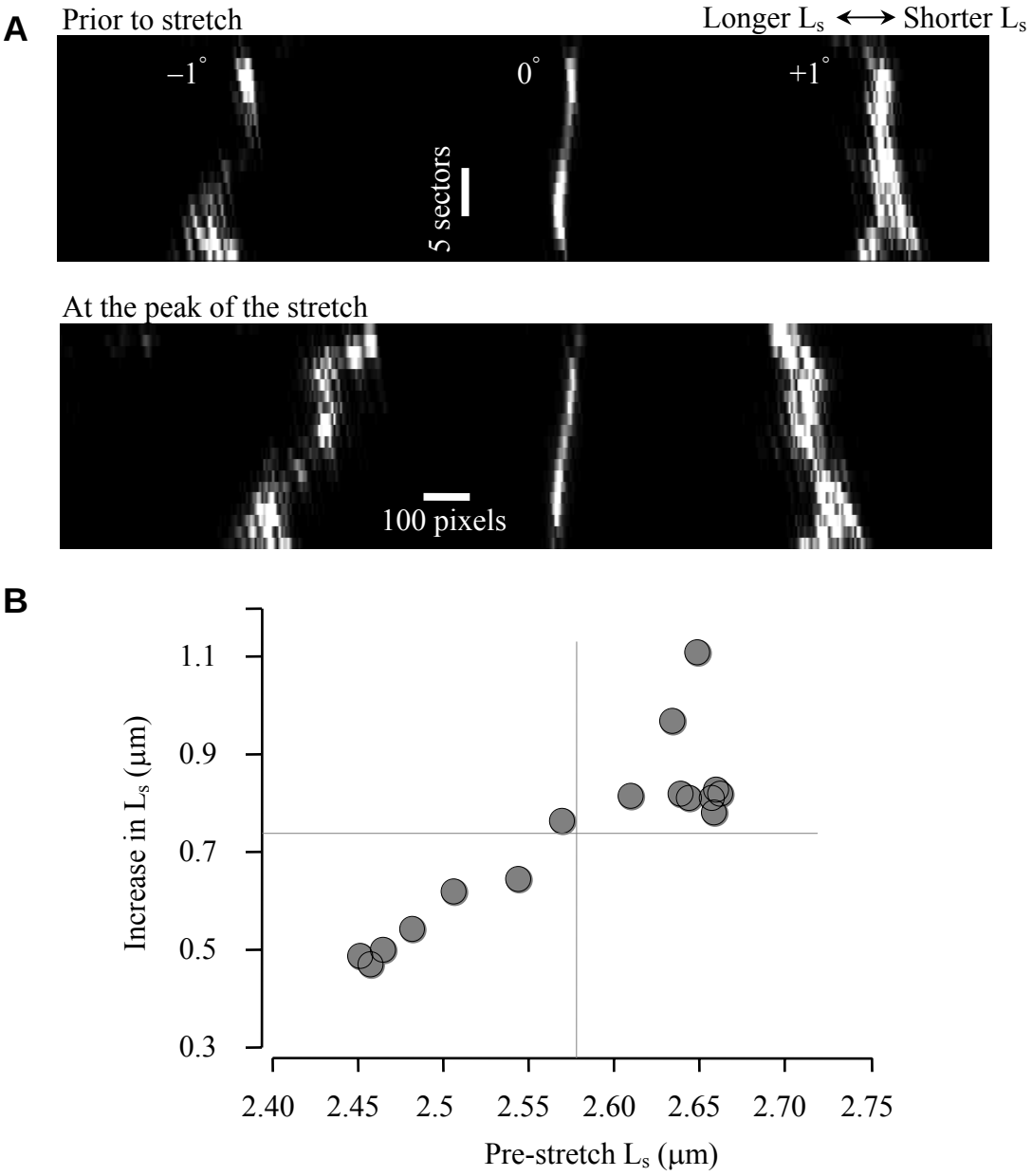

FIGURE 2.6: Representative diffraction images and L_s of an activated fiber during the single stretch protocol. (*A*) L_s were computed from the diffraction images of the activated fibers obtained 100 ms before (top) and at the peak of the stretch (bottom). Functional sectors were identified by applying the rate-limiting filter to the pre-stretch L_s obtained from the top image and the remaining sub-functional sectors were eliminated from subsequent analyses. (*B*) For the accepted sectors (n = 16) the increase in L_s is plotted against the pre-stretch L_s. The graph shows a strong correlation between the increase in L_s and pre-stretch L_s ($r = 0.85$, $p < 0.0001$). The solid vertical and horizontal lines represent, respectively, the mean pre-stretch L_s and the mean increase in L_s of the accepted segment. The graph indicates that sectors with pre-stretch L_s longer than the mean L_s stretched more than the mean increase in L_s (top-right quadrant).

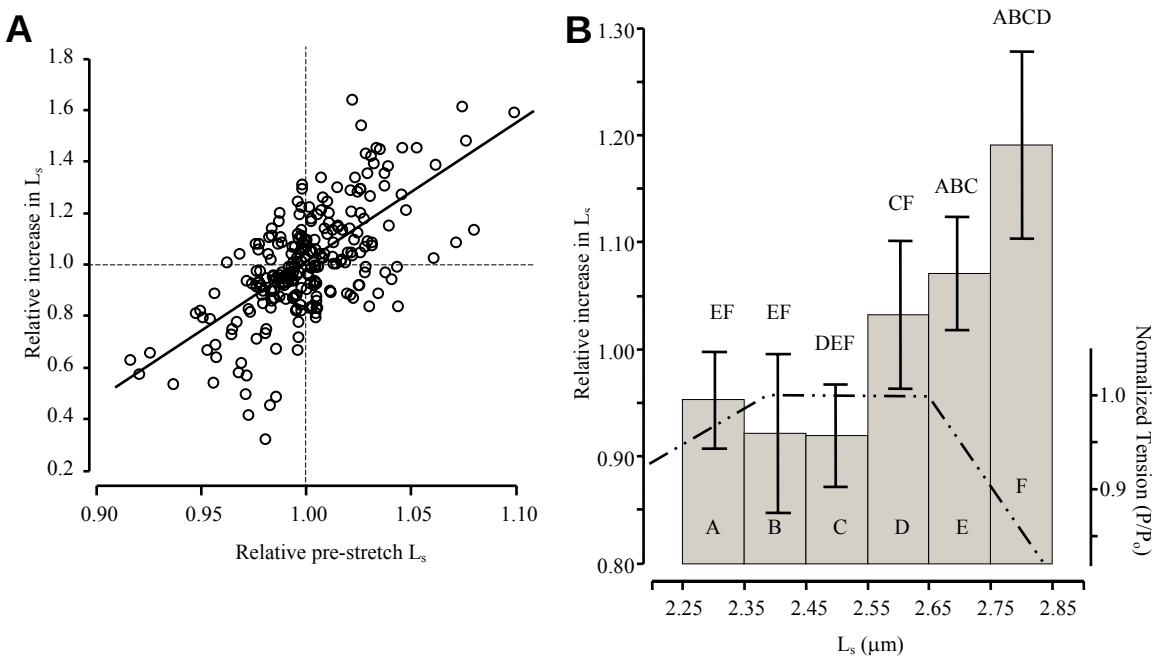

FIGURE 2.7: Effect of pre-stretch L_s on strain. (*A*) Effect of relative pre-stretch L_s on extensibility of sectors during stretch. The *x* axis represents relative pre-stretch L_s, the ratio of sector pre-stretch L_s to the mean L_s of the segment. The *y* axis represents relative increase in L_s, the ratio of increase in sector L_s to the mean L_s increase. The linear fit (solid line) indicates a strong correlation between relative pre-stretch L_s and relative increase in L_s ($r = 0.65$, $p = 0.0001$, slope = 5.4). The graph indicates that sectors with longer pre-stretch L_s than the mean extend more than the mean extension of the segment and the sectors with shorter pre-stretch L_s than the mean extend less than the mean. (*B*) The relative increase in L_s versus pre-stretch L_s. The accepted data from all 16 fibers were pooled and the relative increases in L_s of sectors were assigned to six different groups (A–F) according to the pre-stretch L_s values. The *y* axis on the left hand side of the graph represents relative increase in L_s as a ratio of increase in L_s to mean increase in the accepted segment and the *x* axis represents pre-stretch L_s of the sectors in μm. The groups were divided uniformly in the pre-stretch L_s range of 2.25 to 2.85 μm with an interval size of 0.1 μm. The group means and the error bars representing 95% confidence intervals for the means are shown in the figure. One-way ANOVA for comparing the group means resulted in a significant *F*-statistic ($F = 8.31$) indicating differences among groups. The *post hoc* comparisons identified pair-wise differences ($p < 0.05$) as indicated above the bars of the histogram (e.g., group A is different from groups E and F). The L_s at which the shift in trend occurred coincided approximately with the beginning of the descending limb of the length-tension relationship (‗ . . , *y* axis on right hand side) for *soleus* muscles of rats.

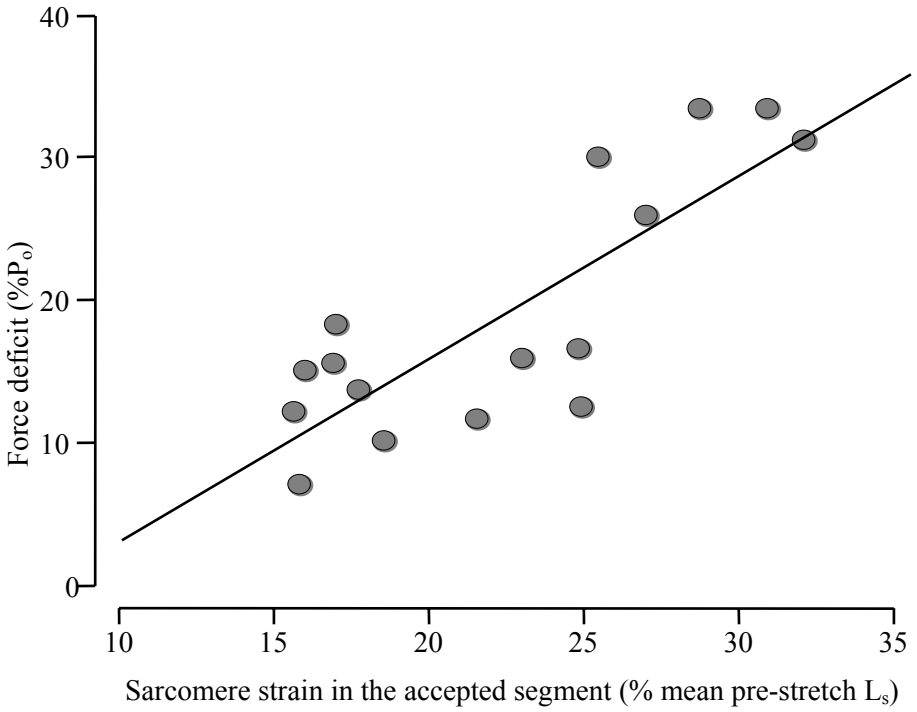

FIGURE 2.8: Relationship between the force deficit and sarcomere strain. Deficit in force produced by the activated fibers following the single stretch protocol correlated with the sarcomere strain in the accepted segment ($r = 0.82$, $p = 0.0001$). The solid line represents a straight line fit to the observed data (slope = 1.29).

References

Brenner, B. 1983. Technique for stabilizing the striation pattern in maximally calcium-activated skinned rabbit psoas fibers. *Biophys. J.* 41:99-102.

Brooks, S. V. and J. A. Faulkner. 1996. The magnitude of the initial injury induced by stretches of maximally activated muscle fibres of mice and rats increases in old age. *J. Physiol* 497:573-580.

Brooks, S. V., E. Zerba, and J. A. Faulkner. 1995. Injury to muscle fibres after single stretches of passive and maximally stimulated muscles in mice. *J. Physiol* 488:459-469.

Brown, L. M. and L. Hill. 1991. Some observations on variations in filament overlap in tetanized muscle fibres and fibres stretched during a tetanus, detected in the electron microscope after rapid fixation. *J. Muscle Res. Cell Motil.* 12:171-182.

Butterfield, T. A. and W. Herzog. 2006. Effect of altering starting length and activation timing of muscle on fiber strain and muscle damage. *J. Appl. Physiol* 100:1489-1498.

Chase, P. B. and M. J. Kushmerick. 1988. Effects of pH on contraction of rabbit fast and slow skeletal muscle fibers. *Biophys. J.* 53:935-946.

Close, R. I. 1972. Dynamic properties of mammalian skeletal muscles. *Physiol Rev.* 52:129-197.

Faulkner, J. A. 2003. Terminology for contractions of muscles during shortening, while isometric, and during lengthening. *J Appl. Physiol* 95:455-459.

Friden, J., M. Sjostrom, and B. Ekblom. 1983. Myofibrillar damage following intense eccentric exercise in man. *Int. J. Sports Med.* 4:170-176.

Galler, S. and K. Hilber. 1994. Unloaded shortening of skinned mammalian skeletal muscle fibres: effects of the experimental approach and passive force. *J. Muscle Res. Cell Motil.* 15:400-412.

Goldman, Y. E. and R. M. Simmons. 1984. Control of sarcomere length in skinned muscle fibres of Rana temporaria during mechanical transients. *J Physiol* 350:497-518.

Gordon, A. M., A. F. Huxley, and F. J. Julian. 1966a. Tension development in highly stretched vertebrate muscle fibres. *J. Physiol* 184:143-169.

Gordon, A. M., A. F. Huxley, and F. J. Julian. 1966b. The variation in isometric tension with sarcomere length in vertebrate muscle fibres. *J. Physiol* 184:170-192.

Hilber, K. and S. Galler. 1998. Improvement of the measurements on skinned muscle fibres by fixation of the fibre ends with glutaraldehyde. *J. Muscle Res. Cell Motil.* 19:365-372.

Hunter, K. D. and J. A. Faulkner. 1997. Pliometric contraction-induced injury of mouse skeletal muscle: effect of initial length. *J. Appl. Physiol* 82:278-283.

Julian, F. J. and D. L. Morgan. 1979. The effect on tension of non-uniform distribution of length changes applied to frog muscle fibres. *J. Physiol* 293:379-392.

Julian, F. J. and R. L. Moss. 1980. Sarcomere length-tension relations of frog skinned muscle fibres at lengths above the optimum. *J. Physiol* 304:529-539.

Kawai, M. and I. D. Kuntz. 1973. Optical diffraction studies of muscle fibers. *Biophys. J* 13:857-876.

Krueger, J. W. and A. Denton. 1992. High resolution measurement of striation patterns and sarcomere motions in cardiac muscle cells. *Biophys. J* 61:129-144.

Lieber, R. L. and J. Friden. 1993. Muscle damage is not a function of muscle force but active muscle strain. *J. Appl. Physiol* 74:520-526.

Lieber, R. L., K. P. Roos, B. A. Lubell, J. W. Cline, and R. J. Baskin. 1983. High-speed digital data acquisition of sarcomere length from isolated skeletal and cardiac muscle cells. *IEEE Trans. Biomed. Eng* 30:50-57.

Lombardi, V. and G. Piazzesi. 1990. The contractile response during steady lengthening of stimulated frog muscle fibres. *J. Physiol* 431:141-171.

Macpherson, P. C., R. G. Dennis, and J. A. Faulkner. 1997. Sarcomere dynamics and contraction-induced injury to maximally activated single muscle fibres from soleus muscles of rats. *J. Physiol* 500:523-533.

Macpherson, P. C., M. A. Schork, and J. A. Faulkner. 1996. Contraction-induced injury to single fiber segments from fast and slow muscles of rats by single stretches. *Am. J. Physiol* 271:C1438-C1446.

Martyn, D. A. and A. M. Gordon. 1992. Force and stiffness in glycerinated rabbit psoas fibers. Effects of calcium and elevated phosphate. *J. Gen. Physiol* 99:795-816.

McCully, K. K. and J. A. Faulkner. 1985. Injury to skeletal muscle fibers of mice following lengthening contractions. *J. Appl. Physiol* 59:119-126.

Moisescu, D. G. and R. Thieleczek. 1978. Calcium and strontium concentration changes within skinned muscle preparations following a change in the external bathing solution. *J Physiol* 275:241-262.

Morgan, D. L. 1990. New insights into the behavior of muscle during active lengthening. *Biophys. J.* 57:209-221.

Myers, J., R. Tirosh, R. C. Jacobson, and G. H. Pollack. 1982. Phase-locked loop measurement of sarcomere length with high time resolution. *IEEE Trans. Biomed. Eng* 29:463-466.

Newham, D. J., D. A. Jones, G. Ghosh, and P. Aurora. 1988. Muscle fatigue and pain after eccentric contractions at long and short length. *Clin. Sci. (Lond)* 74:553-557.

Newham, D. J., G. McPhail, K. R. Mills, and R. H. Edwards. 1983. Ultrastructural changes after concentric and eccentric contractions of human muscle. *J. Neurol. Sci.* 61:109-122.

Ogilvie, R. W., R. B. Armstrong, K. E. Baird, and C. L. Bottoms. 1988. Lesions in the rat soleus muscle following eccentrically biased exercise. *Am J Anat.* 182:335-346.

Panchangam, A., R. S. Witte, D. R. Claflin, M. O'Donnell, and J. A. Faulkner. 2006. A novel optical imaging system for investigating sarcomere dynamics in single skeletal muscle fibers. D. L. Farkas, D. V. Nicolau, and R. C. Leif, editors. SPIE, San Jose, CA, USA. 608808-608811.

Patel, T. J., R. Das, J. Friden, G. J. Lutz, and R. L. Lieber. 2004. Sarcomere strain and heterogeneity correlate with injury to frog skeletal muscle fiber bundles. *J. Appl. Physiol* 97:1803-1813.

Roos, K. P., R. J. Baskin, R. L. Lieber, J. W. Cline, and P. J. Paolini. 1980. Digital data acquisition and analysis of striated muscle diffraction patterns with a direct memory access microprocessor system. *Rev. Sci. Instrum.* 51:762-767.

Rudel, R. and F. Zite-Ferenczy. 1979. Do laser diffraction studies on striated muscle indicate stepwise sarcomere shortening? *Nature* 278:573-575.

Rudel, R. and F. Zite-Ferenczy. 1980. Efficiency of light diffraction by cross-striated muscle fibers under stretch and during isometric contraction. *Biophys. J* 30:507-516.

Stephenson, D. G. and D. A. Williams. 1982. Effects of sarcomere length on the force-pCa relation in fast- and slow-twitch skinned muscle fibres from the rat. *J. Physiol* 333:637-653.

Talbot, J. A. and D. L. Morgan. 1996. Quantitative analysis of sarcomere non-uniformities in active muscle following a stretch. *J. Muscle Res. Cell Motil.* 17:261-268.

Talbot, J. A. and D. L. Morgan. 1998. The effects of stretch parameters on eccentric exercise-induced damage to toad skeletal muscle. *J. Muscle Res. Cell Motil.* 19:237-245.

Wood, S. A., D. L. Morgan, and U. Proske. 1993. Effects of repeated eccentric contractions on structure and mechanical properties of toad sartorius muscle. *Am. J. Physiol* 265:C792-C800.

CHAPTER 3

STRETCHES OF MAXIMALLY ACTIVATED PERMEABILIZED SINGLE MUSCLE FIBERS INCREASE THE HETEROGENEITY OF RESTING SARCOMERE LENGTH

Introduction

Contraction-induced injury to single fibers of skeletal muscle is caused by severe lengthening contractions and results in focal disruption of single sarcomeres, or small groups of sarcomeres, that are both in series and in parallel with intact sarcomeres (Brooks et al., 1995; Brown and Hill, 1991). The focal disruption appears to result from excessive lengthening of sarcomeres that were already at longer lengths prior to the lengthening contraction (Macpherson et al., 1996; Morgan, 1990; Talbot and Morgan, 1996). When individual sarcomeres are lengthened beyond thick and thin filament overlap, passive structural elements within sarcomeres become the sole force-bearing structures and consequently are at risk of being damaged (Brooks et al., 1995; Higuchi et al., 1988; Wang et al., 1993). Despite the involvement of passive structural elements in contraction-induced injury, the passive mechanical properties of single fibers following lengthening contractions have not been studied previously.

When a maximally activated single fiber is lengthened, increases in the lengths of sarcomeres (L_s) within the fiber are not uniform (Julian and Morgan, 1979b; Lombardi and Piazzesi, 1990; Macpherson et al., 1997; Panchangam et al., 2007). During

lengthening contractions of permeabilized single fibers, the regions of the fiber that had the longest L_s during a maximal isometric activation just prior to the stretch were those that were strained to the greatest degree during the stretch (Chapter 2). Thus the regions containing longer sarcomeres were more likely to be damaged by a subsequent strain (Macpherson et al., 1997; Morgan, 1990). Following the lengthening contraction, these differences in the regional strains should be manifested as history-dependent changes in regional passive mechanical properties (Campbell and Moss, 2002; Granzier and Wang, 1993).

Our purpose was to study, with high spatial resolution, the effects of a single lengthening contraction on the passive properties of single fibers. We measured the average L_s of multiple regions of permeabilized single fibers rapidly, during passive stretches applied before and after a single severe lengthening contraction (strain > 25%) with a high-resolution laser scanning technique (Panchangam et al., 2007; Panchangam et al., 2006) to test the hypothesis that a severe lengthening contraction increases the variability in the L_s of a passive fiber.

Materials and methods

Fiber preparation and measurements

The permeabilized fiber preparation, experimental setup, and force, cross-sectional area (CSA) and L_s measurements are described in detail in Chapter 2. Briefly, permeabilized single fiber segments ("fibers") were obtained from *soleus* muscles of adult male rats (n = 5; age 6–10 months). A single fiber was subsequently placed in a temperature-controlled (15°C) fluid-exchange bath filled with relaxing solution. The fiber

was mounted on two short lengths of stainless steal tubing, one connected to a force transducer and the other to the lever arm of a servomotor, and secured with 10-0 monofilament nylon suture ties. The fiber length (L_f) was defined as the length between the innermost ties when mean resting L_s was ~2.5 μm. The length of the fiber being probed optically (L_{op}) was obtained by measuring from the end of the transducer tubing to the end of the servomotor tubing and then subtracting the width of the spot of the laser used for laser diffraction measurements. Within L_{op}, diffraction patterns were obtained from 20 contiguous regions, hereafter termed 'sectors,' by passing a laser beam (wave length, 650 nm) briefly (100 μs) along each sector and capturing the resulting patterns with a charge coupled device camera. L_s corresponding to each of the 20 sectors was calculated from the captured diffraction patterns using the Bragg formulation for one-dimensional gratings (Cleworth and Edman, 1972; Kawai and Kuntz, 1973; Leung, 1983). The time taken for the measurement of the L_s of each of the 20 sectors along the full fiber length (20 sectors) was ~2 ms.

Experimental protocol

The passive properties of permeabilized single fibers in response to stretch are dependent on the previous strain history of the fiber (Granzier and Wang, 1993; Helmes et al., 1999). Therefore, in order to compare the responses of single fibers to a given passive stretch, the variation in the passive properties due to the past history must be minimized. Fig. 3.1 *A* shows the passive stress response of a permeabilized single fiber to eleven, repetitive cycles of passive stretch and release of strain magnitude = 0.33 L_f, strain rate = 0.54 $L_f\ s^{-1}$ and inter-cycle separation = 4.5 min. With each repetitive cycle, the normalized peak passive stress decreased in a curvilinear fashion that was dependent

on the number of previous cycles. During the first four cycles, the passive strain decreased rapidly, but then plateaued with little change in passive stress between cycle 6 and 11 (Fig. 3.1 *B*). After cycle 6, the passive stress relative to that of the previous cycle decreased by less than 2%. Consequently, in contrast to the significant effect of the previous history on the passive stress response during the first five cycles, the passive properties of fibers were essentially free from any effect of the previous history of repetitive cycling after cycle 6.

Consequently, throughout the remainder of the study, each fiber was subjected to a background of eleven equally spaced passive stretch-release cycles and the 'intervention', either a maximum isometric contraction, or a lengthening contraction, was interjected ~3 min after cycle 8. Comparisons of passive properties were made among the pre-intervention cycle (cycle 8) and the three post-intervention cycles 9, 10, and 11. This approach of comparing fiber properties after the fiber stress response to repetitive cycling had stabilized, ensured that any differences in passive properties between the pre-intervention cycle and each of the post-intervention cycles were due to the interventions alone and not due to passive stretching of fibers. The comparisons of stress and L_s among the pre-intervention and the post-intervention cycles were carried out, specifically, at two time-points within each cycle (Fig. 3.2 *A*), one at 100 ms prior to the cycle ('pre-cycle'), and the other at the peak of the cycle where the length of the fiber was maximum ('peak-cycle').

Fibers were assigned to either an isometric contraction group that served as a control group (n = 5), or a lengthening contraction group that served as an experimental group (n = 16). Fibers in the lengthening contraction group were activated maximally by

first immersing the fibers in a low-[Ca^{2+}] preactivating solution for 3 min and then immersing them in a high-[Ca^{2+}] activating solution (Chapter 2). During maximum activation, the fibers were stretched by a magnitude of 0.27 L_f at a velocity of 0.54 L_f s^{-1} (Fig. 3.2 *B*). Immediately following the stretch, the fibers were returned to their original length at the same speed. Upon returning to original length, the fibers were shortened rapidly (step shortening) by a length of 0.22 L_f and held for 40 ms. Fibers were then returned rapidly to their original lengths (step stretch) and allowed to generate maximum isometric force for up to 10 s, before being returned to the relaxing solution. The interval between completion of the intervention and the beginning of cycle 9 was ~30 s. The fibers in the isometric activation group were activated maximally, but not stretched. The total duration of the activation was approximately the same for both the groups.

Before the steady background of passive stretch-release cycles began, the mean resting L_s of the fibers was adjusted to ~2.7 μm. This resting L_s was chosen because during the isometric activation phase of the contraction, the mean L_s within the fiber shortens up to 6%. This length, for *soleus* muscles of rats, ensured that the lengthening contraction was initiated at the mean L_s near the middle of the plateau region, or at the beginning of the descending limb of the length-tension relationship (Stephenson and Williams, 1982).

Force deficit measurements

Force deficit (Macpherson et al., 1996), defined as the percentage reduction in peak isometric force (P_o) following a single lengthening contraction, was calculated as the difference in the isometric force generated by a maximally activated fiber measured before and after the single lengthening contraction. Following a single lengthening

contraction, force deficit was measured twice. The first measurement was made immediately after the lengthening contraction, as soon as the fiber had been returned to its original length (Fig. 3.2 *B*). The second measurement was made 15 min after the lengthening contraction (after cycle 11). The final force deficit was calculated as the mean value of these two force deficit measurements.

Selection criteria

Diffraction patterns produced by the fibers during the maximal isometric contraction phase were visually inspected and fibers were rejected without replacement if the diffraction patterns were faint or diffuse. For each fiber, a rate-limiting filter (described in Chapter 2) was applied to L_s profiles to eliminate compliant end-sectors from all analyses. Fibers were rejected if the mean pre-cycle L_s (Fig. 3.2 *A*) measured prior to any of the post-intervention cycles (cycle 9, 10, and 11) varied by more than 2% of the mean pre-cycle L_s measured prior to the pre-intervention cycle (cycle 8). Fibers that had gross markers of damage at the end of the protocol such as tears were also rejected.

Statistical Analysis

Variability in pre-cycle or peak-cycle L_s of a fiber was computed as the standard deviation of L_s of all the accepted sectors of that fiber. Within the isometric contraction group, or the lengthening contraction group, the differences in a given quantity (e.g., the peak passive stress) among the cycles (8–11) were assessed by a univariate one-way analysis of variance (ANOVA). If the *F*-statistic of the ANOVA showed significance, the differences were determined by Tukey's HSD *post hoc* tests (Fig. 3.53, Fig. 3.6, and Fig. 3.7). The level of significance was set *a priori* at $p < 0.05$. Linear regression models were

used to determine the influence of the stretch magnitude of a sector during the lengthening contraction on the change in pre-cycle L_s of that sector due to the lengthening contraction (Fig. 3.8). The correlation coefficient (r, Pearson's product moment) and the significance level of the correlation are also presented (Fig. 3.8).

Results

In the lengthening contraction group, a total of 12 fibers were selected based on the selection criteria described earlier. For the lengthening contraction group, the lengths of fibers were L_f = 1.36 ± 0.15 mm (mean ± SD, n = 12) and L_{op} = 1.05 ± 0.12 mm. The CSA was 6720 ± 1420 μm^2 (range = 5220–10210 μm^2), P_o was 0.91 ± 0.17 mN and peak isometric stress was 138 ± 23 kN m^{-2}. For the fibers of the isometric contraction group (n = 5), the fiber dimensions were L_f = 1.27 ± 0.26 mm, L_{op} = 1.03 ± 0.25 mm, and CSA = 6680 ± 883 μm^2, P_o was 0.89 ± 0.12 mN, and peak isometric stress was 136 ± 18 kN m^{-2}. The values for the two groups were not different. After applying the rate-limiting filter, rejection of sectors occurred at both the ends in some fibers and in some other fibers, rejection occurred only at one end. The number of sectors in the accepted segments varied from 12 to 20. Following the application of rate-limiting filter in the lengthening contraction group, the average lengths of the accepted segments were 0.89 ± 0.13 mm and the average lengths in the isometric contraction group were 0.86 ± 0.11 mm.

Representative fiber

Representative records of stress and L_s of a fiber from the lengthening contraction group are presented in Fig. 3.3. When compared with the peak passive stress during cycle 8, the peak passive stress during cycle 9 was 7.9% lower. During the subsequent cycles,

the peak passive stress recovered and reached pre-intervention levels by cycle 11. This observation indicated that the effect of the lengthening contraction on the peak passive stress was temporary. No such differences were observed in the 'resting' stress of the fiber prior to the cycles, where the fiber was relaxed at its original length.

For the same representative fiber, Fig. 3.4 shows the effect of lengthening contraction on the L_s profile, the modulation of L_s with the sector number along the fiber. In comparison with the profile of the pre-cycle L_s prior to cycle 8, the profile of pre-cycle L_s prior to cycle 9 was highly dispersed (Fig. 3.4 *A*). This observation indicated that the lengthening contraction increased the variability in pre-cycle L_s of the fiber. The profiles of the pre-cycle L_s prior to subsequent cycles (prior to cycle 10 and cycle 11), became less dispersed when compared with the profile prior to the cycle 9. Despite the slight decrease in the dispersion of L_s profiles, the dispersion prior to cycle 11 was still at elevated levels when compared with the dispersion prior to cycle 8. Following the lengthening contraction, although the dispersion in the profiles increased, the mean level of the profiles (mean pre-cycle L_s, horizontal lines) did not change (< 2%).

Compared with the increases in the dispersion of the profiles of pre-cycle L_s, the increases in those of the peak-cycle L_s were similar, but at diminished levels (Fig. 3.4 *B*). The increase in the dispersion of both pre-cycle and peak-cycle L_s profiles indicated that lengthening contractions caused sector-level differences in the L_s. Furthermore, during each cycle (cycles 8 through 11), the dispersion for the profiles of peak-cycle L_s was less than the dispersion for the profiles of pre-cycle L_s. This observation supported the hypothesis that the variability in L_s was reduced, when fibers were stretched passively (Granzier et al., 1991; Granzier and Pollack, 1990).

Pooled data – stress and mean L_s

During each cycle, the peak passive stress of the fibers in the lengthening contraction group and the isometric contraction (controls) group are shown in Fig. 3.5. For fibers of the lengthening contraction group, the peak passive stress during the cycle 9 was 8.1 ± 6.2 % lower than the peak passive stress during cycle 8. During the subsequent cycles, the peak passive stress recovered and by cycle 11 the peak passive stress returned to the pre-intervention levels. In contrast to the fibers of lengthening contraction group, in the fibers of isometric contraction group, reductions in the peak passive stress were not observed during the passive cycles.

To determine if a reduction in the peak passive stress could be produced with a passive stretch of the fiber instead of a lengthening contraction, the lengthening contraction was replaced with a passive stretch of the same magnitude and velocity. In two fibers that were subjected to this protocol, no differences in the peak passive stress were observed between the pre-intervention cycle and any of the post-intervention cycles. These observations suggested that only lengthening contractions have an effect on the peak passive stress of fibers during passive stretch-release cycles.

Following the lengthening contraction, the force deficit of the lengthening contraction group was 17.4 ± 8.2 % P_o indicating the occurrence of a severe contraction-induced injury. In spite of the severity of the damage, the mean peak-cycle L_s of the fibers during the post-intervention cycles remained unchanged compared with the mean peak-cycle L_s during the pre-intervention cycle (Fig. 3.6 *A*). The mean sarcomere strain, calculated as the percent increase in mean L_s of the fiber from the pre-cycle state to the peak-cycle state, during the post-intervention cycles also did not change when compared with the mean sarcomere strain during the pre-intervention cycle (Fig. 3.6 *B*).

Sector-level responses

Following lengthening contractions of fibers, sector-level changes were observed in the L_s profiles. Compared with the variability in pre-cycle L_s prior to cycle 8, the variability in pre-cycle L_s prior to the cycle 9 (i.e., immediately following the lengthening contraction), increased ~3-fold from 0.02 ± 0.01 μm to 0.06 ± 0.04 μm (Fig. 3.7 *A*). From the highest level of variability in the pre-cycle L_s prior to cycle 9, the variability in the pre-cycle L_s prior to the subsequent cycles declined, but remained elevated prior to the cycle 11, where it was ~2-fold higher than the variability prior to cycle 8, at 0.04 ± 0.03 μm. Similarly, the variability in peak-cycle L_s (Fig. 3.7 *B*) increased immediately following the lengthening contraction (during cycle 9) and then slowly decreased during the subsequent cycles (cycles 10 and 11). In contrast with the sustained increase in the variability in pre-cycle L_s, the increase in the variability in peak-cycle L_s was eliminated by cycle 11. Such differences in the variability of the L_s were not observed in the fibers of the isometric contraction group.

For each sector of the fibers in the lengthening contraction group, the magnitude of stretch during the lengthening contraction was measured. The change in pre-cycle L_s was also computed by subtracting the pre-cycle L_s prior to the cycle 8 from the pre-cycle L_s prior to the cycle 11. The data from all the fibers were pooled (total, 190 sectors) and plotted with stretch magnitude on the *x*-axis and change in pre-cycle L_s on the *y*-axis (Fig. 3.8). A linear regression model fitted to the data indicated a strong correlation ($r = 0.71$; $p < 0.0001$) between the stretch magnitude during the lengthening contraction and the change in the pre-cycle L_s at the sector level.

Discussion

Testing the hypothesis that lengthening contractions increase the variability in L_s of passive fibers required spatially resolved measurements of L_s in multiple sectors of passive fibers before and after lengthening contractions. We measured the L_s in 20 contiguous sectors of permeabilized single fibers within a period of 2 ms just prior to and at the peak of 33% passive stretches applied before and after a severe lengthening contraction. The comparisons of passive stress, mean L_s and variability in L_s of the fibers, made for the passive stretches applied before and after the injury, revealed that lengthening contractions result in: (*i*) short-term changes in the passive stress of the fibers, and (*ii*) both short-term and long-term changes in the sector-level L_s. The short-term changes in the fiber stress were eliminated within 10 min. In contrast, the sector-level changes in the L_s persisted beyond 10 min. The increased variability in L_s following lengthening contractions could not have been discovered with a single-sector measurement of L_s, hence a key contribution of this study is the multiple-sector measurements of L_s along the full length of the passive fibers.

When passive stretches of large strains consistent with loss of thick and thin filament overlap were applied to single fibers, the contractile performance of the fibers were compromised (Higuchi et al., 1988; Wang et al., 1993; Brooks et al., 1995). In the present study, the magnitude of passive stretch-release cycles was chosen to be moderate so that individual sectors were not stretched to an L_s at which myofilament overlap was lost. Therefore, the repetitive cycling of the fibers was not likely to impair the contractile performance of the fibers (Brooks et al., 1995; Higuchi et al., 1988; Macpherson et al., 1996).

Effect of past history on L_s non-uniformity

During lengthening contractions of single fibers, the applied stretch is not distributed uniformly along length of the fibers (Julian and Morgan, 1979a; Lombardi and Piazzesi, 1990; Panchangam et al., 2007). Consequently, the non-uniform lengthening of fiber sectors reflects differences in the past history of different sectors. The present study showed that the sectors that underwent greater magnitudes of stretch during the lengthening contraction subsequently became longer, when fibers were relaxed following the lengthening contraction. Similarly, the sectors that underwent smaller magnitudes of stretch during the lengthening contraction became shorter when fibers were relaxed. These observations support the hypothesis that following a lengthening contraction, the increased variability in the L_s of the passive fibers is due to the non-uniform strain history of the fiber sectors that occurred during the preceding lengthening contraction.

Alterations to passive structural elements

The giant molecule titin, that spans the half-sarcomere, connecting the A-band to the I-bands and the Z lines (Furst et al., 1988; Labeit and Kolmerer, 1995; Maruyama et al., 1985), is a major contributor for the passive tension generated by the single fibers (Magid and Law, 1985; Prado et al., 2005). Titin also plays an important role in restoring sarcomeres to their original lengths following a stretch (Helmes et al., 1996; Trombitas et al., 1993; Trombitas et al., 1997). In the present study, a greater pre-cycle L_s for those sectors that underwent greater magnitudes of stretch during the lengthening contraction suggests that, in these sectors, the mechanism by which the sarcomeres are restored to their original lengths had failed. We suggest that, in the sectors that failed to regain their

original lengths during relxation following the lengthening contraction, the titin molecules and, possibly, some other passive structural elements were altered.

Implications of increased variability in resting L_s

The results indicated that, during a passive stretch immediately following contraction-induced injury to permeabilized single fibers, (*i*) the variability in L_s was high, and (*ii*) the peak stress was low. In such conditions, if the fiber was activated maximally again, an even greater variability in L_s was likely to develop due to (*i*) the increased variability in the initial L_s (Denoth et al., 2002), and (*ii*) the reduced passive stress (Granzier et al., 1991; Granzier and Pollack, 1990). If such a fiber was subjected to a second lengthening contraction, the variability would increase even further (Chapter 2), increasing the likelihood of a more severe damage due to the increased heterogeneity in the L_s (Morgan, 1990; Patel et al., 2004). In contrast, after 10 min of relaxation, if a second lengthening contraction was applied the peak stress and the L_s variability would recover closer to the pre-intervention levels, and consequently the second lengthening contraction may not be as injurious. Thus our observations predict that, following a series of lengthening contractions, the extent of contraction-induced damage will increase with the frequency and increasing number of the contractions. The extent of damage is likely to be reduced, when periods of relaxation and rest are inserted between successive lengthening contractions.

Summary

Lengthening contractions did not alter (*i*) the stress, (*ii*) the mean L_s, and (*iii*) the strain of the fibers during passive stretches. In contrast, the variability in L_s was

increased. At the peak of the passive stretch, the increase in the variability in L_s was eliminated. We conclude that lengthening contractions cause differential sector-level changes in the passive length-tension properties of permeabilized single fibers and these changes can be explained based on the modifications to the past-history of fiber sectors.

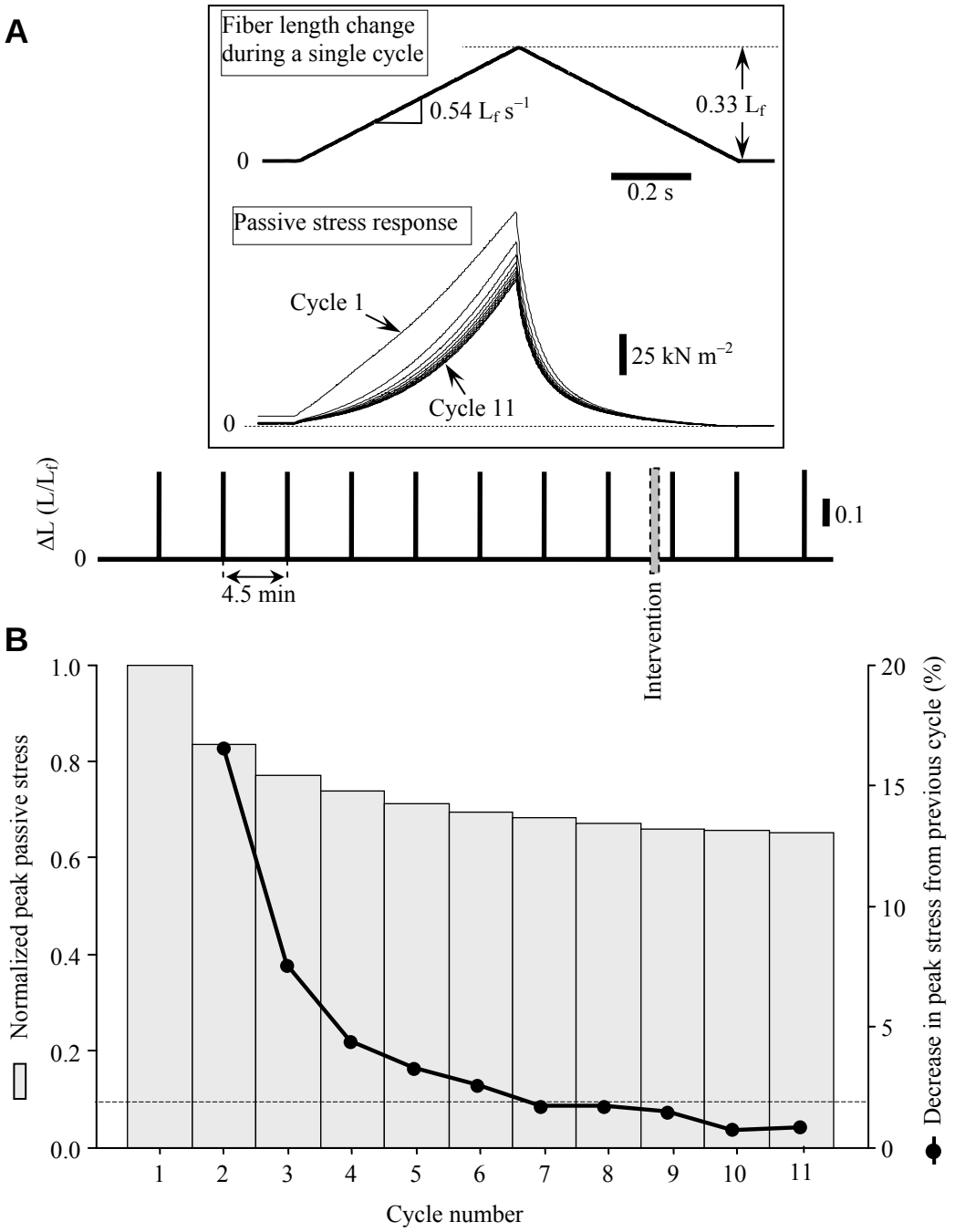

FIGURE 3.1: Passive stress response of a representative fiber to repetitive cycles of stretch and release. (*A*) The change in fiber length and the corresponding stress response to 11 cycles of passive stretch and release. (*B*) Normalized peak passive stress (closed bars, *y*-axis on the left hand side) was obtained by dividing the peak stress during each cycle with the peak stress during the first cycle. The percent decrease in peak passive stress during each cycle with reference to the previous cycle is shown on the *y*-axis on the right hand side.

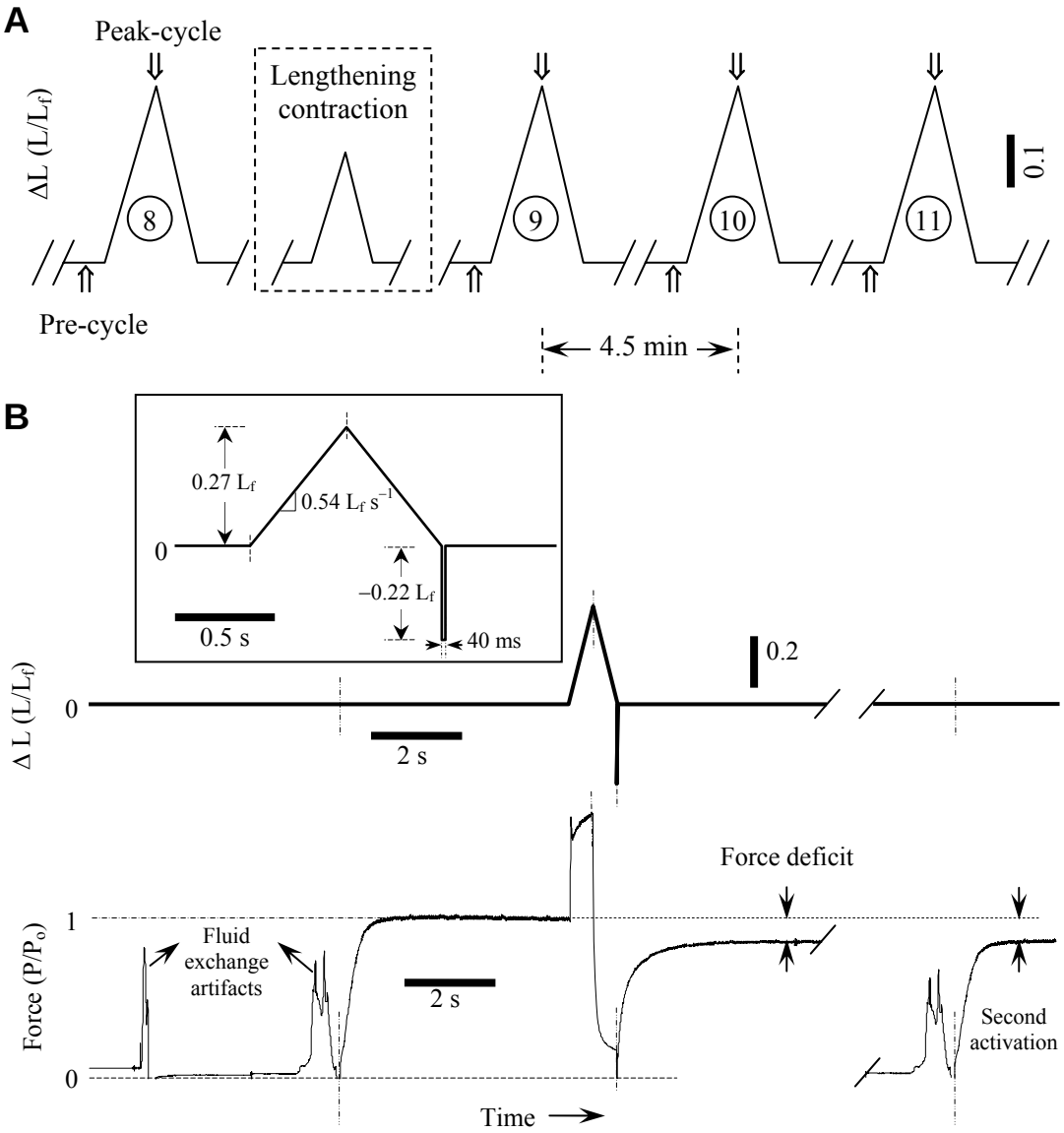

FIGURE 3.2: Experimental protocol. (*A*) Comparisons of stress and L_s were made among the pre-intervention cycle (cycle 8) and each of the post-intervention cycles (cycles 9, 10, and 11) at two time-points within the cycles, pre-cycle (⇑) and peak-cycle (⇓).The lengthening contraction protocol was performed between cycle 8 and cycle 9. (*B*) Lengthening contraction protocol. Change in fiber length during the lengthening contraction is shown in the inset. The force response of a sample fiber during the intervention (bottom) is shown on same time scale. Upon maximal activation of the fiber, force developed rapidly and reached a steady state (P_o). Peak force during the lengthening contraction was ~2-fold higher than P_o. The zero of the force transducer was established during the 40 ms hold following the step-shortening of the fiber. P_o both before and after the lengthening contraction were measured relative to the force transducer zero.

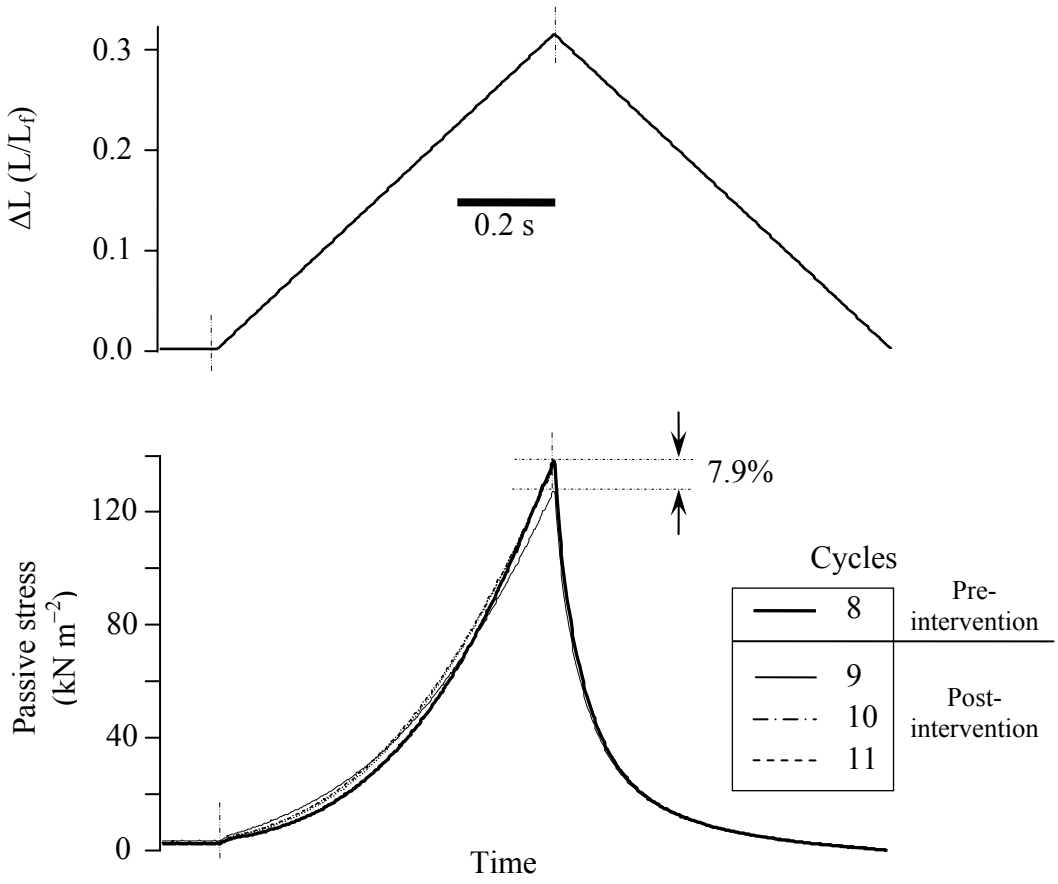

FIGURE 3.3: Effect of lengthening contraction on the stress response of a representative fiber to the passive stretch-release cycles. Top panel shows the change in fiber length during each cycle. The passive stress responses of the fiber to cycles 8–11 are superimposed (bottom panel).

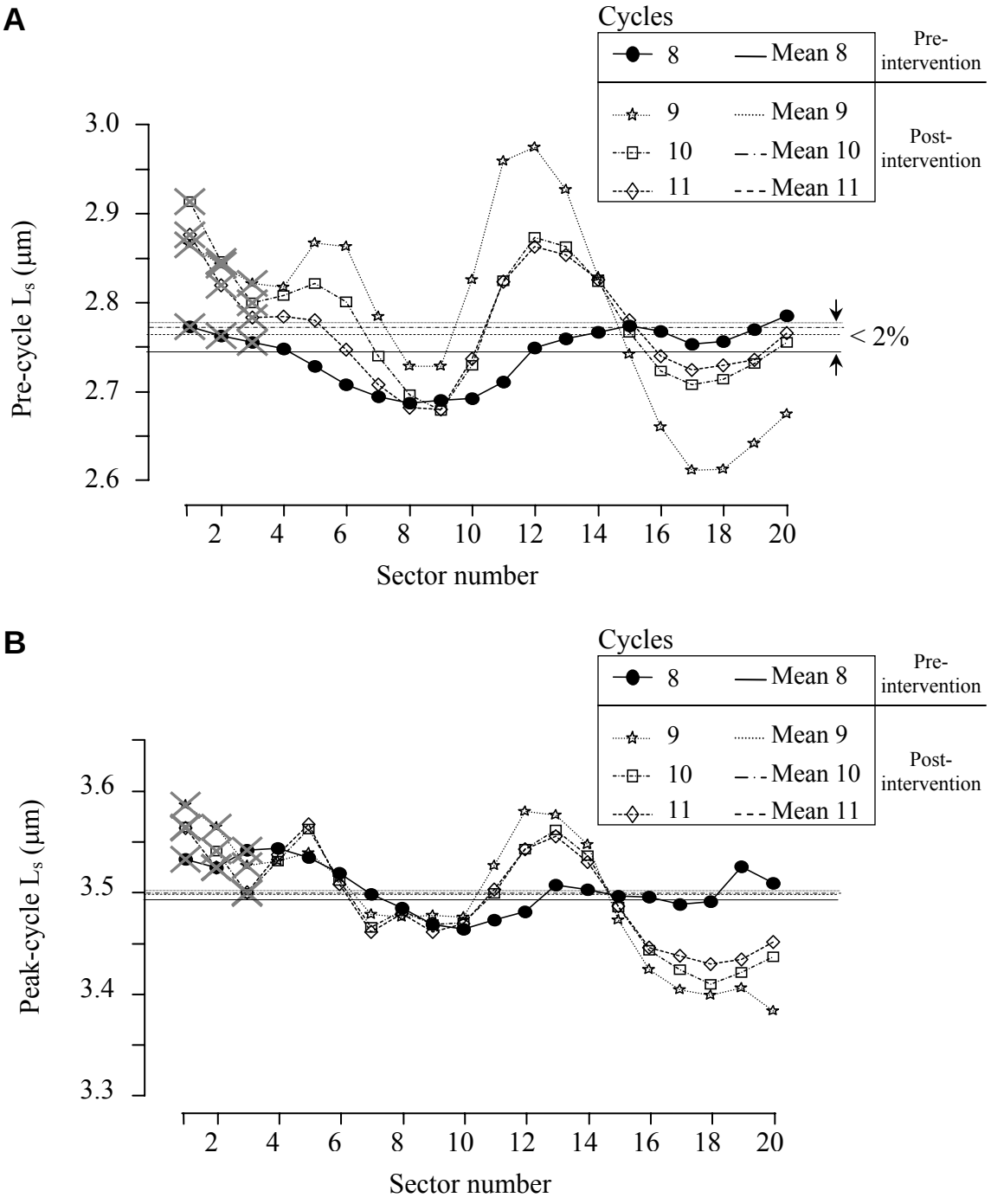

FIGURE 3.4: L_s profiles of the same representative fiber shown in Fig. 3.3. (*A*) Profiles of pre-cycle L_s of the fiber are overlaid on each other for comparison. Sectors eliminated (×) using the rate-limiting filter were not included in the analyses. Note that the rate-limiting filter eliminated only the sectors at the left end of the fiber. (*B*) Overlaid peak-cycle L_s profiles show a similar trend as that of the pre-cycle L_s profiles.

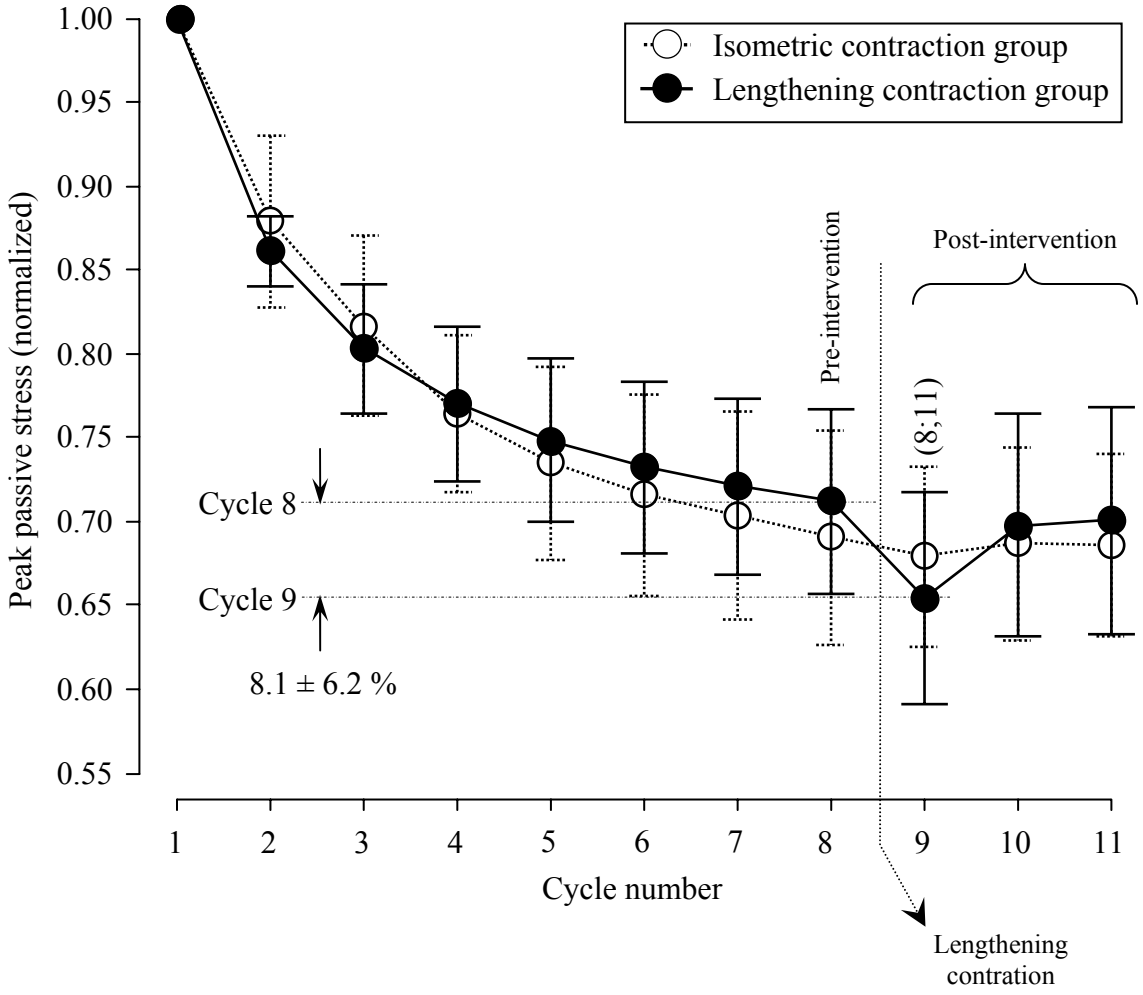

FIGURE 3.5: Peak passive stress during the cycles. Peak passive stress during each cycle was normalized by the peak passive stress during the first cycle. The error bars represent SD in the normalized peak passive stress measurements. In the lengthening contraction group, one-way ANOVA to assess differences in the peak passive stress among cycles 8–11 resulted in a significant *F*-statistic. *Post-hoc* tests revealed differences ($p < 0.05$) in peak passive stress between the cycle 9, and each of cycle 8 and cycle 11 as indicated in the figure within parentheses above cycle 9.

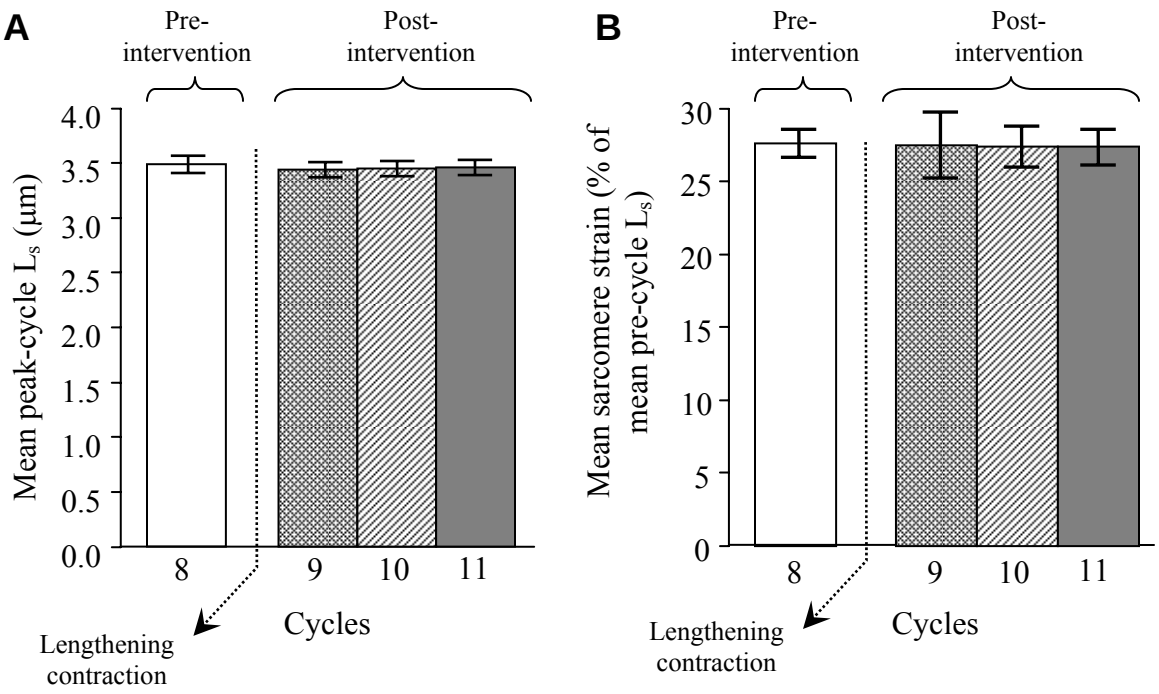

FIGURE 3.6: Comparison of mean peak-cycle L_s and mean sarcomere strain among the cycles. (*A*) Error bars represent the SD of mean pre-cycle L_s computed from all the 12 fibers contained in the lengthening contraction group. ANOVA of the mean peak-cycle L_s showed no differences among cycles. (*B*) The error bars represent the SD of the mean sarcomere strains during the cycles of all the 12 fibers. ANOVA of the mean sarcomere strain showed no differences among cycles.

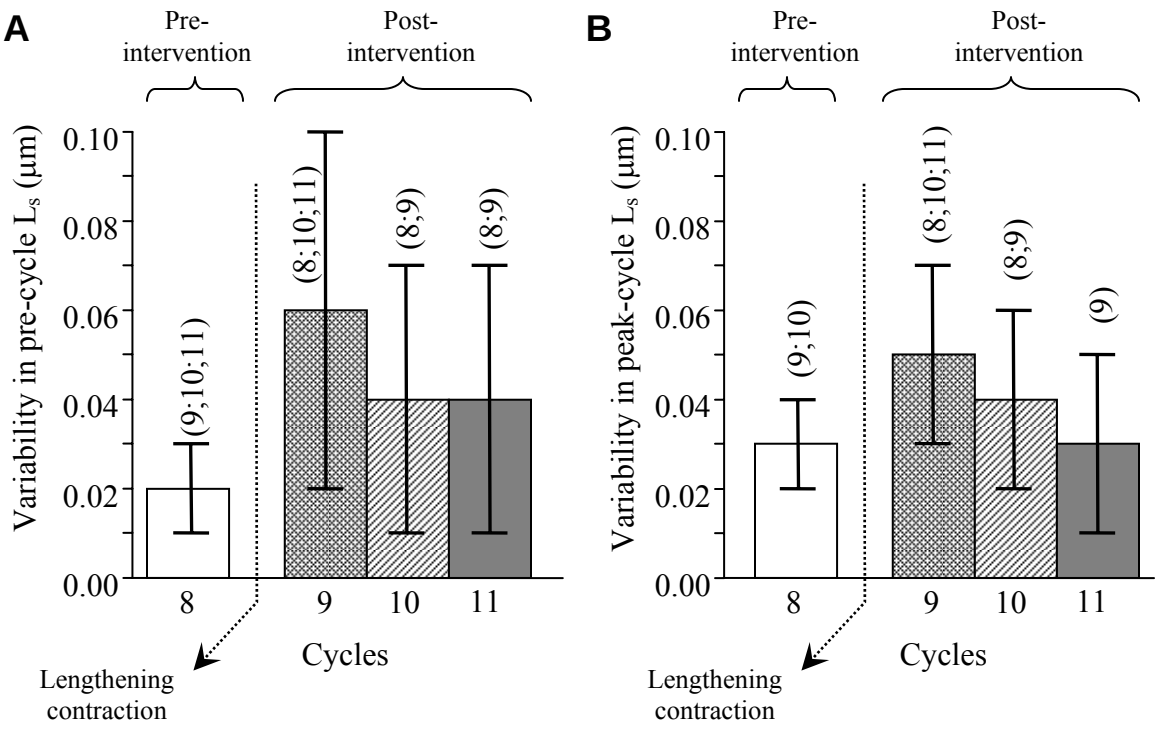

FIGURE 3.7: Comparisons of the variability in L_s. (*A*) One-way ANOVA of the variability in the pre-cycle L_s showed differences among cycles ($F = 2.9 > F_{crit} = 2.8$). The results of the *post-hoc* comparisons between individual cycles are indicated in the figure within parentheses above each cycle; e.g., the pre-intervention cycle 8 showed differences ($p < 0.05$) with each of the post-intervention cycles 9, 10, and 11. (*B*) Although, ANOVA did not show significant differences, the *F*-statistic was close to the critical value ($F = 2.5$; $F_{crit} = 2.8$). *Post-hoc* comparisons between cycles showed differences between the pre-intervention cycle 8 and each of two post-intervention cycles, 9 and 10, but no difference with post-intervention cycle 11.

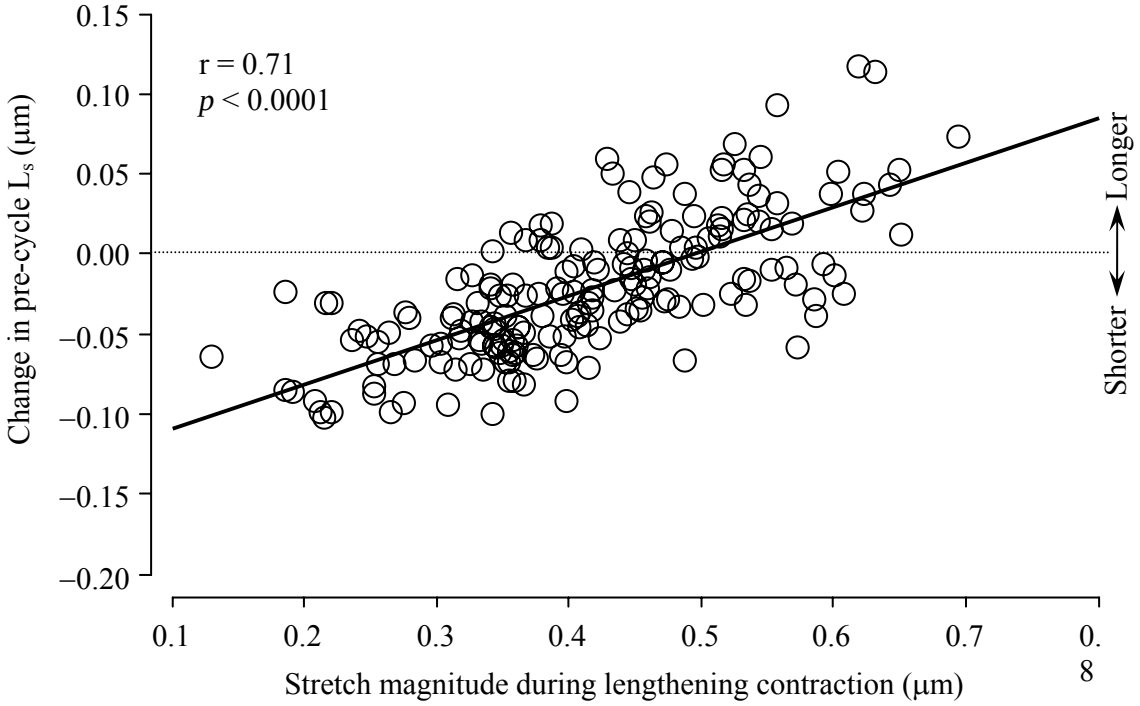

FIGURE 3.8: Effect of sarcomere stretch during lengthening contraction on the change in pre-cycle L_s. The change in pre-cycle L_s was computed by subtracting the pre-cycle L_s prior to cycle 8 from the pre-cycle L_s prior to cycle 11. The data points above the dashed horizontal line represent the sectors with permanently increased pre-cycle L_s.

References

Brooks, S. V., E. Zerba, and J. A. Faulkner. 1995. Injury to muscle fibres after single stretches of passive and maximally stimulated muscles in mice. *J. Physiol* 488:459-469.

Brown, L. M. and L. Hill. 1991. Some observations on variations in filament overlap in tetanized muscle fibres and fibres stretched during a tetanus, detected in the electron microscope after rapid fixation. *J. Muscle Res. Cell Motil.* 12:171-182.

Campbell, K. S. and R. L. Moss. 2002. History-dependent mechanical properties of permeabilized rat soleus muscle fibers. *Biophys. J* 82:929-943.

Cleworth, D. R. and K. A. Edman. 1972. Changes in sarcomere length during isometric tension development in frog skeletal muscle. *J Physiol* 227:1-17.

Denoth, J., E. Stussi, G. Csucs, and G. Danuser. 2002. Single muscle fiber contraction is dictated by inter-sarcomere dynamics. *J Theor. Biol.* 216:101-122.

Furst, D. O., M. Osborn, R. Nave, and K. Weber. 1988. The organization of titin filaments in the half-sarcomere revealed by monoclonal antibodies in immunoelectron microscopy: a map of ten nonrepetitive epitopes starting at the Z line extends close to the M line. *J Cell Biol.* 106:1563-1572.

Granzier, H. L., H. A. Akster, and H. E. ter Keurs. 1991. Effect of thin filament length on the force-sarcomere length relation of skeletal muscle. *Am J Physiol* 260:C1060-C1070.

Granzier, H. L. and G. H. Pollack. 1990. The descending limb of the force-sarcomere length relation of the frog revisited. *J Physiol* 421:595-615.

Granzier, H. L. and K. Wang. 1993. Passive tension and stiffness of vertebrate skeletal and insect flight muscles: the contribution of weak cross-bridges and elastic filaments. *Biophys. J* 65:2141-2159.

Helmes, M., K. Trombitas, T. Centner, M. Kellermayer, S. Labeit, W. A. Linke, and H. Granzier. 1999. Mechanically driven contour-length adjustment in rat cardiac titin's unique N2B sequence: titin is an adjustable spring. *Circ. Res.* 84:1339-1352.

Helmes, M., K. Trombitas, and H. Granzier. 1996. Titin develops restoring force in rat cardiac myocytes. *Circ. Res.* 79:619-626.

Higuchi, H., T. Yoshioka, and K. Maruyama. 1988. Positioning of actin filaments and tension generation in skinned muscle fibres released after stretch beyond overlap of the actin and myosin filaments. *J Muscle Res. Cell Motil.* 9:491-498.

Julian, F. J. and D. L. Morgan. 1979a. Intersarcomere dynamics during fixed-end tetanic contractions of frog muscle fibres. *J. Physiol* 293:365-378.

Julian, F. J. and D. L. Morgan. 1979b. The effect on tension of non-uniform distribution of length changes applied to frog muscle fibres. *J. Physiol* 293:379-392.

Kawai, M. and I. D. Kuntz. 1973. Optical diffraction studies of muscle fibers. *Biophys. J* 13:857-876.

Labeit, S. and B. Kolmerer. 1995. Titins: giant proteins in charge of muscle ultrastructure and elasticity. *Science* 270:293-296.

Leung, A. F. 1983. Light diffractometry for determining the sarcomere length of striated muscle: an evaluation. *J. Muscle Res. Cell Motil.* 4:473-484.

Lombardi, V. and G. Piazzesi. 1990. The contractile response during steady lengthening of stimulated frog muscle fibres. *J. Physiol* 431:141-171.

Macpherson, P. C., R. G. Dennis, and J. A. Faulkner. 1997. Sarcomere dynamics and contraction-induced injury to maximally activated single muscle fibres from soleus muscles of rats. *J. Physiol* 500:523-533.

Macpherson, P. C., M. A. Schork, and J. A. Faulkner. 1996. Contraction-induced injury to single fiber segments from fast and slow muscles of rats by single stretches. *Am. J. Physiol* 271:C1438-C1446.

Magid, A. and D. J. Law. 1985. Myofibrils bear most of the resting tension in frog skeletal muscle. *Science* 230:1280-1282.

Maruyama, K., T. Yoshioka, H. Higuchi, K. Ohashi, S. Kimura, and R. Natori. 1985. Connectin filaments link thick filaments and Z lines in frog skeletal muscle as revealed by immunoelectron microscopy. *J Cell Biol.* 101:2167-2172.

Morgan, D. L. 1990. New insights into the behavior of muscle during active lengthening. *Biophys. J.* 57:209-221.

Panchangam, A., D. R. Claflin, M. L. Palmer, and J. A. Faulkner. 2007. Magnitude of sarcomere extension correlates with initial sarcomere length during lengthening of activated single fibers from soleus muscle of rats. *Biophys. J (submitted)*.

Panchangam, A., R. S. Witte, D. R. Claflin, M. O'Donnell, and J. A. Faulkner. 2006. A novel optical imaging system for investigating sarcomere dynamics in single skeletal muscle fibers. D. L. Farkas, D. V. Nicolau, and R. C. Leif, editors. SPIE, San Jose, CA, USA. 608808-608811.

Patel, T. J., R. Das, J. Friden, G. J. Lutz, and R. L. Lieber. 2004. Sarcomere strain and heterogeneity correlate with injury to frog skeletal muscle fiber bundles. *J. Appl. Physiol* 97:1803-1813.

Prado, L. G., I. Makarenko, C. Andresen, M. Kruger, C. A. Opitz, and W. A. Linke. 2005. Isoform diversity of giant proteins in relation to passive and active contractile properties of rabbit skeletal muscles. *J Gen. Physiol* 126:461-480.

Stephenson, D. G. and D. A. Williams. 1982. Effects of sarcomere length on the force-pCa relation in fast- and slow-twitch skinned muscle fibres from the rat. *J. Physiol* 333:637-653.

Talbot, J. A. and D. L. Morgan. 1996. Quantitative analysis of sarcomere non-uniformities in active muscle following a stretch. *J. Muscle Res. Cell Motil.* 17:261-268.

Trombitas, K., M. L. Greaser, and G. H. Pollack. 1997. Interaction between titin and thin filaments in intact cardiac muscle. *J. Muscle Res. Cell Motil.* 18:345-351.

Trombitas, K., G. H. Pollack, J. Wright, and K. Wang. 1993. Elastic properties of titin filaments demonstrated using a "freeze-break" technique. *Cell Motil. Cytoskeleton* 24:274-283.

Wang, K., R. McCarter, J. Wright, J. Beverly, and R. Ramirez-Mitchell. 1993. Viscoelasticity of the sarcomere matrix of skeletal muscles. The titin-myosin composite filament is a dual-stage molecular spring. *Biophys. J* 64:1161-1177.

CHAPTER 4

SARCOMERE DYNAMICS DURING LENGTHENING CONTRACTIONS OF PERMEABILIZED SINGLE FIBERS OF *SOLEUS* MUSCLES OF RAT

Introduction

For permeabilized single muscle fibers, a lengthening contraction of stretch magnitude > 25% results in focal disruption of small groups of randomly distributed sarcomeres within the fibers (Macpherson et al., 1996). Electron micrographs of relaxed fibers following the lengthening contraction reveal overstretched sarcomeres that are both in series and in parallel with the intact sarcomeres. The initiation of contraction-induced injury during single stretches of activated permeabilized single muscle fibers is influenced by several mechanical factors including initial length, strain, and force developed during the stretch (Macpherson et al., 1996; Macpherson et al., 1997). Although contraction-induced injury is initiated by mechanical events (Wood et al., 1993; Warren et al., 1993; Brooks et al., 1995; Macpherson et al., 1996; Talbot and Morgan, 1998), the mechanism responsible for the focal nature of the injury has not been determined.

When activated single muscle fibers are stretched, the initial increase in force is extremely rapid (fast phase) and then gives way to a more gradual rise in force (slow phase) over the remaining portion of the stretch (Katz, 1939; Flitney and Hirst, 1978). For a single sarcomere operating on the plateau, or the descending limb, of the length-

tension relationship (Gordon et al., 1966; Edman, 2005) an increase in force with stretch during the slow phase is not explained by cross-bridge models of force generation (Harry et al., 1990). Morgan (Morgan, 1990) explained the force increase during the slow phase by incorporating non-uniformities in the lengths of sarcomeres (L_s) into his computer models. Furthermore, he hypothesized that lengthening of fibers during the slow phase would lead to uncontrolled elongation of the longest, presumably the weakest, sarcomeres. Such uncontrolled lengthening of sarcomeres has not been observed directly. Furthermore, experimental findings from single myofibril preparations do not support this hypothesis (Telley et al., 2006).

Our purpose was to study the dynamics of sarcomere lengthening in permeabilized single fibers undergoing a lengthening contraction. This was achieved by acquiring the L_s continuously from 20 contiguous regions at high rates (500 s^{-1}). With this approach, we tested the hypothesis that, during the course of a severe lengthening contraction (strain > 25%), all the sectors of permeabilized single fibers exhibit stable lengthening behavior.

Materials and methods

The permeabilized fibers preparation, experimental setup, and force measurements were described in (Chapter 2). Briefly, segments of permeabilized single fibers ("fibers") obtained from *soleus* muscles of adult male rats (n = 5; age 6–10 months) were placed in a temperature-controlled fluid exchange bath filled with relaxing solution (see 'solutions' in Chapter 2) maintained at 15°C. Fibers were mounted on two short lengths of stainless steal tubing, one connected to a force transducer and the other to

the lever arm of a servomotor. The fibers were secured to the tubing with 10-0 monofilament nylon suture ties. Fiber length (L_f) was defined as the length between the innermost ties when the mean resting L_s of the fiber was ~2.5 μm. The length of the fiber being probed optically (L_{op}) was obtained by measuring from the end of the transducer tubing to the end of the servomotor tubing and then subtracting the width of the spot of the laser used for laser diffraction measurements (Cleworth and Edman, 1972; Kawai and Kuntz, 1973; Leung, 1983).

Data acquisition

A diode laser (wavelength, ~650 nm and e^{-2} width, ~180 μm) was used for the laser diffraction measurements. Complete interrogation of L_{op} was carried out as described in Chapter 2. Within L_{op}, the laser beam was translated with an acousto-optic beam deflector (AOBD) through 20 contiguous regions, hereafter termed 'sectors,' by stopping at each sector momentarily for 100 μs and scanning the resulting diffraction patterns on a charge coupled device sensor. One complete readout from the sensor, a 'scan,' is a 2048 element array of 8-bit unsigned integers representing the intensity profile of a single diffraction pattern containing one undiffracted order (0º) and two diffracted first-orders (–1º, and +1º). A complete set of scans corresponding to all 20 sectors of the fiber, referred to collectively as a 'sweep,' required 2 ms.

Sweeping was accomplished by generating a stair-step waveform of total amplitude proportional to L_{op} to the driver of the AOBD that translated the beam along the fiber in equally-spaced intervals. For continuous interrogation of the fiber, the stair-step waveform was generated to the AOBD driver continuously at 10 k updates s^{-1} and the sensor was scanned at 10 k scans s^{-1} (sweep rate, 500 sweeps s^{-1}). All scans were

stored in a computer for determination of the L_s. Similarly, force and servo data were sampled simultaneously at 10 k samples s^{-1} and stored in a computer. When fiber length was changed, the step-height of the stair-step waveform was adjusted proportionally, thereby adjusting the interval between adjacent laser spots to ensure the entire L_{op} was interrogated (Fig. 2.3). The stair-step waveforms were pre-calculated for a given protocol and stored in the computer. All inputs and outputs were gated by a single trigger pulse generated simultaneously on several trigger lines.

Determination of L_s and velocity

Diffraction patterns (scans) corresponding to a given sector of a given fiber during the lengthening contraction protocol were retrieved from the stored patterns (Fig. 4.1 *A*). From these retrieved patterns, sub-patterns corresponding to each first-order (−1º, or +1º) were separated. Each series of first-order patterns was analyzed separately to identify the diffraction peaks. Within a series of first-order patterns (Fig. 4.1 *B*), the peak of the initial pattern ('initial peak') was assessed with centroid method using the following equation:

$$\hat{p}_I = \frac{\sum_p I(p) \cdot p}{\sum_p I(p)} \tag{1}$$

where, $I(p)$ is intensity at pixel p and $\hat{p}_I$ is the centroid of the pattern I.

The shift in the peak of each subsequent pattern was assessed relative to the initial peak using a cross-correlation method. The cross-correlation (r) between two patterns $I_2(p)$ and $I_1(p)$ (Fig. 4.2 *C*) was computed using the following equations:

$$r(d) = \frac{\sum_p (I_1(p) - \bar{I}_1) \cdot (I_2(p-d) - \bar{I}_2)}{\sqrt{\|I_1\| \cdot \|I_2\|}}, \tag{2}$$

$$\|I\| = \sum_{p} (I(p) - \bar{I})^2 , \tag{3}$$

and

$$\bar{I} = \frac{\sum_{p} I(p)}{N} \tag{4}$$

where, N is the total number of pixels in the pattern I.

The shift in $I_2(p)$ relative to $I_1(p)$ is taken as the value of d where the cross-correlation was maximum (Fig. 4.2 *C*). Shifts were then added to the initial peak to obtain the actual peaks. After the first-order diffraction peaks in each series (−1º, or +1º) were assessed, L_s at each time-point was calculated using the standard grating equation $\lambda = L_s \sin \theta$, where θ is the half-angle between the two diffracted orders (–1º, and +1º), and λ is the wavelength of the laser. Velocity of sarcomeres, hereafter just velocity, within each sector was computed from the continuous L_s record of that sector. For each sector, the velocity at each time-point was estimated as the average slope of the continuous L_s record within a window of 20 ms.

Experimental protocol

Prior to the experimental protocol, the mean resting L_s of a fiber was set at ~2.7 μm because the sarcomeres within L_{op} shorten up to 6% upon maximal activation. This ensured that, during a lengthening contraction, fibers were lengthened on the descending limb of the length-tension relationship (Stephenson and Williams, 1982). Relaxed fibers (n = 14) were activated by first soaking them in a low-[Ca^{2+}] pre-activating solution for 3 min and then exposing them to a high-[Ca^{2+}] activating solution. Upon rapid activation (Moisescu and Thieleczek, 1978), fibers were allowed to generate maximum isometric

force (P_o) for a few seconds. Fibers were then stretched by a magnitude of 0.27 L_f at a speed of 0.54 L_f s^{-1} (Fig. 4.2). Immediately following the stretch, the fibers were returned to their original lengths at the same speed. Upon returning to original lengths, the fibers were shortened rapidly (step shortening) by a length of 0.22 L_f and held for 40 ms. Fibers were then returned rapidly to their original lengths (step stretch) and allowed to generate maximum isometric force for up to 10 s before being returned to the relaxing solution. Ten minutes following the relaxation, fibers were maximally activated again and post-stretch P_o was recorded. Laser diffraction patterns, force, and servo data were acquired continuously throughout the single stretch lengthening contraction protocol. Force deficit (Macpherson et al., 1996), the percentage reduction in P_o following the stretch, was calculated from the P_o measurements before and after the single stretch protocol. Values of force deficit were estimated twice, once immediately after the single stretch protocol was completed, and once during the subsequent maximal activation that occurred 10 min later. The final force deficit was taken as the mean value of these two estimates.

Selection criteria

Diffraction patterns produced by the fibers during the steady-state activation phase (just prior to the lengthening) were visually inspected and fibers were rejected without replacement if the diffraction patterns were faint or diffuse. During maximal isometric activation, compliant sectors at the ends of the fiber, near the attachment points were identified using a rate-limiting filter (Chapter 2) and were eliminated from the subsequent analyses. The compliant end-sectors were eliminated because these sectors may be affected by the attachment procedure (Chase and Kushmerick, 1988). Fibers that had gross markers of damage at the end of the protocols, such as tears, were also rejected.

Results

The lengths of the fibers were L_f = 1.36 ± 0.15 mm (mean ± SD, n = 14) and L_{op} = 1.05 ± 0.12 mm. During a maximal isometric activation prior to the stretch, fibers produced a P_o of 0.91 ± 0.17 mN (stress, 138 ± 23 kN m^{-2}). After applying the rate-limiting filter, the number of sectors in the accepted segments varied from 11 to 20. Consequently, the accepted segments measured 0.89 ± 0.13 mm long and the mean L_s of the fibers were 2.54 ± 0.12 μm (range = 2.33–2.73μm). Within the accepted segment, the observed values of both sarcomere strain (21 ± 7 % of the mean pre-stretch L_s) and the sarcomere velocity (48 ± 12 % of the mean pre-stretch L_s s^{-1}) were less than the applied values of fiber strain (27 % L_f) and fiber velocity (54 % L_f s^{-1}). Following the single stretch protocol, the fibers produced a force deficit of 17.8 ± 8 % P_o.

<u>L_s and velocities of a representative fiber</u>

During the single lengthening contraction protocol, the force response of a representative fiber during the stretch (Fig. 4.3 *A*) contained two distinct phases, an early phase of rapid rise in force (fast phase) and a later phase of slow rise in force (slow phase). The transition between these two phases was marked by a brief reduction in force, referred to as the 'breakpoint'. The breakpoint has been observed in numerous studies on single fibers (Flitney and Hirst, 1978; Stienen et al., 1992; Getz et al., 1998; Bagni et al., 2002). At the peak of the stretch, the force was ~2-fold higher than the P_o (1.79 ± 0.32 mN).

After applying the rate-limiting filter 3 sectors at the left end of the fiber were eliminated from the analyses (Fig. 4.3 *B*). For all the accepted sectors, hereafter termed 'sectors,' the continuous records of L_s were computed (Fig. 4.3 *C*). During the course of

the stretch within the lengthening contraction protocol, L_s of the sectors increased at steady rates. The velocities of 3 sectors corresponding to three different values of pre-stretch L_s are shown in Fig. 4.3 *C* (bottom panel). During the first ~20 ms of the stretch, all the 3 sectors were stretched by 14 ± 8 nm at uniformly increasing velocities. Following the first 20 ms and near the breakpoint, the longest sector underwent rapid lengthening to reach its peak velocity at 3.2 μm s^{-1}. Following the rapid lengthening, the velocity of the sector declined sharply and reached a stable level at 1.3 μm s^{-1}. In contrast to the longest sector, the shortest sector underwent a brief shortening to reach a velocity of –0.3 μm s^{-1}, followed by a sharp lengthening to reach a relatively stable level of velocity at 0.6 μm s^{-1}. Beyond the breakpoint and during the slow phase of force increase, all the sectors stretched at stable levels of velocities with brief periods of acceleration followed by deceleration.

Velocity map

Continuous records of L_s, and velocities of all the sectors from all fibers (n = 204) were pooled and presented in a grayscale map (Fig. 4.4). The grayscale intensity of each pixel on each L_s trace (white arrows) indicates the instantaneous velocity of the sector at that length. Although some sarcomeres underwent rapid lengthening at high velocities (~3 μm s^{-1}; white arrows), the rapid lengthening was arrested within the first ~100 ms of the stretch. The highest velocity observed in any sector at any time was 3.3 μm s^{-1}. Following the first 100 ms of the stretch and during the slow phase, the sarcomeres lengthened at steady velocities (range = 0.48–1.9 μm s^{-1}) with brief periods of acceleration followed by deceleration. The maximum duration of any single period of

acceleration in any sector never exceeded 0.1 s. The range of velocities during these periods was 0.72 ± 0.27 μm s^{-1} (maximum range, 1.42 μm s^{-1}). Also, none of the sectors accelerated continuously to lengths that are consistent with loss of filament overlap [see length-tension relationship of *soleus* muscles of rats (Stephenson and Williams, 1982) in Fig. 4.4].

Relative velocities

For each sector of a given fiber, the velocity at each time-point was divided by the mean velocity of all the fiber sectors at that time-point to obtain the relative velocity of sarcomeres in that sector. Similarly, for each sector of a given fiber, the relative pre-stretch L_s was computed by dividing the pre-stretch L_s of that sector by the mean of all sectors in that fiber. Sectors from all fibers were pooled (n = 204) and then assigned to one of 5 groups according to the relative pre-stretch L_s value. Then, at each time-point during the stretch, the mean relative velocities of all sectors contained in each group were computed. The mean relative velocities are then compared among groups (Fig. 4.5). Near the breakpoint for force, sectors whose relative pre-stretch L_s was greater than 100% (i.e., sectors longer than their neighbors) underwent rapid lengthening at ~100% higher velocity than the mean velocity. The rapid lengthening was immediately arrested and beyond the breakpoint, the relative velocities were stable, but at a higher level (~20%) than the mean. This observation indicated that during a lengthening contraction, the fiber sectors that began at longer lengths compared to the mean underwent rapid lengthening initially, but the high lengthening velocities of these longer sectors were quickly stabilized at levels higher than the rate of lengthening of the fiber. In contrast, the sectors with relative pre-stretch L_s lower than 100% (i.e., sectors shorter than their neighbors),

underwent rapid shortening below the mean rate of lengthening. This rapid shortening was arrested within ~100 ms and thereafter the relative velocities of these shorter sectors reached a stable level of velocity, ~33% lower than the mean velocity of the fiber.

Discussion

We tested the hypothesis that, during lengthening contractions of permeabilized single fibers, all sectors of the fibers exhibit stable lengthening behavior. Testing this hypothesis required continuous monitoring of the L_s of multiple, serially connected sectors of a fiber at a high rate. This was accomplished by sequentially measuring the L_s of each of 20 sectors of a fiber (Panchangam et al., 2007) within ~2 ms time period and then repeating the process continuously 500 times s^{-1} throughout the lengthening contraction. This rapid measurement technique permitted, for the first time, study of the dynamic behavior of serially-connected sectors in permeabilized single fibers undergoing a lengthening contraction. Based on the high resolution L_s and velocity records obtained from permeabilized single fibers from *soleus* muscles of adult male rats undergoing severe lengthening contractions, we concluded that sectors of the fibers lengthened at stable rates. Although during an early phase of the lengthening contraction, rapid lengthening of some sectors was observed, such rapid lengthening was quickly arrested and thereafter, these sectors continued to lengthen at stable rates.

No evidence of uncontrolled lengthening

The magnitude of the lengthening contraction, a 27 % strain, was chosen to produce moderate to high deficits of force following the contraction (Macpherson et al., 1996). The observed force deficits were high enough to expect severe damage to the

ultrastructure of the fibers. If the ultrastructural damage was caused by the process of uncontrolled lengthening (Morgan, 1990), one or more of the following should have been evident during the stretch, (*i*) at least a few sectors should have undergone excessive lengthening to $L_s > 4.0$ μm with progressively increasing velocities, and (*ii*) to compensate for the overstretching of some sectors, at least a few sectors should have shortened or remained at the same lengths during most part of the stretch. Neither one of these predicted consequences that would have strengthened the hypothesis of uncontrolled lengthening was observed in our L_s or velocity records.

Although rapid lengthening was observed in the first 100 ms of the stretch, the percent increase in L_s (the sarcomere strain) during this period was too modest (< 5%) to cause any significant damage to the ultrastructure of the fiber (Brooks et al., 1995; Brooks and Faulkner, 1996; Macpherson et al., 1996; Panchangam et al., 2007). Most of the damage must have occurred during the slow phase of force increase. Therefore, if the process of uncontrolled lengthening existed, such process must likely have occurred during the slow phase. While the occurrence of rapid non-uniformity in L_s during the slow phase would have been consistent with the hypothesis of uncontrolled lengthening, such rapid non-uniformity was not observed in our experiments.

By continuously measuring the lengths of all half-sarcomeres in single myofibrils, investigators concluded that uncontrolled lengthening may not occur during lengthening contractions (Rassier et al., 2003; Telley et al., 2006). As these investigators did not report any evidence of force deficit to the myofibrils, it was not clear if the mechanical conditions present during their experiments were suitable to trigger the predicted process of uncontrolled lengthening (Morgan and Proske, 2006). In the present study, all stretch

parameters i.e., initial L_s, magnitude of strain, and stretch velocity, were chosen to produce severe damage to the fibers, as was evident from the magnitude of force deficits we report. Furthermore, the fibers were first passively stretched on the descending limb of the length-tension relationship and then maximally activated to ensure that lengthening contractions were initiated near the beginning of the descending limb of the length-tension relationship. Consequently, the mechanical conditions were sufficient to initiate uncontrolled lengthening of sarcomeres if such event were to occur. Despite these precautions, a continuous increase in sector velocity that would have strengthened the hypothesis of uncontrolled lengthening was never observed. The lack of any continuous increases in sector velocity indicates that the events of uncontrolled lengthening were not present in sufficient scales to explain the observed deficit in force.

Stability of sarcomeres during the stretch

The sector velocities during the slow phase were characterized by brief periods of acceleration and deceleration. Within this phase of continuous variation in velocity, if the sarcomeres within a sector ever became unstable, they would accelerate continuously until loss of filament overlap rather than decelerate. Since the sectors decelerated in our experiments, the predicted instability of sarcomeres (Morgan, 1990) could not likely have occurred. Furthermore, this variation in velocity was observed in all sectors irrespective of their pre-stretch L_s. From these observations we concluded that during stretches of maximally activated fibers, the sectors are in a dynamic stability.

In permeabilized single fibers that underwent lengthening contractions and were subsequently relaxed, the sectors that underwent greater strains during the lengthening contraction, failed to shorten completely to their original lengths indicating that the

passive elastic elements within these sectors were modified (Chapter 3). The present study shows that, although the sectors that underwent greater strains must have lengthened at higher average velocities, the lengthening velocities of these sectors were at stable levels. When combined these observations suggest that during lengthening contractions, the passive elastic elements might play a role in the stabilization of the sarcomeres contained within sectors (Telley et al., 2006).

Monitoring the L_s of sectors when fibers were stretched on the descending limb and then held isometrically, provides insights into the inherent stability of the sarcomere system at longer lengths (Telley et al., 2006). Under these circumstances, the sarcomere system is freed from any dynamic, velocity-dependent effects (Minajeva et al., 2001; Telley et al., 2006) thereby allowing the observation of inherent stability of sarcomeres at long lengths under steady-state conditions. Our experimental protocol involved a ramp stretch of activated fibers immediately followed by a ramp shortening. Consequently, our results pertain to the dynamic stability, but do not indicate inherent stability of the activated sarcomere system at long lengths.

Summary

During stretches of activated permeabilized fibers, we observed rapid lengthening of sectors when the force response of the fibers to stretch changed from a phase of fast rise to a phase of slow rise. These rapid length changes were quickly arrested and the rate of lengthening continued at steady levels. Based on the observations, we conclude that during lengthening contractions, fiber sectors undergo lengthening at stable rates. Furthermore, the present findings did not support the hypothesis of uncontrolled

lengthening of sarcomeres. Taken together with other available evidence in the literature, the findings suggested that during lengthening contractions of single fibers, the passive elastic elements might play a dynamic role in stabilizing the sarcomere system.

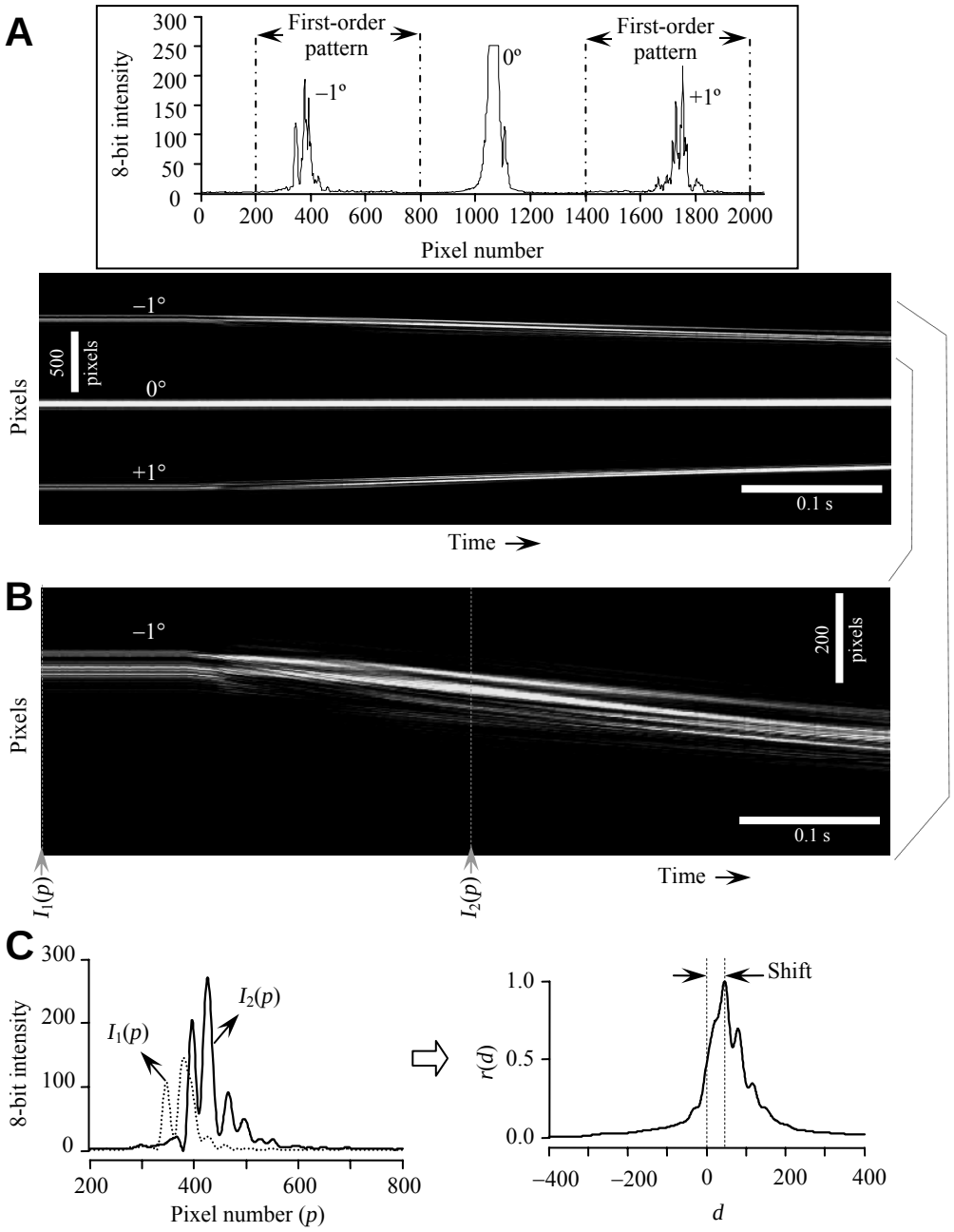

FIGURE 4.1: Determination of L_s. (*A*) Top: The intensity profile of an example diffraction pattern. Bottom: Time-varying diffraction patterns corresponding to one sector of a fiber are presented in a grayscale map. (*B*) Within the time-varying series of first-order patterns, the peak of the first pattern ($I_1(p)$) was assessed by the centroid method and subsequent peaks were assessed with a cross-correlation method. (*C*) *Left*: Intensity profiles of the patterns $I_1(p)$ and $I_2(p)$. *Right*: The cross-correlation coefficient between $I_1(p)$ and $I_2(p)$ (r, y axis) as a function of the delay (d, x axis) was computed. The shift in the peak of $I_2(p)$ relative to the peak of $I_1(p)$ is the value of the delay where the cross-correlation coefficient reached its maximum.

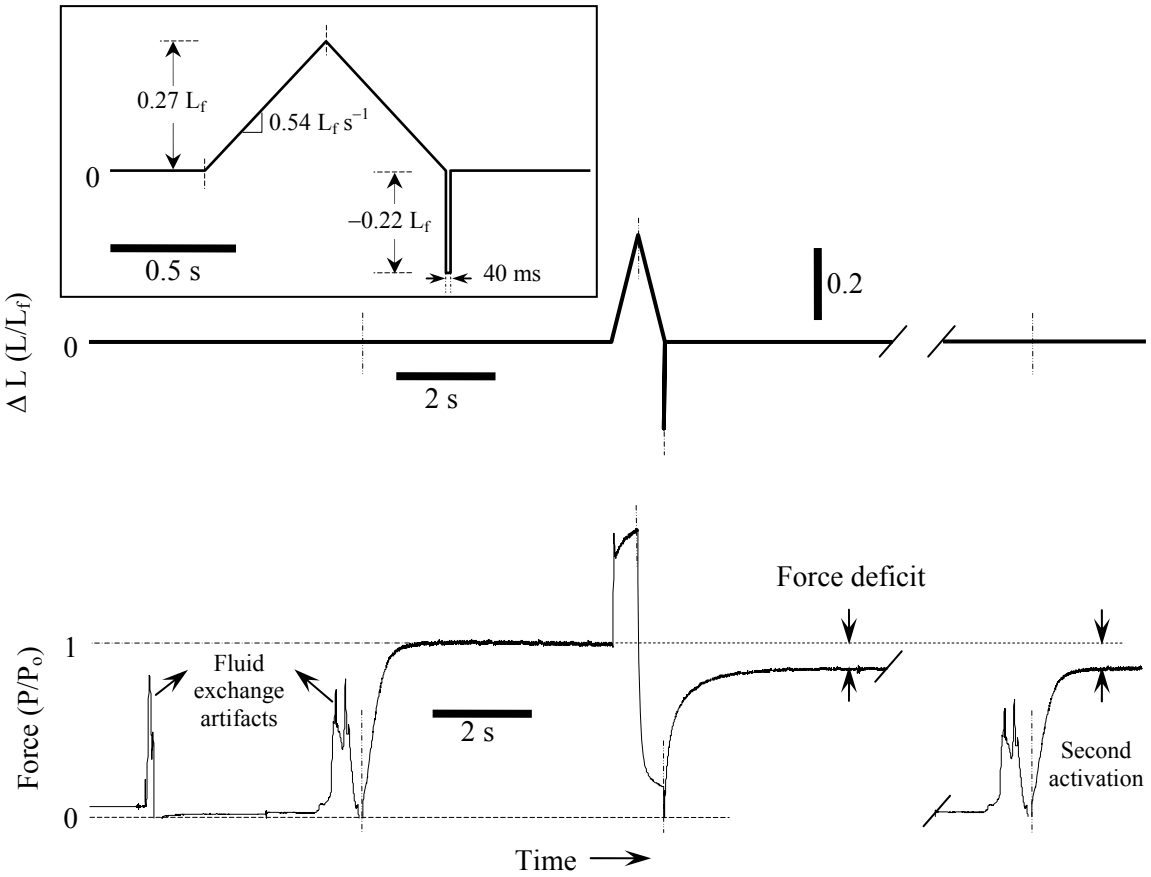

FIGURE 4.2: Single lengthening contraction protocol. (*A*) Change in fiber length during a single stretch lengthening contraction protocol is shown in the inset. (*B*) The force response of a sample fiber during the lengthening contraction protocol is shown on same time scale. The zero of the force transducer was established during the 40 ms hold following the step-shortening of the fiber. P_o both before and after the lengthening contraction were measured relative to the force transducer zero.

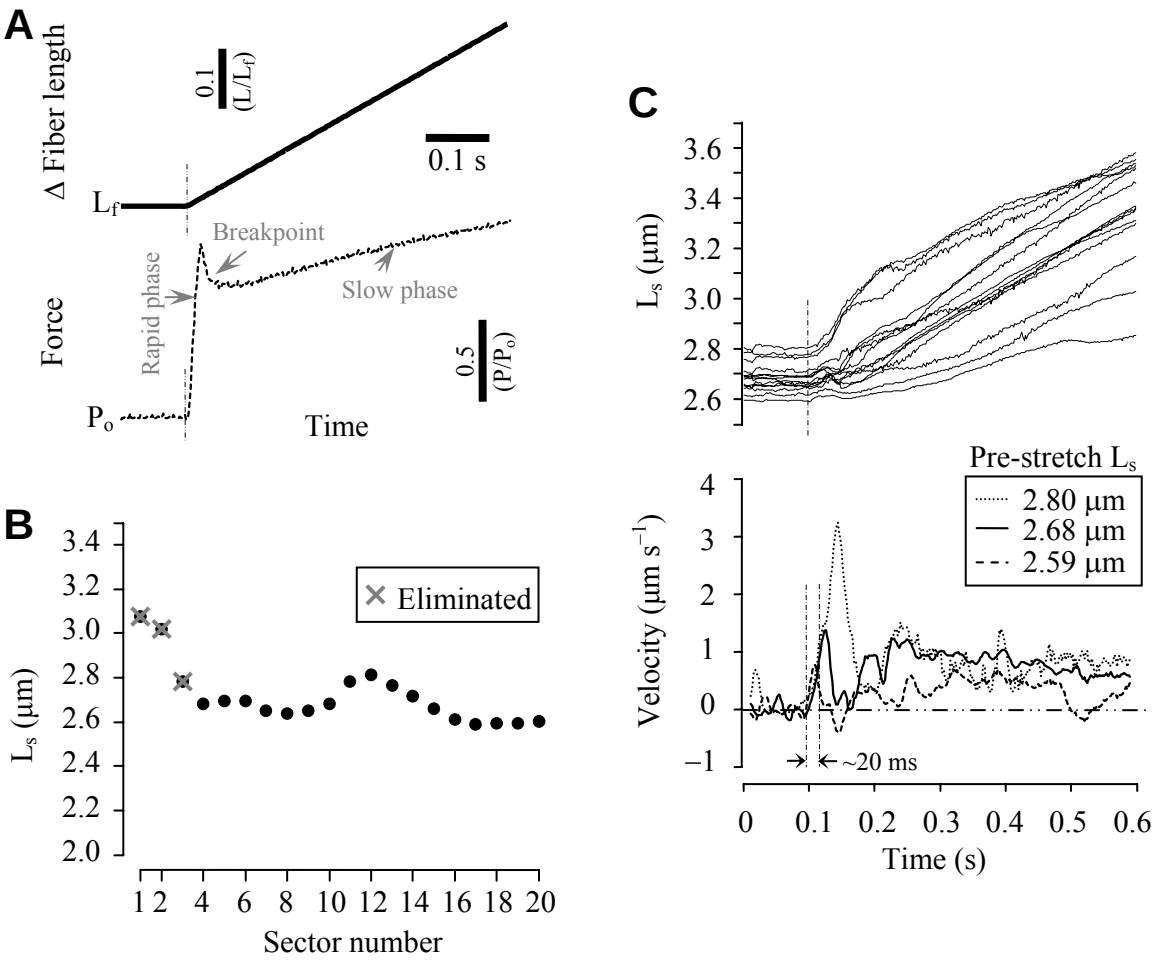

FIGURE 4.3: L_s and velocity data of a representative fiber. (*A*) Force response of the fiber during the stretch is shown in the bottom panel. (*B*) Sector exclusion map of the fiber. Note that sectors exclusion occurred only at the left end. (*C*) The continuous L_s records of all sectors of the fiber (top) show a stable lengthening behavior of the sectors. Velocities corresponding to 3 sectors (bottom) show uniform acceleration during the first 20 ms. Velocity changes were rapid near breakpoint of the force, but these rapid changes were arrested immediately, within ~100 ms.

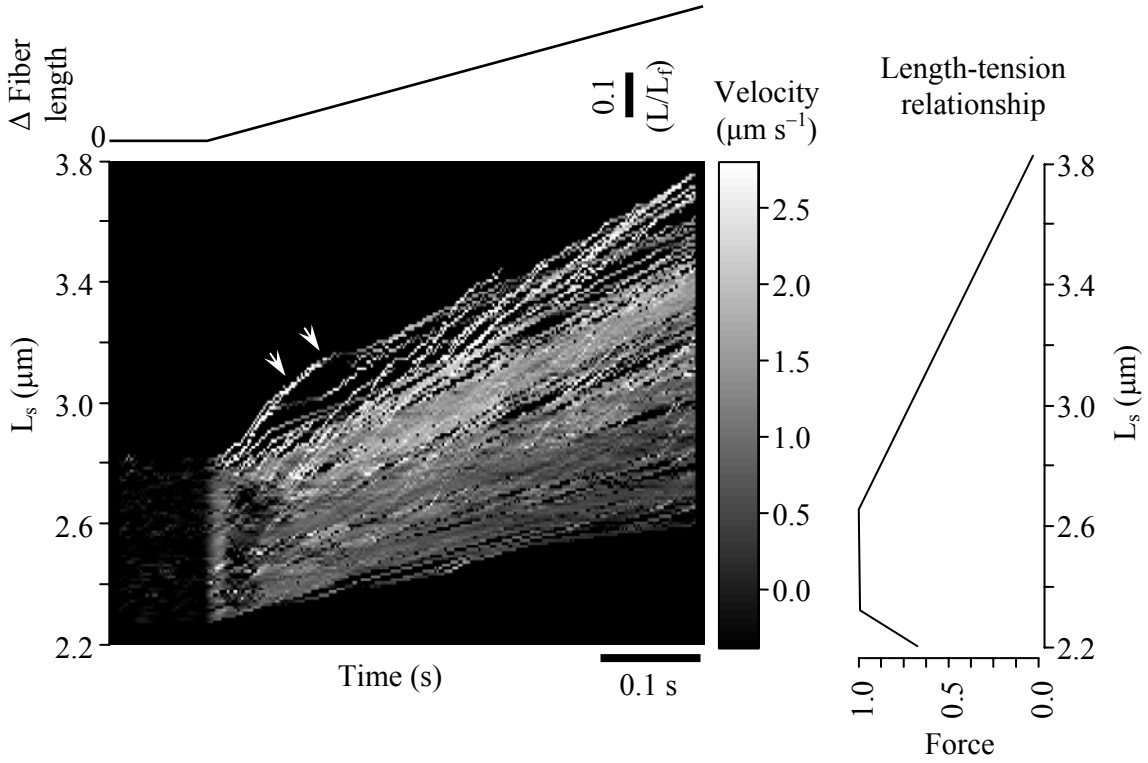

FIGURE 4.4: Sarcomere dynamics during the stretch. Left: The grayscale value at each pixel on each L_s trace (indicated by white arrows) represents the average velocity of the sectors as indicated in the color bar to the right. Right: The length-tension relationship for *soleus* muscles of rat.

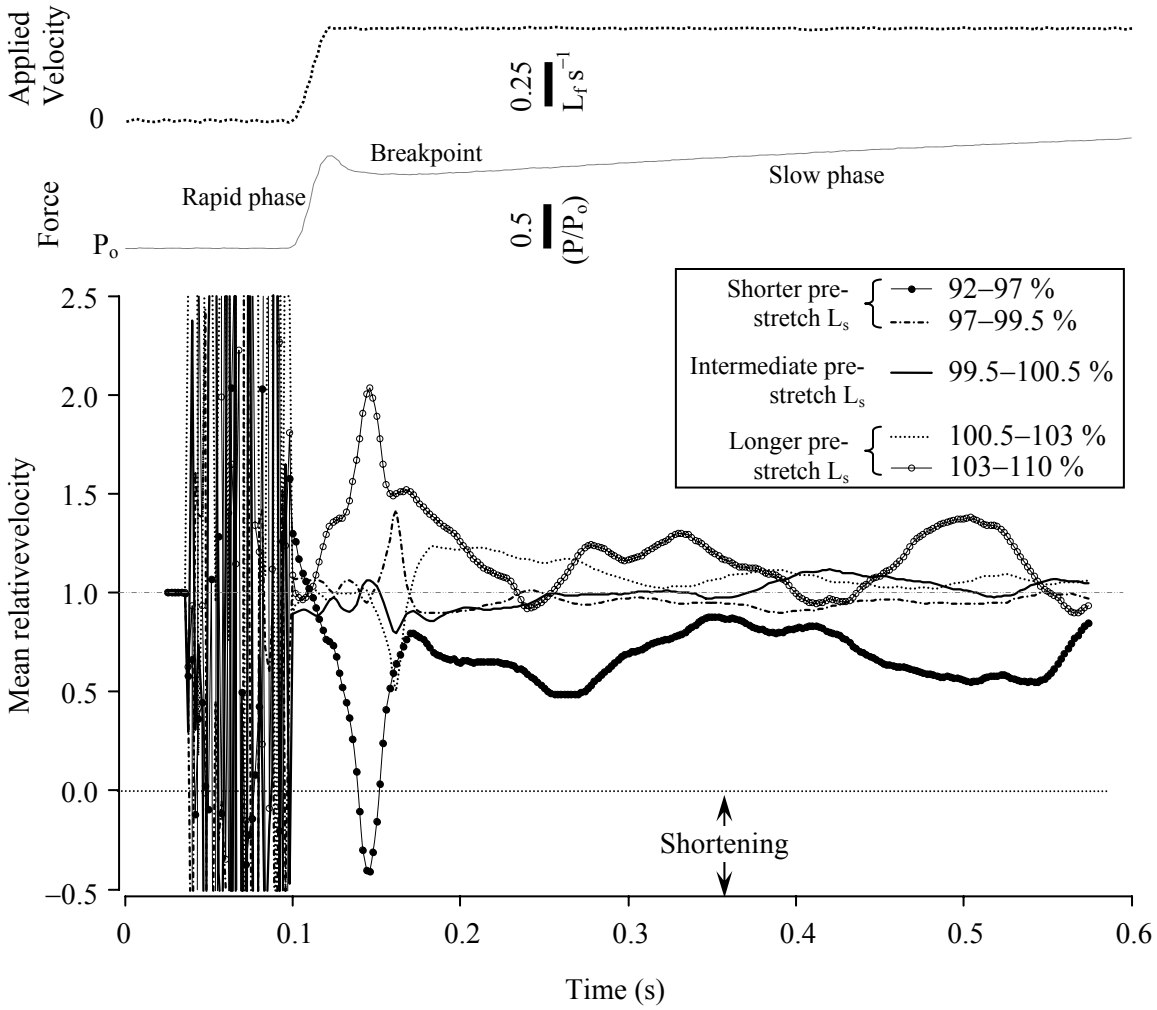

FIGURE 4.5: Mean relative velocities. Sectors are assigned to each one of 5 groups based on their relative pre-stretch L_s [L_s (μm)/mean fiber L_s (μm)]. The relative pre-stretch L_s bounds of each group are as indicated in the figure. The mean relative velocity (sector velocity/mean fiber velocity) in each group was computed by averaging the relative velocities of all sectors contained in that group at each time-point. Examples of applied stretch velocity and the corresponding force response are shown on the top.

References

Bagni, M. A., G. Cecchi, B. Colombini, and F. Colomo. 2002. A non-cross-bridge stiffness in activated frog muscle fibers. *Biophys. J.* 82:3118-3127.

Brooks, S. V. and J. A. Faulkner. 1996. The magnitude of the initial injury induced by stretches of maximally activated muscle fibres of mice and rats increases in old age *J. Physiol* 497:573-580.

Brooks, S. V., E. Zerba, and J. A. Faulkner. 1995. Injury to muscle fibres after single stretches of passive and maximally stimulated muscles in mice. *J. Physiol* 488:459-469.

Chase, P. B. and M. J. Kushmerick. 1988. Effects of pH on contraction of rabbit fast and slow skeletal muscle fibers. *Biophys. J.* 53:935-946.

Cleworth, D. R. and K. A. Edman. 1972. Changes in sarcomere length during isometric tension development in frog skeletal muscle. *J Physiol* 227:1-17.

Edman, K. A. 2005. Contractile properties of mouse single muscle fibers, a comparison with amphibian muscle fibers. *J. Exp. Biol.* 208:1905-1913.

Flitney, F. W. and D. G. Hirst. 1978. Cross-bridge detachment and sarcomere 'give' during stretch of active frog's muscle. *J Physiol* 276:449-465.

Getz, E. B., R. Cooke, and S. L. Lehman. 1998. Phase transition in force during ramp stretches of skeletal muscle. *Biophys. J* 75:2971-2983.

Gordon, A. M., A. F. Huxley, and F. J. Julian. 1966. The variation in isometric tension with sarcomere length in vertebrate muscle fibres. *J. Physiol* 184:170-192.

Harry, J. D., A. W. Ward, N. C. Heglund, D. L. Morgan, and T. A. McMahon. 1990. Cross-bridge cycling theories cannot explain high-speed lengthening behavior in frog muscle. *Biophys. J.* 57:201-208.

Katz, B. 1939. The relation between force and speed in muscular contraction. *J Physiol* 96:45-64.

Kawai, M. and I. D. Kuntz. 1973. Optical diffraction studies of muscle fibers. *Biophys. J* 13:857-876.

Leung, A. F. 1983. Light diffractometry for determining the sarcomere length of striated muscle: an evaluation. *J. Muscle Res. Cell Motil.* 4:473-484.

Macpherson, P. C., R. G. Dennis, and J. A. Faulkner. 1997. Sarcomere dynamics and contraction-induced injury to maximally activated single muscle fibres from soleus muscles of rats. *J. Physiol* 500:523-533.

Macpherson, P. C., M. A. Schork, and J. A. Faulkner. 1996. Contraction-induced injury to single fiber segments from fast and slow muscles of rats by single stretches. *Am. J. Physiol* 271:C1438-C1446.

Minajeva, A., M. Kulke, J. M. Fernandez, and W. A. Linke. 2001. Unfolding of titin domains explains the viscoelastic behavior of skeletal myofibrils. *Biophys. J* 80:1442-1451.

Moisescu, D. G. and R. Thieleczek. 1978. Calcium and strontium concentration changes within skinned muscle preparations following a change in the external bathing solution. *J Physiol* 275:241-262.

Morgan, D. L. 1990. New insights into the behavior of muscle during active lengthening. *Biophys. J.* 57:209-221.

Morgan, D. L. and U. Proske. 2006. Sarcomere popping requires stretch over a range where total tension decreases with length. *J Physiol* 574:627-628.

Panchangam, A., D. R. Claflin, M. L. Palmer, and J. A. Faulkner. 2007. Magnitude of sarcomere extension correlates with initial sarcomere length during lengthening of activated single fibers from soleus muscle of rats. *Biophys. J (submitted)*.

Rassier, D. E., W. Herzog, and G. H. Pollack. 2003. Dynamics of individual sarcomeres during and after stretch in activated single myofibrils. *Proc. Biol. Sci.* 270:1735-1740.

Stephenson, D. G. and D. A. Williams. 1982. Effects of sarcomere length on the force-pCa relation in fast- and slow-twitch skinned muscle fibres from the rat. *J. Physiol* 333:637-653.

Stienen, G. J., P. G. Versteeg, Z. Papp, and G. Elzinga. 1992. Mechanical properties of skinned rabbit psoas and soleus muscle fibres during lengthening: effects of phosphate and Ca2+. *J Physiol* 451:503-523.

Talbot, J. A. and D. L. Morgan. 1998. The effects of stretch parameters on eccentric exercise-induced damage to toad skeletal muscle. *J. Muscle Res. Cell Motil.* 19:237-245.

Telley, I. A., R. Stehle, K. W. Ranatunga, G. Pfitzer, E. Stussi, and J. Denoth. 2006. Dynamic behaviour of half-sarcomeres during and after stretch in activated rabbit psoas myofibrils: sarcomere asymmetry but no 'sarcomere popping'. *J. Physiol* 573:173-185.

Warren, G. L., D. A. Hayes, D. A. Lowe, and R. B. Armstrong. 1993. Mechanical factors in the initiation of eccentric contraction-induced injury in rat soleus muscle. *J. Physiol* 464:457-475.

Wood, S. A., D. L. Morgan, and U. Proske. 1993. Effects of repeated eccentric contractions on structure and mechanical properties of toad sartorius muscle. *Am. J. Physiol* 265:C792-C800.

CHAPTER 5

SUMMARY

Overview

The purpose of this dissertation was to clarify the mechanisms of initial injury during lengthening contractions of permeabilized single muscle fibers. The first objective was to develop an apparatus that enables rapid measurements of lengths of sarcomeres along segments of permeabilized single muscle fibers. This objective was met by developing a laser scanning system that rapidly reports the length of sarcomeres in 20 contiguous regions, hereafter termed 'sectors', that span the full length of ~1 mm long fibers at a rate of 500 s^{-1}. In addition to enabling rapid measurements of sarcomere lengths, this apparatus also allowed simultaneous measurements of the force and the length of fibers.

The second objective was to use this apparatus to test specific hypotheses regarding the dynamic behavior of sarcomeres during lengthening contractions of permeabilized single fibers. The hypotheses were that (*i*) during the lengthening of maximally activated permeabilized single fibers, the sectors that contain longer sarcomeres during the preceding isometric activation period undergo more elongation than the regions that contain shorter sarcomeres; (*ii*) severe lengthening contractions increase the variability in the lengths of sarcomeres of passive fibers; and (*iii*) during the

course of a severe lengthening contraction, all the sectors of permeabilized single fibers exhibit stable lengthening behavior. The findings of this study are summarized as follows.

Sarcomere length predicts sarcomere extension (Chapter 2)

The first study involved the measurements of lengths of sarcomeres within multiple sectors of each fiber at two time-points during a 27% lengthening contraction. The first time-point was just prior to the beginning of the lengthening and the second time-point was at the peak of the lengthening contraction, when the strain of the fiber reached the maximum. From these data, the relationship between the sarcomere lengths of the sectors prior to the lengthening contraction and the elongation of individual sectors during the lengthening contraction was determined. The results of the first study are summarized as follows.

This study is the first to show experimentally that, (*i*) during lengthening contractions, longer sarcomeres are extended more than their serially-connected, shorter neighbors, and (*ii*) sarcomeres operating on the descending limb of the length-tension relationship are stretched more than their neighbors that are connected serially and that are operating on the plateau, or the ascending limb of the length-tension relationship. Consequently, this study established that non-uniformities in L_s during lengthening contractions are due to non-uniformities in sarcomere lengths during the isometric phase of the contraction just prior to lengthening. During contraction-induced injury, the link between the pre-stretch sarcomere length and the extent of damage (Macpherson et al., 1997; Talbot and Morgan, 1998) was drawn solely from theoretical models (Morgan,

1990) and was attributed to the excessive strain placed on the longer sarcomeres. With direct experimental evidence, the present study established the link between pre-stretch sarcomere length and the increased likelihood of injury following a severe strain. The findings supported the hypothesis that contraction-induced injury results when groups of sarcomeres that are at longer lengths in the activated fibers, when exposed to a severe lengthening contraction, are stretched excessively compared with their serially connected neighboring sarcomeres that are at shorter lengths and undergo structural damage.

Lengthening contractions increase variability in sarcomere lengths (Chapter 3)

In the second study, in addition to the measurements of sarcomere lengths prior to and at the peak of a 27% lengthening contraction, lengths of sarcomeres were measured just prior to and at the peak of 33% passive stretches applied before and after the lengthening contraction. Comparisons of sarcomere lengths made among these passive stretches revealed differences that were caused by the lengthening contraction. Prior to the experimental protocol, the fibers were subjected to repetitive cycles of stretch and release to minimize the effects of past history of strain on the passive properties of fibers. This approach ensured that, following the minimization of the history-dependent effects, the observed changes in the lengths of sarcomeres are due only to the lengthening contraction.

The study demonstrated that lengthening contractions increase the variability in sarcomere lengths of passive fibers. The increase in variability of sarcomere lengths was greatest immediately following the lengthening contraction and then declined to a lower, but still elevated level. Sarcomeres that were extended the most during the lengthening

contraction did not return to their resting lengths when the fibers were relaxed. This observation suggested that passive elements within the severely extended sarcomeres underwent irreversible changes. Based on these observations, we conclude that lengthening contractions alter the passive length-tension relationships of individual sarcomeres. For fibers that were stretched passively, the variability in sarcomere lengths was eliminated at long lengths. This observation is consistent with the premise that passive elastic elements minimize the non-uniformities in the lengths of sarcomeres in stretched fibers (Granzier et al., 1991).

Compared with the peak stress during a 33% passive stretch applied to the fibers prior to a lengthening contraction, the peak stress during a subsequent passive stretch applied immediately after the lengthening contraction, was 8% lower. For passive fibers, the variability in sarcomere lengths was greatest immediately after the lengthening contraction. Under these circumstances, when the fibers were activated maximally a second time, the variability in sarcomere lengths would be even higher (Denoth et al., 2002) and the likelihood of damage would be increased (Macpherson et al., 1997; Patel et al., 2004). Based on these observations, a second lengthening contraction initiated immediately after the first lengthening contraction causes more damage to the fiber than if the lengthening contraction were initiated after some prolonged period of relaxation. This hypothesis forms a basis for future studies of contraction-induced injury that involve multiple lengthening contractions with varying periods of relaxation and rest in between each of the contractions.

The rate of change of sarcomere length during lengthening contractions (Chapter 4)

The third study involved continuous measurements of the lengths of sarcomeres of all the sectors of permeabilized fibers. From these continuous records of sarcomere length, continuous records of the velocity of the sarcomeres contained in each sector were computed. From these measurements, during a severe lengthening contraction, the dynamic behavior of the fiber sectors was studied. The findings of this study are summarized as follows.

For some sectors that were composed of sarcomeres at long lengths, rapid lengthening was observed during an early phase of the stretch, but the rapid lengthening was arrested quickly and transitioned to a lengthening at steady rates. This finding contradicts the hypothesis that the sarcomeres at the longest lengths prior to a lengthening contraction, undergo rapid and sudden lengthening during the lengthening contraction, to extreme long lengths where thick and thin filament overlap in those sarcomeres would be lost (Morgan, 1990). Some individual events at the level of single sarcomeres that cannot be detected with the laser diffraction technique cannot be ruled out, but rapid lengthening of the sectors was not observed in the present study. Therefore, we conclude that the rapid lengthening events have not taken place on a scale sufficient to explain the extent of damage observed in these studies.

Based on steady-state models of force generation, sarcomeres at longer lengths are at greater risk of undergoing rapid elongation (Morgan, 1990; Schachar et al., 2002; Zahalak, 1997). In contrast, in the present study sarcomeres in all sectors, even those undergoing the greatest strains, elongated at steady rates. This stable stretch behavior when combined with the finding in Chapter 3 that, the sectors that underwent greater

strains during a lengthening contraction, were unable to return to their original sarcomere lengths in a relaxed state following the lengthening contraction, suggests that passive elastic elements play a role in stabilizing the stretch during the lengthening contraction. We propose that the elastic protein filament titin, that spans each half-sarcomeres and connects A-bands to I-bands and Z-disks, might play a major role in the stabilization of the sarcomeres during a lengthening contraction. Lateral connections between sarcomeres in adjacent myofibrils (Lazarides, 1980) may also be involved in this stabilization process. Additional studies are required to resolve precisely the structures involved in this stabilization process.

Future applications of the technique

Compared with previous studies (Lieber and Baskin, 1983; Macpherson et al., 1997), the multiple-sector measurements of lengths of sarcomeres offer an enhanced view of the contractile behavior of single muscle fibers at rest and during contractions. The current approach can be extended even further to provide insights into the behavior of sarcomeres contained within sectors: (*i*) the width of a first-order diffraction pattern indicates the variability in L_s within each sector (Kawai and Kuntz, 1973); and (*ii*) the sub-structure of the first-order diffraction pattern can be used to gain deeper insights into the sarcomere length dynamics of populations within individual sectors (Sidick et al., 1992; Yeh et al., 1980). The laser scanning technique described here provides both the width and the sub-structure of the first-order patterns corresponding to multiple sectors along the entire length of a fiber. These additional data have the potential to provide insightful physiological information contained within the sectors. Although originally

designed for measurements on permeabilized fibers, this technique can be easily extended to other preparations such as mechanically skinned and intact single fibers.

Future research

The current thesis focused exclusively on the sarcomere dynamics in permeabilized fibers from *soleus* muscles of adult rats. The *soleus* muscles of the rats contain predominantly slow, type 1 fibers. The future research will take into consideration the differences between different fiber types (type 1 and type 2) and different age groups (adult and old). Compared with type 1 fibers of adult animals, both type 2a and 2b fibers (Macpherson et al., 1996) and fibers from the old animals (Brooks and Faulkner, 1996) are more susceptible to contraction-induced injury. The study of the differences in sarcomere dynamics between the fiber types and the age groups will enhance significantly the understanding of the mechanisms of contraction-induced injury. Also, compared with type 1 fibers of adult animals, both type 2 fibers and the fibers from old animals appear to develop greater heterogeneity in the lengths of sarcomeres (personal observations). This increased heterogeneity should manifest itself in the broadening of the first-order diffraction spots. Future research will include investigation of the broadening of first-order diffraction spots to clarify the dynamic behavior of sarcomeres contained within individual fiber sectors.

References

Brooks, S. V. and J. A. Faulkner. 1996. The magnitude of the initial injury induced by stretches of maximally activated muscle fibres of mice and rats increases in old age. *J. Physiol* 497:573-580.

Denoth, J., E. Stussi, G. Csucs, and G. Danuser. 2002. Single muscle fiber contraction is dictated by inter-sarcomere dynamics. *J Theor. Biol.* 216:101-122.

Granzier, H. L., H. A. Akster, and H. E. ter Keurs. 1991. Effect of thin filament length on the force-sarcomere length relation of skeletal muscle. *Am J Physiol* 260:C1060-C1070.

Kawai, M. and I. D. Kuntz. 1973. Optical diffraction studies of muscle fibers. *Biophys. J* 13:857-876.

Lazarides, E. 1980. Intermediate filaments as mechanical integrators of cellular space. *Nature* 283:249-256.

Lieber, R. L. and R. J. Baskin. 1983. Intersarcomere dynamics of single muscle fibers during fixed-end tetani. *J. Gen. Physiol* 82:347-364.

Macpherson, P. C., R. G. Dennis, and J. A. Faulkner. 1997. Sarcomere dynamics and contraction-induced injury to maximally activated single muscle fibres from soleus muscles of rats. *J. Physiol* 500:523-533.

Macpherson, P. C., M. A. Schork, and J. A. Faulkner. 1996. Contraction-induced injury to single fiber segments from fast and slow muscles of rats by single stretches. *Am. J. Physiol* 271:C1438-C1446.

Morgan, D. L. 1990. New insights into the behavior of muscle during active lengthening. *Biophys. J.* 57:209-221.

Patel, T. J., R. Das, J. Friden, G. J. Lutz, and R. L. Lieber. 2004. Sarcomere strain and heterogeneity correlate with injury to frog skeletal muscle fiber bundles. *J. Appl. Physiol* 97:1803-1813.

Schachar, R., W. Herzog, and T. R. Leonard. 2002. Force enhancement above the initial isometric force on the descending limb of the force-length relationship. *J Biomech.* 35:1299-1306.

Sidick, E., A. Knoesen, J. K. Xian, Y. Yeh, and R. J. Baskin. 1992. Rigorous analysis of light diffraction by a striated muscle fibre. *Proc. Biol. Sci.* 249:247-257.

Talbot, J. A. and D. L. Morgan. 1998. The effects of stretch parameters on eccentric exercise-induced damage to toad skeletal muscle. *J. Muscle Res. Cell Motil.* 19:237-245.

Yeh, Y., R. J. Baskin, R. L. Lieber, and K. P. Roos. 1980. Theory of light diffraction by single skeletal muscle fibers. *Biophys. J* 29:509-522.

Zahalak, G. I. 1997. Can muscle fibers be stable on the descending limbs of their sarcomere length-tension relations? *J Biomech.* 30:1179-1182.